Draft

A Hydrodynamic and Water Quality Model for the Lower Charles River Basin, Massachusetts

Prepared for:

United States Environmental Protection Agency
Region 1
1 Congress Street
Boston, MA 02114

Prepared by:

Tetra Tech, Inc.
10306 Eaton Place, Suite 340
Fairfax, VA 22030
and
Numeric Environmental Services

November 2005

Table of Contents

List of Tables

List of Figures

Figures are located in the attached document

1 INTRODUCTION

This report documents the development, calibration, and verification of a coupled hydrodynamic and water quality modeling system to support the implementation of a eutrophication total maximum daily load (TMDL) for the Lower Charles River Basin (the Basin) in metropolitan Boston, Massachusetts. The Basin is targeted for TMDL development to address water quality impairments associated with excessive algal blooms. The companion report *DRAFT – Total Maximum Daily Load for Eutrophication in the Lower Charles River Basin* (Tetra Tech 2005) discusses the water quality impairments in greater detail. The Basin represents the section for the river between the Watertown Dam and the New Charles River Dam where the river flows into Boston Harbor. To develop the TMDL, a three dimensional-time variable water quality model is needed to simulate algal dynamics and dissolved oxygen levels in the Basin and to determine acceptable pollutant load allocations for nutrients and heat that will result in attaining water quality standards.

The organization of the report is as follows: The remainder of this section provides background material and defines the purpose and scope of the study. Section 2 provides additional background information on the Basin and data available to support model development, calibration, and verification. Section 3 documents the configuration, calibration, and verification of the hydrodynamic and transport component of the model. Section 4 documents the configuration, calibration, and verification of the water quality component of the model. Section 5 summarizes the study and discusses application of the modeling system to support TMDL development. Three appendices (A, B, and C) provide details on the formulation of the hydrodynamic and water quality models and quantitative measures proposed for use in evaluating model calibration and verification.

1.1 Background

With the passage of the Clean Water Act (CWA), demonstrable progress has been made in reducing water pollution from point sources. The goal of the CWA, however, still remains to be met. The nation will not be able to attain or maintain water quality standards by solely controlling point sources. There are some situations where nonpoint source controls will be necessary in order to solve existing water quality problems and mitigate threats to designated water uses. One of the CWA tools available to help devise holistic, integrated approaches to solving point and nonpoint source problems is the establishment of TMDLs under Section 303(d).

In April of 1991 the United States Environmental Protection Agency's (EPA) Office of Water Assessment and Protection Division published *Guidance for Water Quality Based decisions: the TMDL Process*. In July 1992, EPA published the final *Water Quality Planning and Management Regulation* (40 CFR Part 130). Together these documents describe the roles and responsibilities EPA and the States have in meeting the requirements of Section 303(d) of the CWA, particularly the continued integration of point and nonpoint source controls.

The CWA requires States to identify and report to EPA their water quality-limited waters following public participation. In addition, the States are required to develop TMDLs for those

waterbodies that are listed as not meeting their designated uses.

TMDLs result in a distribution of pollutant loading intended to meet water quality standards. In many cases, the determination of loadings and exploration of alternatives relies on the description of the waterbody's interactions through the use of modeling systems. When the interactions of flow, loading, internal chemical and biological processes are too involved to be solved through the use of statistical and data analysis techniques, computer simulation models are often employed. The model(s) employed in examining the relationships between loading and waterbody systems must be carefully selected and crafted to recognize the key features of the system and gain the acceptance of the affected community and program regulators.

The Massachusetts Department of Environmental Protection (MADEP) has included the Basin on the State's 2002 and 2004 section 303(d) lists for the following pollutants (MAEOEA 2003 and 2004):

- Unknown toxicity
- Priority organics
- Metals
- Nutrients
- Organic enrichment/low dissolved oxygen
- Pathogens
- Oil and grease
- Taste, odor and color
- Noxious aquatic plants
- Turbidity

The TMDL modeling tools described in this report address the nutrient, low dissolved oxygen, and noxious aquatic plant impairments. The noxious aquatic plants listing refers to excessive algae growth in the Basin. It is believed that increased nutrient loads to the Basin are causing the excessive algal growth, which in turn causes the low dissolved oxygen levels. For more detail on the water quality impairments addressed by this modeling effort, refer to the companion report, *DRAFT – Total Maximum Daily Load for Eutrophication in the Lower Charles River Basin* (Tetra Tech 2005).

The pollutants of concern for this TMDL modeling study are those pollutants that are thought to be directly causing or contributing to the excessive algal growth in the Basin and pollutants that will or might require reductions to attain the applicable Massachusetts Water Quality Standards (MAWQS). Phosphorus is a primary pollutant of concern and heat or thermal load has been identified as a potential pollutant of concern for contributing to excessive algal growth and the proliferation of undesirable blue-green algae species in the Lower Basin.

In summary, factors contributing to the above water quality problems include: large tributary stormwater and CSO loads of algal nutrients and oxygen demanding substances, vertical salinity and temperature induced stratification of the Basin during low flow summer months, and release of algal nutrients from and exertion of dissolved oxygen demand by bottom sediments within the Basin during low flow summer months.

1.2 Purpose of Modeling

Modeling for TMDL development presents some special constraints. TMDLs often have hard deadlines requiring that analysis be completed in spite of technical complexity and data limitations. TMDLs require loading estimates to support allocations although there is significant flexibility in the spatial and temporal detail required in the final distribution of nonpoint source loadings. TMDL modeling is often used to evaluate various interpretations of water quality standards and measures of designated uses. For the selected modeling approach to be successfully applied it must be accepted by the user community as being sensitive to their needs and concerns. The type and detail of analysis required can be derived from careful examination of the goals, objectives, and needs analysis. If implementation of the TMDL is likely to result in an expensive and significant management effort, a more sophisticated and detailed modeling approach is often warranted.

Typically models used in TMDL analysis are in the public domain and accepted by the State and the EPA Region. The review of the selected modeling system must be able to withstand the scrutiny of the user community, nationally recognized experts, and state and federal reviewers. This requires the use of clearly identified procedures for selecting and designing modeling approaches that are accepted and result in successful decision-making.

For development of eutrophication TMDLs in waterbodies having complex physical and biogeochemical dynamics, a three-dimensional (3-D) time variable water quality model is generally needed to simulate algal dynamics and dissolved oxygen levels and to determine acceptable pollutant load allocations for nutrients and heat that result in attaining water quality standards. The complex hydrodynamics of the Basin, including salinity and temperature stratification, salinity intrusion through the ship locks, and the power plant thermal discharge, require the use of a 3-D hydrodynamic model with dynamically coupled salinity and temperature prediction to simulate transport and mixing, and to provide transport for a eutrophication or water quality model. Although water column nutrient cycling and algae dynamics coupled with 3-D transport and mixing in the Basin can be represented by a number of available water quality models, the ability to predict sediment oxygen demand and nutrient fluxes requires a model formulation that includes sediment diagenesis. The Environmental Fluid Dynamics Code (EFDC) model has been selected as the modeling system to be used for this study and is described in Section 3.

1.3 Scope and Approach

Model development was undertaken using a team approach. Tetra Tech, Inc., under contract to the EPA, developed the hydrodynamic model component, while Numeric Environmental Services (Numeric), under contract to the New England Interstate Water Pollution Control Commission (NEIWPCC) and later Tetra Tech, developed the linked water quality model. Tetra Tech supported the water quality model development and calibration effort by providing technical guidance (QA/QC and final assembly of this report). Both Tetra Tech and Numeric participated in a Technical Advisory Committee (TAC) for the project, which will be convened by the Charles River Watershed Association (CRWA). Model development will be accomplished

in two phases. This report documents Phase I, involving model configuration and calibration and verification to existing data and information. Phase II will include application of the model for allocation scenario simulations to support development of the TMDL.

Following calibration and verification of the water quality model, the model will be used to evaluate point and nonpoint source loading allocations and reduction scenarios (or options), considering critical conditions and the established TMDL endpoints. There are numerous combinations of loads that can meet the TMDL endpoints. Using the information provided through stakeholder interaction, scenarios that best meet the stakeholders' needs will be assessed and adjusted to produce acceptable loadings. In addition, watershed and in-stream best management practices (BMPs) will be considered for nonpoint source load reduction.

TMDL scenario simulations will be designed based on current load allocations and various alternative load allocations developed in conjunction with the stakeholders, regulatory agencies and the technical advisory group. The calibrated and verified hydrodynamic and water quality models will be reconfigured as appropriate based on TMDL allocation simulation scenarios using both calibration kinetic parameters and implicit margin of safety parameters derived from sensitivity and uncertainty analyses. The simulation scenario results and analysis, including a comparison of implicit and explicit margin of safety approaches, will be documented in a report.

2 THE LOWER CHARLES RIVER SYSTEM

The Lower Charles River Basin is targeted for TMDL development to address water quality impairments associated with excessive algal blooms. The Basin represents the section of the river between the Watertown Dam and the New Charles River Dam where the river flows into Boston Harbor. The lower portion of the Basin is impounded and has a long retention time during low flows, allowing algal blooms to become well established and severe during the summer months. This region is also density stratified because of intrusion of saline water into the Basin from Boston Harbor during lock opening. An existing shoreline, near-surface thermal discharge from the Kendall Square power plant is also a possible contributor to the density stratification and elevated near-surface temperature. The severity of the blooms is attributed primarily to (1) high nutrient loadings from wastewater treatment facilities (WWTFs) in the upper watershed, urban stormwater drainage systems, and combined sewer overflows (CSOs); (2) thermal loadings from the power plant discharges into the lower Basin; and (3) long retention times. The sediment bed in the impounded portion of the Basin between Boston and Cambridge is characterized by a thick layer of mud, which is a source of sediment oxygen demand and nutrient fluxes into the lower water column. This condition, combined with the summer density stratification, results in low bottom water dissolved oxygen.

Conditions in the Basin are further complicated by a proposed expansion of the Kendall Square power plant's capacity and relocation of the existing near-shore, near-surface thermal discharge to a bottom diffuser. A study conducted for the power plant owners (Mirant) indicated that the diffuser could reduce or eliminate density stratification in portions of the impoundment. The reduction in stratification could have complex effects on water quality in the impounded portion of the Basin. Reduced stratification would likely result in higher dissolved oxygen levels in the bottom of the Basin, but could also result is higher near-surface nutrient levels as diagenetic fluxes from the sediment are mixing upward in the water column.

2.1 Physical Setting

This Section provides a brief overview of the study area. For more detailed information, refer to the companion document *DRAFT – Total Maximum Daily Load for Eutrophication in the Lower Charles River Basin* (Tetra Tech 2005).

The Basin is located in eastern Massachusetts and flows through portions of Norfolk, Middlesex, and Suffolk Counties. The Basin is at the downstream end of the Charles River Watershed, approximately 1.2 miles upstream from its outlet to Boston Harbor and the Atlantic Ocean. The Basin is an impounded section of the Charles River that is 8.6 miles long and covers approximately 675 acres. The majority of this area exists in the lower portion of the Basin downstream of the Boston University (BU) Bridge (Lower Basin). The Lower Basin is 2.6 miles long and has widths varying from 300 to 2,000 feet. Its water volume accounts for approximately 90 percent of the entire water volume of the Basin (MADEP 2000, Zarriello and Barlow, 2002). Water depths range from 6 to 12 feet in the Basin upstream of the BU Bridge and 9 to 36 feet in the Lower Basin.

The entire Charles River Basin drains a watershed area of 308 square miles. Two hundred and sixty-eight square miles of watershed area (upstream watershed) drain over the Watertown Dam into the Basin. The remaining 40 square miles drain directly into the Basin from small tributary streams that are mostly piped and piped stormwater drainage systems serving the surrounding communities. There is also a combined sewer drainage area near the downstream end of the Basin. The Basin is in the heart of a highly urbanized area.

The Boston area has a fairly typical four-season climate and is characterized as humid temperate. There is no wet or dry season as precipitation is reasonably consistent with about 3 inches of rain per month and average annual precipitation of 41.5 inches.

The soils in the surrounding watershed are well- to moderately well-drained soils that are derived from glacial till and outwash. Much of the watershed is identified as "urban land". Soils classified as urban land tend to be near the river in areas that have been filled to eliminate tidal marshes and mud flats (Zarriello and Barlow 2002). Since the Basin is in such a highly urbanized area, much of the area is impervious because of paving.

2.2 Hydrology and Hydrodynamics

During any given year, the Charles River Basin experiences large variations in flow because of the size of the upstream watershed (268 square miles) draining over the Watertown Dam and the highly urbanized watershed that drains directly to the Basin. Daily average river flow data entering the Basin at Watertown Dam (1997-2004) were reviewed. During this period, flows ranged from a low of 52 cubic feet per second (cfs) to a high of 2,143 cfs. Generally, annual high flows at Watertown Dam occur during the spring thaw period and low flows occur during the summer months. Occasionally, and regardless of the time of year, large rain events occur and produce high flow conditions in the Basin.

Of particular interest is the summer period when growth conditions for algae are optimal. The low flows that occur in the Basin during the summer period favor algal growth because of the associated increase in water residence time. For more detailed information on the hydrology and hydrodynamics of the Basin, refer to the companion report *DRAFT – Total Maximum Daily Load for Eutrophication in the Lower Charles River Basin* (Tetra Tech 2005).

2.3 Observational Data to Support Modeling

The calibration and verification of a coupled three-D hydrodynamic and water quality modeling system to support TMDL development requires sufficient field observation data to support calibration and quantify an acceptable level of verification such that confidence is established for use of the modeling system for evaluating various load and wasteload allocation scenarios. Field data collection programs have been ongoing in the Basin since 1998.

Numeric Environmental Services conducted a comprehensive historical data review early in this project. Results of this data review were published in 2002 (*Lower Charles River TMDL Modeling Project – Historical Data Review*, November 22, 2002). The companion document, *DRAFT – Total Maximum Daily Load for Eutrophication in the Lower Charles River Basin*

(Tetra Tech 2005), summarizes the available data, which are deemed adequate for model calibration and verification. The major objective of the data review was to identify and summarize the available sources of site-specific historical data with regard to their utility during the development, testing (calibration and verification), and application of the Lower Charles River Basin Model. Principal data sources reviewed in this report included the following:

- Monitoring and 3-D hydrodynamic and water quality transport modeling conducted by Mirant for their existing and proposed Kendall Power Station heated water discharge to the Basin
- Massachusetts Water Resources Authority (MWRA) monitoring and modeling of combined sewers and overflows to the Basin
- United States Geological Survey (USGS) monitoring and modeling of dry- and wet-weather tributary flow and pollutant loads to the Basin
- Ongoing EPA monitoring of water quality in the Basin since 1998
- Boston Water and Sewer Commission (BWSC) monitoring and modeling of stormwater and CSO discharges to the Basin
- USGS monitoring of benthic sediment nutrient and oxygen fluxes in the Basin
- USGS monitoring and statistical modeling of salt wedge intrusion from Boston Harbor into the Basin
- Metropolitan District Commission (MDC) monitoring of water quality impacts of air diffusers installed in the Basin during the Charles River Artificial De-stratification Project (1978 through 1980s)
- Charles River Watershed Association (CRWA) monitoring and modeling of flow and water quality at and upstream of Watertown Dam (headwaters to the Basin)

Each of these data sources were useful for one, several, or many components of the model development and verification processes. For example, both the EPA water quality monitoring data (summer months of the years 1998 through 2002) and the USGS saltwater wedge intrusion study (June 1998 through July 1999) were required for testing (calibration and verification) of the hydrodynamic and water quality models. The EPA water quality monitoring and USGS sediment flux monitoring data were useful for increasing the understanding of the extent and possible contributing factors to the levels of eutrophication currently found in the Basin during the summer months. The USGS monitoring and analysis of salt wedge intrusion into the Basin during 1998 and 1999 served to improve the understanding of this complex phenomenon, which was included in the 3-d hydrodynamic model as density-induced circulation.

The MWRA, BWSC, and USGS monitoring and transient modeling of dry- and wet-weather tributary and CSO flow inputs and pollutant loads to the Basin were expanded upon and subsequently utilized to define time-series of boundary flow and water quality constituent loading rates required as input to the 3-D hydrodynamic and water quality transport models. Mirant's 3-D modeling of the existing and proposed Kendall Power Station heated water discharges to the Basin and their field data compilations provided a major source of model input data (e.g., conceptual grid layout, bathymetry, and heat loading time series) and potentially useful hydrodynamic modeling techniques that were investigated during initial development of the models for this study.

3 HYDRODYNAMIC AND TRANSPORT MODEL

3.1 Model Description

The public domain EFDC was selected to model both hydrodynamics and water quality in the Lower Charles River Basin. EFDC is a multifunctional surface water modeling system that includes hydrodynamic, sediment-contaminant, and eutrophication components. The EFDC model was originally developed at the Virginia Institute of Marine Science and is currently maintained by Tetra Tech with support from the EPA. EFDC has been used for more than 80 modeling studies of rivers, lakes, estuaries, coastal regions and wetlands in the U.S. and abroad. The EFDC model is capable of 1-, 2-, and 3-D spatial resolution. The model utilizes a curvilinear-orthogonal horizontal grid and a sigma terrain following vertical grid. The EFDC model's hydrodynamic component employees a semi-implicit, conservative finite volume solution scheme for the hydrostatic primitive equations with either two or three level time stepping. Salinity and temperature transport are dynamically coupled with choice of high accuracy advection schemes including MPDATA and COSMIC. Additional hydrodynamic component features include simulation drying and wetting, representation of hydraulic control structures, vegetation resistance, wave-current boundary layers, and wave induced currents. An embedded single port buoyant jet module is included for coupled near and far field mixing analysis. The EFDC model includes a variable configuration eutrophication component for simulation of aquatic carbon, nitrogen, and phosphorous cycles. The full configuration of state variables is based on the CE-QUAL-ICM model including sediment diagenesis. The configuration can be readily reduced to WASP5 equivalent configurations. Coupled EFDC hydrodynamic and water quality applications include Peconic Bays, NY; the Christina River Basin, DE; the Cape Fear River Estuary, NC; Mobile Bay, AL; the Yazoo River Basin, MS; Tenkiller Lake, OK; as well as a number of smaller water bodies. Details of the EFDC model's hydrodynamic and eutrophication components are provided in Appendices A and B, respectively.

3.2 Model Configuration

The general procedure for the application of the EFDC model to the Lower Charles River Basin follows a sequence of steps beginning with model set-up or configuration. Model configuration involves the construction of a horizontal grid of the waterbody and interpolation of bathymetric data to the grid, construction of EFDC input files, and compilation of the source code with appropriate parameter specification of array dimensions. The EFDC input files include the master input file (efdc.inp); files specifying the grid and bathymetry (cell.inp, celllt.inp, dxdy.inp, lxly.inp, mask.inp); atmospheric forcing files (aser.inp and wser.inp); an inflow-outflow file (qser.inp); salinity and temperature boundary condition and inflow concentration files (sser.inp and tser.inp); power plant withdrawal, temperature rise and discharge file (qwrs.inp); water column initial salinity and temperature concentration distribution files (salt.inp and temp.inp), respectively; and a screen print control file (show.inp) (Tetra Tech 2002a).

The horizontal grid that constructed the Basin used curvilinear horizontal grid cells and was constructed using an orthogonal mapping procedure (Ryskin and Leal 1983). Figure 3.1 shows the grid of the entire model region from just below the Watertown Dam to the New Charles

River Dam. The horizontal coordinate system used by the model is a localized UTM system. The horizontal grid has 56 active water cells. Bathymetry or water depth data collected by the USGS was interpolated to the horizontal model grid using an arithmetic average of all data points falling within a specific cell. Since exact vertical datum information was not available, the vertical datum reference was assumed to be at the mean water level of the wide portion of the river and that collected depths were relative to this assumed datum. Figure 3.2 shows an expanded view of the grid in the down-stream area. A single narrow cell represents the boat locks at the New Charles River Dam. A barrier between cells is used to represent the bridge constriction between the old and new dams. The cell containing the Mirant Kendall Square power plant cooling water withdrawal and discharge is also shown. Figure 3.3 shows the USGS 1998-99 discrete monitoring stations that were used for model calibration. The model vertical grid utilizes 8 sigma layers having varying thickness throughout the horizontal model domain. Sensitivity analyses of vertical resolution, using 5, 8, and 10 layers, indicated that 8 layers provided the best representation of vertical stratification.

3.3 Hydrodynamic Model Forcing Functions

Hydrodynamics in the Lower Charles River Basin model is forced by a combination of inflows and outflows and local wind surface wind stress. Inflows include the upstream river inflow at the Watertown Dam (Figure 3.4), inflow from smaller tributaries, CSOs, and distribution runoff along the river. The tributary, CSO, and distributed inflows were determined by a Stormwater Management Model (SWMM) of the Basin drainage area (Huber and Dickinson, 1988). Outflow at the New Charles River Dam includes both gravity-driven flow through sluice gates and pumped outflow to control river level during high inflow events. Since complete gauging information was not available for these outflows, the net outflow was estimated as the sum of inflows plus surface rainfall minus evaporation (Figure 3.6). Kendall Square power plant cooling water withdrawal and the subsequent return of temperature-elevated cooling water flow to the river significantly influences local hydrodynamics and thermodynamics in the Basin in the area upstream of the old dam and Museum of Science. Power plant records of cooling flow and temperature rise were included in the configuration using the EFDC model's power plant cooling withdrawal and discharge simulation module.

The intrusion of dense saline water from Boston Harbor due to boat lock openings at the New Charles River Dam is also a significant hydrodynamic forcing. Saline water entering the Basin creates bottom density currents that propagate upstream, forming a high-salinity layer in the bottom of the river primarily between late spring and early fall. The presence of the high-density saline bottom layer contributes significantly to maintaining a stable stratification and corresponding reduction in vertical mixing during this period. In the earlier phases of this study, the effects of the boat locks were represented by converting lockage per day information (Figure 3.5) into a pair of inflow and outflow time series representing inflow of high salinity harbor water and the corresponding outflow of lower salinity water from the river (Figure 3.6). Introduction of the inflow series in the lower layers and the outflow series in the upper layers of the horizontal cell representing the lock tended to introduce a dynamic inconsistency that manifested itself in the form of intense vertical mixing and under-representation of stratification in the region of the river observed to have salinity intrusion. The final configuration of the model represents salinity intrusion due to lock opening by setting the daily salinity in the lock cell to the

harbor salinity for a specified period of time proportional to the number of lock openings occurring that day. This was found to be more dynamically consistent in that the hydrodynamics of the lock exchange were determined by the model's numerical representation of the hydrodynamic processes.

Atmospheric forcing functions for the model were developed from National Climatic Data Center (NCDC) records from Logan Airport and included wind speed and direction, atmospheric pressure, air temperature, relative humidity, rainfall, and cloud cover at approximately hourly intervals. Wind speed and direction are used internally in the model to provide surface wind stress forcing, while wind speed is used in the prediction of water surface latent and sensible heat exchange. Wind speed is also used in determination of surface reaeration rates in the eutrophication component of the model. Wind speeds were internally adjusted in the model using input directional sheltering coefficients determined during the thermal calibration. Cloud cover information was externally used to estimate incoming solar short wave radiation and internally used in the estimation of net long wave radiation.

All model forcing data were assembled for a 5 year period spanning 1998 through 2002. Initial conditions for the hydrodynamic model included a constant water surface elevation corresponding to mean water level in the wide downstream region of the river, water temperature representative of early January 1998, and a zero initial salinity.

3.4 Hydrodynamic Model Calibration and Validation

Physical data for the hydrodynamic model calibration were limited to discrete salinity and temperature profiles measured by USGS during 1998 and 1999. During this period, the USGS periodically measured vertical salinity and temperature profiles at 69 stations in the Basin. Figure 3.3 shows the location of 13 of these stations selected for model calibration comparison based on the spatial coverage and extent of data available at each station. A number of the stations fall within the same horizontal model cell.

Salinity calibration involved the adjustment of the relationship between number of lock openings per day and the daily interval for which the salinity in the lock cell was set to harbor salinity. Figures 3.7 through 3.19 show continuous model predicted surface and bottom layer salinities over the entire simulation period and blowups with discrete near-surface and near-bottom USGS observations over the observational period during 1998 and 1999. The most downstream stations, 5-29 (Figures 3.7 through 3.11), show the annual time scale signal of salinity intrusion in response to lock opening during the late spring to early fall. At these stations the model predicts vertical salinity stratification fairly well. However, noticeable in these comparisons is the fact that the model predicted that bottom salinities drop rapidly in late fall and remain low until the following spring, while the observation data indicate a relatively large retention of high salinity water near the bottom. The reason for this retention is not immediately evident, but could indicate non-quantified continuous leakage through the locks or an over-response to river flow flushing of salinity as river flows increase during the winter and spring. Since water quality conditions during the winter and early spring are not critical, this deficiency in model performance was not judged to be a major flaw. Intermediate stations, 36-52 (Figures 3.12 through 3.16), show higher inter-annual variability in salinity intrusion. The upstream stations,

57-62 (Figures 3-17 through 3-19), show that the model over-predicts salinity intrusion, but when present, vertical stratification is maintained. Figures 3.20 and 3.21 show scatter plots of model-predicted and observed surface and bottom salinity for all times at the 69 USGS observation stations. Although there is excessive scatter in the bottom salinity comparison (Figure 3.20) the general trend for the model to predict observed values is evident. The scatter in surface salinity (Figure 3.21) is less intensive with the model tending to slightly under-predict surface salinity.

Temperature calibration involved the adjustment of surface heat exchange parameters including wind speed reduction by wind sheltering and wind speed dependent latent and sensible heat transfer coefficients, as well as the solar short wave radiation adsorption rate with depth over the water column. Figures 3.22 through 3.34 show continuous model-predicted surface and bottom layer temperatures over the entire simulation period and blowups with discrete near-surface and near-bottom USGS observations over the observational period during 1998 and 1999. Visual comparison of model predictions and observations is quite good at all stations, including stations 24, 29, 36, and 43 (Figures 3-25 through 3-28), which are most significantly influenced by the Kendall Square power plant discharge. Figures 3.35 and 3.36 show scatter plots of model predicted and observed surface and bottom temperature for all times at the 69 USGS observation stations. Correlation between model predicted and observed temperature for both the bottom and surface is very good with correlation coefficients of 0.92 for the bottom and 0.98 for the surface.

Salinity and temperature verification involved the visual comparison of model predicted and observed quantities at 4 EPA monitoring stations (Figure 3.37) during 2002. Figures 3.38 through 3.41 show salinity comparisons for the period between June and September 2002. The model tends to perform reasonably well in predicting increasing bottom salinity in response to lock opening during this period. Model-predicted surface salinities remain low and in agreement with observations. Figures 3.42 through 3.45 show temperature comparisons at the same four stations. The model performs very well in predicting surface temperature, but tends to over-predict bottom temperatures in June and early July. Table 3-1 summarizes relative mean absolution errors (RMAs) between model predictions and observations for surface salinity and temperature in three model zones and at five stations. The high surface salinity RMAs are unduly influenced by the low salinity observational values, typically less than 2 practical salinity units (psu), used to normalize the relative errors.

Table 3-2 summarizes RMAs between model predictions and observations for bottom salinity and temperature at three stations. All temperature errors in these two tables are less than the accepted 25 percent upper bound for transport variables suggested in the EPA's Estuary Wasteload Allocation guidance document (USEPA 1990). The average of the surface and bottom salinity errors, 28 and 30 percent, respectively, is somewhat high relative to the 25 percent guidance, but still deemed acceptable.

Table 3-1. Relative mean absolute errors for surface salinity and temperature, June-October 2002

Location	Salinity Error (%)	Temperature Error (%)
Lower Basin	39	5
Upper Basin	30	4
BU Basin	24	4
Science Mus.	38	7
CRBL02	19	6
CRBL03	29	5
CRBL12	23	3
TMDL21	19	4
Average	31	5

Table 3-2. Relative mean absolute errors for bottom salinity and temperature, June-October 2002

Location	Salinity Error (per cent)	Temperature Error (per cent)
TMDL22	31	18
TMDL25	21	6
CRBL11	38	21
Average	30	15

4 WATER QUALITY MODEL

A transient, 3-D linked hydrodynamic-water quality model has been developed to simulate hydrodynamic, biogeochemical and water quality transport processes in the Lower Charles River Basin. Following its calibration and verification using historical field water quality data, the linked model will be used to investigate the combined water quality impacts of the following inputs to the Basin: (1) dry- and wet-weather tributary flow and pollutant loads, (2) existing and possible future heated water discharges from the Kendall and Blackstone Power Stations, (3) salt-water intrusion from Boston Harbor, and (4) release of algal nutrients from and loss of bottom water dissolved oxygen to benthic sediments. Ultimately, the validated model will be used to assess the impacts of these sources and sinks on levels of eutrophication, under alternative management scenarios. A map of the Basin is shown in Figure 4.1.

4.1 Water Quality Modeling Objectives

Water quality standards for dissolved oxygen are not currently met during summer. Significant algal blooms also occur during summer months, as the result of warm water temperatures and inputs of nitrogen and phosphorous to the Basin. These factors have contributed to non-attainment of its designated uses as a fishable and swimable surface water resource.

In order to address the causes of and possible control of these eutrophication problems, TMDL modeling tools have been developed. Testing (calibration and verification) and application of these tools will increase understanding of eutrophication processes in the Basin and serve to better define the relative water quality impacts of the following factors:

- Flow inputs
- Nutrient inputs
- Harbor water inputs
- Benthic sediment nutrient and oxygen fluxes
- Algal growth dynamics
- Vertical stratification
- Atmospheric forcing and nutrient inputs
- Heat inputs

4.2 Water Quality Model Description

A detailed description of the EFDC water quality model (EFDC-WQM) is contained in Appendix B. A brief summary of the water column and sediment diagenesis model components is given below.

4.2.1 Water Column Sub-Model

The water column sub-model was used to simulate processes occurring from the water surface to the benthic sediment interface. State variables simulated during the current model application are shown in Figure 4.2. Major model compartments include dissolved and particulate organic matter (carbon, nitrogen, and phosphorus), inorganic nitrogen and phosphorus, and

phytoplanktonic algae and dissolved oxygen. Organic carbon, nitrogen, and phosphorus matter is further subdivided into refractory and labile particulate and dissolved forms. Refractory organic particulates break down very slowly to dissolved organic forms, whereas labile organic particulates break down faster. Both refractory and labile particulate organics settle out of the water column and deposit onto the surface layer of benthic sediments. The benthic sediment sub-model, which is discussed in Section 4.2.2, was used to simulate buildup and diagenesis (conversion to inorganic forms) of deposited organics and subsequent release of inorganic forms from benthic sediments, during anoxic bottom water conditions. The sediment sub-model was also used to predict sediment oxygen demand at the water-sediment interface.

Dissolved organic carbon, nitrogen, and phosphorus are converted into inorganic forms by processes such as hydrolysis and bacterial activity. Utilization of dissolved organic carbon during respiration of heterotrophic bacteria consumes dissolved oxygen. Similarly, dissolved organic nitrogen and phosphorus are converted by bacterial activity to ammonium nitrogen (NH4-N) and orthophosphorus (PO4-P), respectively. NH4-N is subsequently oxidized by bacteria to nitrate nitrogen (NO3-N). This process, which is called nitrification, consumes dissolved oxygen. Under conditions of very low dissolved oxygen, NO3-N may be reduced by bacteria to dissolved nitrogen gas, which may subsequently be lost to the atmosphere at the air-water interface. This process, which is called denitrification, consumes dissolved organic carbon.

In the current EFDC-WQM model, algae biomass was subdivided into three forms: blue-green (cyanophycae), green (chlorophycae, chrysophycae, and others) and diatoms (bacillariophycae). Growth, respiration, and mortality of each of these algal groups are controlled in the model by using different optimal water temperature specifications. All three algae forms uptake nitrogen (NH4-N and NO3-N) and phosphorus (dissolved PO4-P) during growth. Similarly, algae release dissolved and particulate organic carbon, nitrogen, and phosphorus due to respiration and mortality. In the current EFDC-WQM model, algae are growth-limited in a multiplicative manner by ambient levels of light, water temperature, and concentrations of inorganic nitrogen (NH4-N and NO3-N) and phosphorus (dissolved PO4-P). Algae take up dissolved oxygen during respiration and release dissolved oxygen during photosynthetic activity. Blue-green algae exhibit a toxic response to salinity levels above 1 part per thousand (ppt). Blue-green algae are not limited by low inorganic nitrogen concentrations, since they can alternatively utilize dissolved nitrogen gas in the water column via nitrogen fixation. Algae also settle out of the water column, contributing their organic carbon, nitrogen, and phosphorus contents to the surface layer of benthic sediments.

The EFDC-WQM water column sub-model of the Basin includes all the above processes and state variables. In addition, loadings of each state variable at each lateral boundary of the Basin were specified on a daily basis, using available field data and results from previous modeling studies by MWRA, USGS, and EPA. Development of these boundary loads are discussed in detail in Section 4.3.

4.2.2 Benthic Sub-Model

The EFDC-WQM water column sub-model was interfaced in real-time with a sediment diagenesis sub-model developed previously by DiToro and Fitzpatrick (1993). The sediment

process model has twenty-seven water quality state variables and their associated mass fluxes, which occur within a 2-layer sediment compartment (Figure 4.3). For this application silica was not simulated. State variables include: three separate classes (G1, G2, and G3) of particulate organic carbon, nitrogen and phosphorus in layer 2 only, and sulfide/methane, ammonium nitrogen, nitrate nitrogen, phosphate phosphorus, and temperature in layers 1 and 2. Fluxes include: three classes (G1, G2, and G3) of particulate organic carbon, nitrogen and phosphorus deposition to layer 2 sediments, ammonium nitrogen, nitrate nitrogen, phosphate phosphorus and sediment oxygen demand releases to bottom waters, and heat transfer through the sediment-water interface and the ground below layer 2.

The nitrate state variable represents the sum of nitrate (NO3) and nitrite (NO2) nitrogen. The three G classes for particulate organic matter (POM) in layer 2, and the two layers used to simulate transformations and fluxes of inorganic substances are described below. In the sediment sub-model, benthic sediments are represented as two layers (Figure 4.4). The upper layer (layer 1) is in contact with the water column and may be oxic or anoxic depending on dissolved oxygen concentration in the overlying water. The lower layer (layer 2) is permanently anoxic. The upper layer depth, which is determined by the penetration of oxygen into the sediments, is at its maximum only about 1 centimeter (cm) thick. Layer 2 is much thicker, on the order of 10 cm to 1 meter.

The sediment sub-model incorporates three basic processes (Figure 4.4): (1) depositional flux of POM, (2) diagenesis, and (3) the resulting sediment flux. The sediment model version used in the current application is driven by net settling of particulate organic carbon, nitrogen and phosphorus from the overlying water to the sediments (depositional flux). Because of the negligible thickness of the upper layer, deposition is considered to be from the water column directly to the lower layer. Within the lower layer, the model simulates the diagenesis (mineralization or decay) of deposited POM, which produces oxygen demand and inorganic nutrients (diagenesis flux). The third basic process is the flux of substances produced by diagenesis (sediment flux). Oxygen demand, as sulfide (in saltwater) or methane (in freshwater), takes three paths out of the sediments: (1) oxidation at the sediment-water interface as sediment oxygen demand, (2) export to the water column as chemical oxygen demand, or (3) burial to deep, inactive sediments. Inorganic nutrients produced by diagenesis takes two paths out of the sediments: (1) release to the water column or (2) burial to deep, inactive sediments.

4.3 Water Quality Model Inflows, Loads, and Forcing Functions

The Lower Charles River Basin receives flows and water quality parameter loads from a total of 91 sources during dry and wet weather. Sources include: the upper Charles River Watershed (entering at the Watertown Dam), 6 streams (Laundry, Hyde, Faneuil and Shepard Brooks, Salt Creek, and the Muddy River), the Stony Brook combined sewer system outfall, 71 separate storm sewer outfalls, 12 CSO outfalls from Cambridge (CAM005, 007, 009, 011, and 017), Boston (BOS049), the MWRA regional interceptor system (MWR201- The Cottage Farm CSO Treatment Facility, 018, 019, 020, 021 and 022), and Boston Harbor (via locks at the New Charles River Dam). Discharge points of these individual sources are shown in Figure 4.5, which was a figure extracted from Breault et al. (2001). In addition to the above inputs, the Basin contributes water to and receives heated cooling water discharges from the Kendall Power

Station. The following sections (4.3.1 through 4.3.6) give details on methodologies and assumptions utilized during this modeling study to define the daily flow and load boundary conditions used by the linked, 3-D hydrodynamic and water quality transport models.

4.3.1 Watertown Dam (Headwater)

In order to be successful in modeling the temporal and spatial variability of hydrodynamics and eutrophication processes within the Basin, flows and water quality loads entering at the Watertown Dam headwater had to be adequately defined. Based on time scale considerations and to keep the size of input data files manageable, it was decided that all input flows and loads, including those at the Watertown Dam, would be defined on a daily basis, for the period between 1998 and 2002.

USGS (Breault et al. 2001) estimated that 90 percent of the total nutrient load and 50 percent of the total flow discharged to the Basin, enter at the Watertown Dam. Fortunately, a large amount of data are available from previous monitoring studies for use in defining flows and loads entering this major input boundary of the Basin.

Major sources of time series flow and water quality data needed to define inputs at the Watertown Dam included: USGS daily flow records at the Waltham gage between 1998 and 2002, USGS daily flow records at the Watertown Dam during water year 2000, MWRA bi-weekly water quality data collected year-round just upstream of the Watertown Dam (1998 through 2002), and EPA bi-weekly water quality data collected only during summer months just upstream of the Watertown Dam (1998 through 2002).

Flows

Flows have been measured on a daily basis at the USGS Waltham gage on the Charles River (01104500) since 1931. The Waltham gage (227 square mile tributary drainage area) is located several miles upstream of the Watertown Dam (268 square mile tributary drainage area) and its daily flows were found to be closely correlated with daily flows measured by USGS at the Watertown Dam, during water year 2000. Figure 4.6 shows daily flows measured at the Waltham gage and the Watertown Dam during water year 2000. Based on a linear regression analysis of the daily flow data in Figure 4.6, daily flows at the Waltham long-term gage were used to predict daily flows at the Watertown Dam for water year 2000.

A comparison of measured and predicted flows at the Watertown Dam is given in Figure 4.7. Predictions closely mimic observations at this important headwater boundary. Daily flows were subsequently predicted for the Watertown Dam for the period between 1998 and 2002 by applying the regression equation determined from the regression in Figure 4.6. Predicted flows for the Watertown Dam and those measured at the Waltham gage are shown in Figure 4.8 for the period between 1998 and 2002. Evident on this plot are both the annual spring periods of high runoff due to rainfall and snowmelt and the lower flow periods during summer and early fall when rainfall/runoff and groundwater discharges to the river are generally lower. Flow boundary conditions input to the EFDC hydrodynamic model at the Watertown Dam headwater were

developed based on the above-predicted daily flow values (cubic meters per day), for the period between January 1, 1998 and December 31, 2002.

Water Quality Constituent Loads

Water quality data have been collected just upstream of the Watertown Dam by MWRA (Station 12) on a year-round bi-weekly basis since 1997. Surface grab samples were analyzed for the following parameters: total nitrogen (organic plus ammonia, nitrite and nitrate), NH4-N, NOx-N, total phosphorus, dissolved PO4-P, total suspended solids (TSS), dissolved oxygen, temperature, salinity, chlorophyll *a*, and phaeopigments. EPA also collected bi-weekly water quality data just downstream of the Watertown Dam between May and October since 1998 (station CRBL02). USGS also collected dry- and wet-weather data in this vicinity on approximately 24 dates during both dry and wet weather in the second half of 1999 and the first half of 2000. The latter two studies tested for water quality parameters similar to those tested by MWRA. However, EPA chlorophyll *a* measurements were not corrected for phaeopigments and EPA PO4-P measurements were conducted on unfiltered samples. MWRA chlorophyll *a* measurements were corrected for phaeopigments and MWRA PO4-P measurements were made on filtered samples. Time series plots comparing water quality data collected near this location during the above EPA and MWRA monitoring studies are shown in Figures 4.9 through 4.22. Differences in reported concentrations occur, especially for chlorophyll *a*, PO4-P, and NOx-N. EPA also tested for total organic carbon (TOC), which has subsequently been found during this modeling study to be well correlated with TSS data collected by MWRA near the Watertown Dam during the period of 1998 through 2002 (Figure 4.18). MWRA TSS concentrations were multiplied by a factor of 1.5 to yield the "MWRA Calculated" TOC concentrations shown in Figure 4.18. This finding is important to the water quality modeling, as organic carbon is an important state variable for which daily input boundary loads must be defined.

The EFDC-WQM model requires that input boundary condition loads be specified for each state variable simulated at frequent time intervals over the simulation period (1998 through 2002). All loads were specified on a daily basis, assuming a linear interpolation between dates when MWRA water quality parameter concentration data were available. Daily water quality parameter loads were determined by multiplying daily stream flow and water quality parameter concentrations followed by conversion to input units of kilograms per day.

Loads of organic carbon were developed based on TOC data and predictions, assuming 20 percent of the TOC is in particulate form and 80 percent is dissolved. It was further assumed that 50 percent of the particulate organic carbon is labile (reactive) and 50 percent is refractory (non-reactive).

Loads of nitrogen state variables were based on the MWRA data for total nitrogen, ammonium nitrogen (NH4-N) and nitrite-plus-nitrate nitrogen (NOx-N). Total organic nitrogen concentrations were determined by subtracting inorganic nitrogen forms (NH4-N and NOx-N) from total nitrogen. It was assumed that 50 percent of the organic nitrogen determined in this manner is particulate and 50 percent is dissolved. It was further assumed that 50 percent of the particulate organic nitrogen is labile and 50 percent is refractory.

Loads of phosphorus state variables were determined based on the MWRA data for total phosphorus and orthophosphate (PO4-P). Total organic phosphorus was determined as the difference between total phosphorus and PO4-P. Total organic phosphorus was assumed to be 50 percent particulate and 50 percent dissolved. In addition, 50 percent of the particulate organic phosphorus was assumed to be labile and 50 percent was assumed to be refractory.

Loads of dissolved oxygen were developed based on the MWRA data in the same manner as described above for carbon, nitrogen, and phosphorus state variables. Loads of algae biomass for blue-green, green, and diatom algal groups were determine based on the MWRA chlorophyll *a* data, assuming a biomass to chlorophyll *a* ratio of 260 (g algal carbon/µg chlorophyll *a*) for blue-green algae, 100 for diatoms, and 60 for the rest of the algae (greens and other groups). Distribution of the resultant total algal biomass into the three algal groups was based on their relative growth rates under ambient water temperature conditions on each day. The growth rate temperature limitation formulation contained in the EFDC-WQM model for the three algal groups was utilized for these calculations. Optimum water temperatures for growth of blue-green, diatom, and green algal groups were set at 31.5, 15.0, and 21.5 degrees centigrade (°C), respectively.

A high correlation has been found (Voorhees 2005) between 30-day average flow passing over the Watertown Dam (headwater) and water color in the Basin. This relation is evident particularly during the spring and early summer when the water exhibits a stained appearance due to flushing of decomposed organic material from the Upper Charles River Watershed. Since penetration of sunlight through the water column is a key factor affecting algal growth, background extinction in the water column was varied as model input, based on the time series of 30-day average headwater flow and field measurements of light extinction made by EPA in the Basin.

Salinity and temperature values (not loads) must be specified for each input boundary. These inputs were determined based on the MWRA data at the Watertown Dam in the same manner as described above for the other state variables.

4.3.2 Tributary and Storm Drain Outfalls

Input flow and water quality load boundary conditions for the 8 tributary streams and 71 separate storm drain outfalls discharging directly to the Basin were determined using field data and models developed previously by USGS (Breault et al. 2001). A map of the locations of the major tributary sub-basins monitored and modeled by USGS is shown in Figure 4.23. This map was extracted from the original USGS report. USGS sub-divided these sub-basins into smaller sub-units for the purpose of SWMM modeling. Locations of the individual inputs from these sub-basins were given previously in Figure 4.5. Tributary stream inputs include: Stony Brook, Laundry Brook, Hyde Brook, Faneuil Brook, Shepard Brook, Salt Creek, and the Muddy River. Stony Brook is conveyed to the Basin via the Stony Brook combined sewer system, with possible additional combined sewer outflows at the old and new Fens Gate Houses on the Muddy River.

Excluding the headwater input at the Watertown Dam, Stony Brook is the largest individual contributor (approximately 90 percent) of peak wet-weather flow, annual flow volume, and annual water quality parameter loads to the Basin (Breault et al. 2001).

Flows

With the exception of Stony Brook, all the USGS developed models utilized the RUNOFF and TRANSPORT sub-models of the EPA's SWMM (Huber et al. 1992) as a basis for computation of flows at each discharge point. The Stony Brook model utilized the RUNOFF and EXTRAN (Extended Transport) sub-models of SWMM to simulate the separate storm sewer portion of Boston's combined sewer system. The SWMM EXTRAN-based Stony Brook model was developed and validated previously by the BWSC.

All 89 of the USGS stormwater RUNOFF and TRANSPORT sub-models were run for the years 1998 through 2002, utilizing historical rainfall data collected every 15 minutes at the MWRA's Ward Street Headwork Facility. The previous USGS SWMM modeling utilized rainfall data at several locations distributed throughout the Basin's watershed. However, rainfall data were not readily available for these locations for the full 5-year historical time period to be simulated during the current modeling study. Accordingly, the MWRA Ward Street rainfall data were chosen for use in characterizing rainfall throughout the Basin's watershed during the current SWMM modeling. Instantaneous SWMM model flow predictions were saved to computer files at a 5-minute time interval for each discharge to the Basin. A new post-processing software utility program was developed to convert these instantaneous model flow predictions to daily total discharge rates at each discharge point to the Basin.

The Stony Brook RUNOFF and EXTRAN sub-model was also run for the years 1998 through 2002 and instantaneous flow predictions were saved to computer file at a 5-minute time interval. The same post-processing software utility was also used to convert Stony Brook flows to daily totals.

Figure 4.24 shows a comparison of daily flows predicted at the Watertown Dam and the total of the storwmater and dry-weather flows predicted using the USGS SWMM models for the period between 1998 and 2002. The Stony Brook sub-basin accounts for approximately 90 percent of the total stormwater inputs to the Basin. A plot of daily rainfall totals measured at the MWRA Ward Street Headwork Facility is shown in Figure 4.25

Water Quality Constituent Loads

USGS conducted 9 wet-weather and 15 dry-weather field monitoring surveys during the second half of 1999 and first half of 2000. Locations monitored included: the Watertown Dam; in the Muddy River, Stony Brook, Laundry Brook, and Faneuil Brook sub-watersheds; and in single-family, multi-family, and commercial sub-watersheds. Locations of these monitoring stations are shown in Figure 4.23. USGS developed wet-weather best-fit linear regression equations for each of these watersheds. These equations relate measured event mean water quality parameter concentrations (EMCs) to rainfall event characteristics such as rainfall duration, total rainfall, maximum rainfall intensity and several measures of antecedent rainfall conditions at the start of

each storm. EMC regressions were developed for numerous monitored water quality parameters, including: specific conductance (a surrogate for salinity), 5-day biochemical oxygen demand (BOD5), TSS, nitrate nitrogen (NOx-N), ammonium nitrogen (NH4-N), total Kjeldahl nitrogen (TKN), and total phosphorus.

USGS analyzed the rainfall time series at several gauging locations distributed over the Basin tributary watershed, using the SYNOP software utility (Woodward-Clyde 1995). SYNOP was used to develop values of the independent regression variables (storm characteristics) for each historical wet-weather event during water year 2000 (October 1999 through September 2000). USGS subsequently used the results of the SYNOP and linear regression analyses to develop wet-weather EMCs for each of the 5 monitored stormwater inputs to the Basin (Watertown Dam, Stony Brook, Muddy River, Landry Brook, and Faneuil Brook) during water year 2000. USGS assumed that wet-weather EMCs for each of the un-monitored sub-basin stormwater discharges were 10 percent higher than those calculated for Laundry Brook.

The current modeling study requires that daily flows and loads be developed using the USGS SWMM models for years other than water year 2000. As a result, the SWMM flow prediction models were run for the period of 1998 through 2002 using the MWRA Ward Street rainfall data. Because of this approach, both the SYNOP and EMC regression analyses also had to be re-done.

The USGS load calculations combined SWMM model flow predictions, regression-based EMCs for wet-weather conditions, and measured mean dry-weather period concentration data were used to calculate daily and annual loads entering the Basin during water year 2000 from each tributary input. For the current modeling study, an enhanced statistical regression methodology was developed and applied to hind-cast wet-weather EMCs and dry-weather discharge concentrations for the 5-year period between 1998 and 2002. SYNOP was first used to analyze the 15-minute rainfall data at the MWRA Ward Street headwork, in order to determine the rainfall characteristics, such as start-time, duration and inter-event antecedent dry period length, for each wet-weather event. A new software utility called ANTICEDE was then developed to calculate a series of wet-weather rainfall-related characteristics for each wet-weather day in the 5-year period. A wet-weather day is any day falling within a SYNOP wet-weather event. Calculated wet-weather day rainfall characteristics included: storm characteristics such as duration, total depth, average intensity, and maximum intensity; and antecedent characteristics such as previous dry period length, previous hours with rainfall less than 0.1, 0.5, and 1.0 inches, and precipitation during the previous 48, 72, 168, and 336 hours. Water year 2000 USGS wet-weather water quality monitoring data for each of the major sub-basins (conductivity, BOD5, TP, NH4-N, NOx-N, TKN, and TSS measured during 9 days) were then used as input to a multi-variable regression analysis using the calculated rainfall characteristics each corresponding wet day. The resultant wet-weather regression equation intercepts and coefficients for the 4 monitored sub-basins (Stony Brook, Muddy River, Laundry Brook, and Faneuil Brook) are given in Tables 4-1 through 4-4, respectively. Wet-weather EMCs of a monitored water quality parameter within a tributary discharge, on a given day, were subsequently predicted as the sum of the regression equation intercept and the product of the regression equation coefficients determined for each of the 13 wet-weather rainfall characteristics in Tables 4-1 through 4-4 and the corresponding characteristic value calculated by the ANTICEDE software utility on that day.

Table 4-1. Regression analysis results used for hindcasting stormwater and tributary water quality under wet-weather conditions in the Stony Brook sub-basin

	Conductivity	BOD5	TSS	NOx	NH4	TKN	TP
intercept	481.95811	107.69278	382.68489	1.87496	-0.89898	6.32199	1.12926
durhrs	0.00000	-1.02078	-6.12071	0.00000	0.00811	-0.09830	-0.01595
totrain "	-40.04148	5.77784	0.00000	-0.04475	0.00000	0.00000	0.00000
aveint "/hr	0	0.00000	0.00000	0.00000	0.00000	0.00000	0.00000
maxint "/hr	0.00000	0.00000	155.94671	0.00000	0.54966	0.00000	0.00000
anti hrs dry	0	0.00000	0.00000	0.00000	0.00000	0.00000	0.00000
anti hrs<.1"	-0.98444	-0.09056	0.00000	0.00000	0.00730	0.00000	0.00000
anti hrs<.5"	0.00000	-0.28222	0.00000	-0.00434	0.00000	0.00000	0.00000
anti hrs<1"	0.00000	0.00000	-0.49291	0.00000	0.00000	-0.00487	-0.00085
antpt 48hr	0.00000	0.00000	0.00000	0.00000	15.98595	0.00000	0.00000
antpt 72hr	0.00000	109.10846	0.00000	5.36132	-8.50492	0.00000	0.00000
antpt 168hr	-261.98435	-49.39862	-251.80650	0.00000	-0.26915	-3.33651	-0.62594
antpt 336hr	0	0.00000	0.00000	0.00000	0.00000	0.00000	0.00000
Wet EMC Mn	100.000	5.700	23.000	0.500	0.100	0.800	0.200
Wet EMC Mx	720.000	28.000	260.000	1.600	0.800	4.600	0.830
Wet EMC Av	280.000	15.000	107.000	1.000	0.400	2.300	0.400
cor coef	0.640	0.960	0.980	0.870	0.960	0.870	0.950
determ coef	0.410	0.920	0.920	0.760	0.930	0.750	0.900

Table 4-2. Regression analysis results used for hindcasting stormwater and tributary water quality under wet-weather conditions in the Muddy River sub-basin

	Conductivity	BOD5	TSS	NOx	NH4	TKN	TP
intercept	355.33504	8.02948	-7.08268	0.78138	-0.19881	2.09667	0.02364
durhrs	0.00000	0.00000	0.00000	0.00000	0.00000	0.00000	0.00000
totrain "	0.00000	-5.20353	0.00000	-0.09730	-0.00720	-0.26163	-0.03896
aveint "/hr	0.00000	0.00000	0.00000	0.00000	0.00000	0.00000	0.00000
maxint "/hr	-410.32977	0.00000	0.00000	0.00000	0.00000	0.00000	0.00000
anti hrs dry	0.00000	0.00000	0.00000	0.00000	0.00000	0.00000	0.00000
anti hrs<.1"	0.00000	0.00000	0.10300	0.00000	0.00387	0.00000	0.00116
anti hrs<.5"	0.00000	0.00000	0.15359	0.00000	0.00000	0.00000	0.00077
anti hrs<1"	0.00000	0.01506	0.00000	0.00000	0.00000	0.00000	-0.00031
antpt 48hr	0.00000	0.00000	-101.28628	1.56583	6.64105	0.00000	0.00000
antpt 72hr	0.00000	0.00000	0.00000	0.00000	-3.69437	0.00000	0.00000
antpt 168hr	0.00000	0.00000	0.00000	0.00000	0.00000	-0.69439	0.00000
antpt 336hr	0.00000	0.00000	0.00000	0.00000	0.00000	0.00000	0.00000
Wet EMC Mn	120.000	4.500	25.000	0.300	0.100	0.900	0.100
Wet EMC Mx	370.000	13.000	65.000	1.100	0.600	2.400	0.400
Wet EMC Av	220.000	7.100	39.000	0.700	0.300	1.500	0.200
cor coef	0.760	0.910	0.970	0.620	0.900	0.840	0.920
determ coef	0.580	0.820	0.940	0.390	0.810	0.700	0.850

Table 4-3. Regression analysis results used for hindcasting stormwater and tributary water quality under wet-weather conditions in the Laundry Brook sub-basin

	Conductivity	BOD5	TSS	NOx	NH4	TKN	TP
intercept	260.94793	11.98115	202.46223	1.47703	1.70577	2.46255	0.61211
durhrs	-1.24884	0.00000	-3.43816	-0.01897	-0.02442	-0.03992	-0.00952
totrain "	-18.08843	-6.02208	0.00000	-0.06332	0.09237	0.00000	0.00000
aveint "/hr	0.00000	0.00000	0.00000	0.00000	0.00000	0.00000	0.00000
maxint "/hr	0.00000	0.00000	0.00000	0.00000	0.00000	0.00000	0.00000
anti hrs dry	0.00000	0.00000	0.00000	0.00000	0.00000	0.00000	0.00000
anti hrs<.1"	0.00000	0.04663	0.00000	0.00000	0.00000	0.00541	0.00098
anti hrs<.5"	0.00000	0.00000	0.00000	0.00000	-0.00380	0.00000	0.00000
anti hrs<1"	0.00000	0.00000	-0.19557	-0.00150	0.00000	0.00000	-0.00076
antpt 48hr	0.00000	0.00000	0.00000	0.00000	0.00000	0.00000	0.00000
antpt 72hr	325.74973	0.00000	-237.84903	0.00000	0.00000	0.00000	0.00000
antpt 168hr	0.00000	-8.12242	-115.73585	0.00000	-0.89732	-2.01123	-0.41319
antpt 336hr	0.00000	0.00000	0.00000	0.00000	0.00000	0.00000	0.00000
Wet EMC Mn	150.000	3.400	16.000	0.300	0.037	0.800	0.100
Wet EMC Mx	310.000	20.000	142.000	1.100	0.800	3.400	0.600
Wet EMC Av	230.000	9.500	44.600	0.700	0.300	1.900	0.200
cor coef	0.930	0.950	0.980	0.930	0.920	0.930	0.960
determ coef	0.860	0.900	0.960	0.870	0.840	0.870	0.920

Table 4-4. Regression analysis results used for hindcasting stormwater and tributary water quality under wet-weather conditions in the Faneuil Brook sub-basin

	Conductivity	BOD5	TSS	NOx	NH4	TKN	TP
intercept	921.89532	18.93639	230.97648	1.17489	1.29401	4.99391	-0.06926
durhrs	0.00000	-0.20750	-4.78261	0.00000	-0.01786	-0.05690	0.00382
totrain "	0.00000	-5.12607	0.00000	-0.45576	0.00000	0.00000	-0.06361
aveint "/hr	0.00000	0.00000	0.00000	0.00000	0.00000	0.00000	0.00000
maxint "/hr	-115.34118	0.00000	0.00000	2.77048	0.00000	0.00000	0.00000
anti hrs dry	0.00000	0.00000	0.00000	0.00000	0.00000	0.00000	0.00000
anti hrs<.1"	-2.12417	0.00000	0.86652	-0.00398	0.00000	0.00000	0.00000
anti hrs<.5"	-2.75418	0.00000	0.00000	0.00000	-0.00212	-0.00698	0.00000
anti hrs<1"	1.44093	0.00000	-0.37698	0.00000	0.00000	0.00000	0.00110
antpt 48hr	0.00000	0.00000	0.00000	0.00000	0.00000	0.00000	0.00000
antpt 72hr	994.09017	0.00000	0.00000	4.39328	0.00000	0.00000	0.00000
antpt 168hr	-326.58514	0.00000	-188.05443	0.00000	-0.74927	-2.37915	0.00000
antpt 336hr	0.00000	0.00000	0.00000	0.00000	0.00000	0.00000	0.00000
Wet EMC Mn	120.000	2.800	29.000	0.300	0.037	0.900	0.100
Wet EMC Mx	530.000	20.000	318.000	2.200	0.800	3.400	0.500
Wet EMC Av	330.000	11.000	96.800	1.100	0.300	1.700	0.200
cor coef	0.990	0.860	0.940	0.940	0.890	0.880	0.900
determ coef	0.990	0.740	0.890	0.890	0.800	0.770	0.810

USGS used the mean values of the stream water quality monitoring data collected within the 5 major sub-basins on 15 dry days in water year 2000 as being representative of average dry weather conditions in the corresponding discharge to the Basin. However, during the current modeling study an examination of the USGS dry-weather concentration data and rainfall data revealed likely significant correlations between dry-weather concentrations and antecedent conditions on those monitoring days. In an effort to better define daily dry-weather loads, a linear regression analysis was also conducted relating dry-weather water quality parameter concentrations measured by USGS during water year 2000 and dry-weather day antecedent rainfall characteristics, including: previous dry period length, previous hours with rainfall less than 0.1, 0.5, and 1.0 inches, and precipitation during the previous 48, 72, 168, and 336 hours. The resultant dry-weather regression equation intercepts and coefficients for the 4 monitored sub-basins (Stony Brook, Muddy River, Laundry Brook, and Faneuil Brook) are given in Tables 4-5 through 4-8, respectively. Dry-weather day concentrations of a monitored water quality parameter within a tributary discharge, on a given day, were subsequently predicted as the sum of the regression equation intercept and the product of the regression equation coefficients determined for each the 7 dry-weather antecedent rainfall characteristics in Tables 4-5 through 4-8 and the corresponding characteristic value calculated by the ANTICEDE software utility on that day.

Table 4-5. Regression analysis results used for hindcasting stormwater and tributary water quality under dry-weather conditions in the Stony Brook sub-basin

	Conductivity	BOD5	TSS	NOx	NH4	TKN	TP
intercept	-378.67838	0.90920	3.23592	0.72079	0.35317	0.66569	-0.8491
durhrs	0.00000	0.00000	0.00000	0.00000	0.00000	0.00000	0.00000
totrain "	0.00000	0.00000	0.00000	0.00000	0.00000	0.00000	0.00000
aveint "/hr	0.00000	0.00000	0.00000	0.00000	0.00000	0.00000	0.00000
maxint "/hr	0.00000	0.00000	0.00000	0.00000	0.00000	0.00000	0.00000
anti hrs dry	0.00000	-0.01528	0.00000	0.00000	0.00000	0.00000	0.00000
anti hrs<.1"	2.69717	0.01556	0.01523	0.00000	0.00058	0.00000	0.00000
anti hrs<.5"	0.00000	0.00000	-0.01362	0.00193	0.00000	0.00160	0.00000
anti hrs<1"	0.00000	0.00000	0.00000	0.00000	0.00000	0.00000	0.00186
antpt 48hr	20579.60982	-139.00855	0.00000	26.00863	-4.01393	-21.34805	0.00000
antpt 72hr	762.40697	0.00000	0.00000	0.00000	0.00000	0.00000	0.00000
antpt 168hr	0.00000	0.00000	-0.55327	0.00000	0.11534	0.20637	0.76019
antpt 336hr	166.64446	0.00000	0.00000	0.17682	-0.05584	-0.02776	0.00000
Dry EMC Mn	100.000	1.000	1.250	1.200	0.200	0.800	0.050
Dry EMC Mx	720.000	3.100	4.000	2.000	0.500	1.300	1.300
Dry EMC Av	460.000	1.200	2.410	1.600	0.400	1.000	0.200
cor coef	0.970	0.990	0.880	0.750	0.830	0.880	0.890
determ coef	0.950	0.990	0.770	0.560	0.680	0.770	0.800

Table 4-6. Regression analysis results used for hindcasting stormwater and tributary water quality under dry-weather conditions in the Muddy River sub-basin

	Conductivity	BOD5	TSS	NOx	NH4	TKN	TP
intercept	204.07710	2.25268	9.11677	0.00000	0.68018	0.00000	0.08465
durhrs	0.00000	0.00000	0.00000	0.00000	0.00000	0.00000	0.00000
totrain "	0.00000	0.00000	0.00000	0.00000	0.00000	0.00000	0.00000
aveint "/hr	0.00000	0.00000	0.00000	0.00000	0.00000	0.00000	0.00000
maxint "/hr	0.00000	0.00000	0.00000	0.00000	0.00000	0.00000	0.00000
anti hrs dry	-3.10265	0.00000	-0.02931	0.00000	-0.00179	0.00000	-0.00046
anti hrs<.1"	5.42139	0.01178	0.00000	0.00000	0.00066	0.00000	0.00044
anti hrs<.5"	-2.03232	0.00000	0.00000	0.00000	0.00000	0.00000	0.00000
anti hrs<1"	0.00000	-0.00605	0.00000	0.00000	0.00000	0.00000	0.00000
antpt 48hr	0.00000	0.00000	0.00000	0.00000	0.00000	0.00000	0.00000
antpt 72hr	0.00000	0.00000	0.00000	0.00000	0.84939	0.00000	0.00000
antpt 168hr	0.00000	0.00000	0.00000	0.00000	-0.36400	0.00000	0.00000
antpt 336hr	72.81491	0.00000	0.00000	0.00000	0.00000	0.00000	0.00000
Dry EMC Mn	59.000	1.000	3.000	0.300	0.300	1.000	0.050
Dry EMC Mx	860.000	4.600	11.000	1.600	0.800	9.000	0.200
Dry EMC Av	400.000	2.400	6.620	0.900	0.500	1.800	0.100
cor coef	0.930	0.480	0.590	0.650	0.920	0.580	0.640
determ coef	0.860	0.230	0.350	0.420	0.840	0.330	0.410

Table 4-7. Regression analysis results used for hindcasting stormwater and tributary water quality under dry-weather conditions in the Laundry Brook sub-basin

	Conductivity	BOD5	TSS	NOx	NH4	TKN	TP
intercept	0.00000	0.19726	4.74462	0.00000	0.00000	1.67448	0.09916
durhrs	0.00000	0.00000	0.00000	0.00000	0.00000	0.00000	0.00000
totrain "	0.00000	0.00000	0.00000	0.00000	0.00000	0.00000	0.00000
aveint "/hr	0.00000	0.00000	0.00000	0.00000	0.00000	0.00000	0.00000
maxint "/hr	0.00000	0.00000	0.00000	0.00000	0.00000	0.00000	0.00000
anti hrs dry	0.00000	0.00000	0.00000	0.00000	0.00000	0.00000	0.00000
anti hrs<.1"	0.00000	0.00000	0.00744	0.00000	0.00000	0.00000	0.00000
anti hrs<.5"	0.00000	0.01009	-0.01512	0.00000	0.00000	-0.00160	0.00000
anti hrs<1"	0.00000	-0.00693	0.00000	0.00000	0.00000	-0.00101	0.00000
antpt 48hr	0.00000	0.00000	0.00000	0.00000	0.00000	0.00000	0.00000
antpt 72hr	0.00000	4.52347	0.00000	0.00000	0.00000	1.08552	0.00000
antpt 168hr	0.00000	0.00000	0.00000	0.00000	0.00000	-0.39197	-0.03388
antpt 336hr	0.00000	0.00000	0.00000	0.00000	0.00000	-0.08182	0.00478
Dry EMC Mn	71.000	1.000	1.250	0.700	0.033	0.600	0.025
Dry EMC Mx	610.000	3.100	4.000	1.800	0.300	1.100	0.100
Dry EMC Av	330.000	1.800	2.720	1.500	0.100	0.700	0.100
cor coef	0.940	0.870	0.900	0.940	0.780	0.980	0.560
determ coef	0.880	0.760	0.800	0.890	0.610	0.960	0.310

Table 4-8. Regression analysis results used for hindcasting stormwater and tributary water quality under dry-weather conditions in the Faneuil Brook sub-basin

	Conductivity	BOD5	TSS	NOx	NH4	TKN	TP
intercept	696.28695	-9.06719	-65.29501	1.37116	-0.97819	-0.31785	0.01268
durhrs	0.00000	0.00000	0.00000	0.00000	0.00000	0.00000	0.00000
totrain "	0.00000	0.00000	0.00000	0.00000	0.00000	0.00000	0.00000
aveint "/hr	0.00000	0.00000	0.00000	0.00000	0.00000	0.00000	0.00000
maxint "/hr	0.00000	0.00000	0.00000	0.00000	0.00000	0.00000	0.00000
anti hrs dry	-2.41088	0.00000	0.00000	0.00000	0.00276	0.00000	0.00000
anti hrs<.1"	4.24994	0.00000	0.00000	0.00553	0.00000	0.00000	0.00000
anti hrs<.5"	0.00000	0.04675	0.26021	0.00000	0.00443	0.01668	0.00267
anti hrs<1"	-1.66303	0.00000	0.00000	0.00000	0.00000	-0.00624	-0.00132
antpt 48hr	0.00000	0.00000	880.55481	0.00000	0.00000	-41.15868	-5.51495
antpt 72hr	917.85468	0.00000	0.00000	0.00000	0.00000	0.00000	0.00000
antpt 168hr	0.00000	5.62226	0.00000	0.62340	0.62334	0.60932	0.00000
antpt 336hr	0.00000	0.00000	12.08990	0.00000	0.00000	0.00000	0.00000
Dry EMC Mn	160.000	1.000	1.250	1.800	0.200	0.800	0.050
Dry EMC Mx	1100.000	22.000	117.000	3.500	2.200	6.400	0.900
Dry EMC Av	670.000	4.800	22.300	2.600	0.600	1.700	0.200
cor coef	0.880	0.620	0.720	0.740	0.720	0.700	0.720
determ coef	0.780	0.380	0.510	0.550	0.520	0.490	0.520

The resultant wet- and dry-weather regression equations and results of the SYNOP analysis of the MWRA Ward Street 15-minute interval rainfall data were subsequently used jointly to generate wet-weather EMCs and dry-weather concentrations on a daily basis and these were tested both visually and statistically against the USGS water year 2000 wet- and dry-weather concentration monitoring data. Statistical measures of correlation, in terms of correlation coefficients and coefficients of determination for each water quality parameter for wet- and dry-weather, are given at the bottom of Tables 4-1 through 4-8. Comparison of regression equation predicted daily water quality parameter concentrations (Conductivity, BOD5, total phosphorus, NH4-N, NOx-N, TKN, and TSS) and corresponding USGS monitored wet- and dry-weather concentrations during water year 2000 are given in Figures 4.26 through 4.32 (Stony Brook), Figures 4.33 through 4.39 (Muddy River), Figures 4.40 through 4.46 (Laundry Brook), and Figures 4.47 through 4.53 (Faneuil Brook).

As is evident from an examination of the plots, several constraints were also imposed on the regression equation calculation results. First, several regression equations for a sub-basin may have exhibited low correlation coefficients (< 0.50) for both or either wet- or dry-weather conditions. In these cases, the regression equations were not used to calculate concentrations. Instead, the mean wet- and/or dry-weather monitoring data were used. Second, predicted wet- and dry-weather concentrations were constrained by the corresponding minimum and/or maximum wet- and dry-weather monitored concentrations for each water quality parameter and sub-basin. For example, if the wet-weather regression equation for Stony Brook yielded a total phosphorus concentration greater than the maximum observed wet-weather total phosphorus value measured by USGS at the Stony Brook monitoring station during water year 2000, then the result was set to the maximum observation.

Figures 4.26 through 4.53 demonstrate that the enhanced statistical methodology used in the current study appears to predict wet- and dry-weather water quality parameter concentrations similar to sub-basin specific monitoring data collected by USGS in water year 2000. Following its calibration, the above-described statistical methodology was subsequently incorporated into a new software utility used to generate input flow and loading boundary conditions for the hydrodynamic and water quality models of the Basin.

A software utility named MAKWQBC was developed in order to allow rapid generation of all required flow and water quality constituent load boundary conditions needed in the EFDC and EFDC-WQM modeling of the Basin. This new software utility uses daily flows predicted using the SWMM models, the above wet- and dry-weather regression results and the SYNOP results to calculate daily flows, water quality parameter concentrations and corresponding loads for each boundary condition input to the Basin model.

USGS did not conduct water quality monitoring at the remaining 72 separate storm sewer outfalls. Therefore, wet- and dry-weather concentrations at the outfalls could not be determined in the manner used above for several of the major streams. Based on personal communications with Rob Breault of USGS (principal investigator in the USGS study), it was determined that wet- and dry-weather concentrations predicted for Laundry Brook would be most appropriate for specifying concentrations at all of the unmonitored separate storm sewer outfalls. This procedure was previously utilized by the USGS for estimating water quality constituent loads to the Basin.

The USGS study did not develop regression equations for water temperature, dissolved oxygen, and chlorophyll *a* in the streams and separate storm sewer outfall discharges. In the current modeling study it was assumed that water temperature and dissolved oxygen were the same as those measured on a bi-weekly basis by MWRA at the Watertown Dam. Chlorophyll *a* was assumed to be zero for the separate storm sewer outfalls and for stream discharges it was assumed to be 50 percent of that measured by MWRA at the Watertown Dam on a given day. Chlorophyll *a* was used to determine algal biomass concentrations and corresponding daily biomass loads for the three algal groups (blue-green, green, and diatoms) based on the same method applied to the Watertown Dam chlorophyll *a* data.

Predicted conductivity, BOD5, TSS, NOx-N, NH4-N, TKN, and total phosphorus concentrations for each stream and separate storm sewer discharge were subsequently used to allocate loads between the appropriate model state variables. Predicted daily conductivities were converted to salinity (ppt) using a constant ratio. Predicted BOD5 concentrations were converted first to ultimate CBOD assuming a first-order decay rate of 0.1 per day (base e). Ultimate CBOD concentrations were subsequently used to determine total organic carbon, assuming a ratio of carbon/oxygen consumed of 2.5. Total organic carbon concentrations determined in this manner were petitioned 20 percent into particulate organic carbon and 80 percent into dissolved organic carbon. It was further assumed that 50 percent of the particulate organic carbon is labile and 50 percent is refractory.

Predicted NOx-N and NH4-N concentrations were utilized directly as state variable inputs. Total organic nitrogen concentrations were determined as the difference between TKN and NH4-N and

total organic nitrogen was split equally between particulate and dissolved fractions. In addition, particulate organic nitrogen was split equally between labile and refractory forms.

Predicted total phosphorus was assumed to be 50 percent inorganic phosphorus and 50 percent organic phosphorus. The organic phosphorus was split equally between particulate and dissolved forms and the particulate organic phosphorus was split evenly between labile and refractory forms.

Daily loads of each water quality state variable were calculated using the above determined concentrations and corresponding daily flows predicted using the USGS SWMM models.

4.3.3 Combined Sewer Overflow Inputs

Daily flows were calculated for each of the 12 CSO inputs using the MWRA Regional CSO Model (Metcalf & Eddy 2000, 2001, and 2002). The CSO model has been updated on an annual basis to reflect changing conditions due to ongoing sewer system modifications and enhancements since 1998. For the current modeling study the 2002 version of the CSO model was assumed to be appropriate for simulating the years 1998 through 2002. This simplifying assumption may result in some over-prediction of CSO activation frequency and discharge volumes during the early portions of the 5-year period simulated with the MWRA CSO model. Locations of the CSO discharges to the Basin are shown in Figure 4.5.

Flows

The MWRA CSO model is based on the SWMM RUNOFF and EXTRAN sub-models, and uses a time step of 10 seconds. Rainfall, snowfall, and air temperature data measured every 15-minutes at 4 MWRA facilities distributed throughout the region were used as input to the model simulations of the years 1998 through 2002. These meteorological monitoring stations were located at the Ward Street, Chelsea Creek and Columbus Park Headwork, and the Reading Pump Station.

Model-predicted instantaneous flows at each CSO were saved to computer file at 15-minute time intervals. Results were integrated to daily total flows for input to the load generation program and the Basin hydrodynamic model. Daily totals for the sum of all the predicted CSO discharges to the Basin are shown in Figure 4.54 for the period between 1998 and 2002.

Water Quality Constituent Loads

MWRA has determined CSO EMCs for BOD5, TSS, NOx-N, NH4-N, TKN, and total phosphorus based on extensive CSO monitoring in recent years (Metcalf & Eddy 1994). Arithmetic mean concentrations and the number of samples tested for each water quality parameter are given in Table 4-9. All CSOs were assumed to have these water quality parameter concentrations during all overflow events.

Table 4-9. EMCs used for CSO inputs to the Basin

Parameter	Arithmetic Mean (mg/l)	Number of Samples
TSS	140.0	869
BOD5	78.0	807
NOx-N	3.4	170
NH4-N	3.1	205
TKN	5.9	182
TP	3.1	181

The MWRA did not develop EMCs for water temperature or dissolved oxygen in CSOs. In the current modeling study it was assumed that CSO water temperature was the same as those measured by MWRA at the Watertown Dam. Dissolved oxygen concentrations in all CSO discharges were assumed to be zero. Chlorophyll *a* and salinity were also assumed to be zero.

MWRA CSO EMCs for BOD5, NOx-N, NH4-N, TKN, and total phosphorus were subsequently used to allocate loads between the appropriate model state variables. Predicted BOD5 concentrations were converted first to ultimate CBOD, assuming a first-order decay rate of 0.23 per day (base e). Ultimate CBOD concentrations were subsequently used to determine total organic carbon, assuming a ratio of carbon/oxygen consumed of 2.5. Total organic carbon concentrations determined in this manner were partitioned 50 percent into particulate organic carbon and 50 percent into dissolved organic carbon. It was further assumed that 50 percent of the particulate organic carbon is labile and 50 percent is refractory.

MWRA CSO EMCs for NOx-N and NH4-N were utilized directly as state variable input concentrations. Total organic nitrogen concentrations were determined as the difference between TKN and NH4-N and total organic nitrogen was split 50 percent and 90 percent between particulate and dissolved fractions, respectively. In addition, particulate organic nitrogen was split equally between labile and refractory forms.

The MWRA CSO EMC for total phosphorus was assumed to be 50 percent inorganic phosphorus and 50 percent organic phosphorus. The organic phosphorus was split equally between particulate and dissolved forms and the particulate organic phosphorus was split evenly between labile and refractory forms.

Daily CSO loads for each discharge were determined by multiplying the CSO model predicted daily flows by the model state variable CSO concentrations given above, followed by units conversion to kilograms per day.

4.3.4 Boston Harbor Water Intrusion at the New Charles River Dam

A significant phenomenon impacting water quality within the Basin is the upstream intrusion of harbor water at depth because of boat lockage through the New Charles River Dam. This highly saline (10 to 31 ppt) cold water (4 to 20 degrees centigrade) wedge, which is denser than the fresh water passing downstream through the Basin, sinks to the deeper portions of the river in the summer months. This stable vertical density stratification restricts the vertical movement of surface oxygen resources, resulting in low or even zero dissolved oxygen concentrations in the bottom waters. The resultant low bottom-water dissolved oxygen likely promotes the release of

nitrogen and phosphorus algal nutrients from benthic sediments. These nutrients are presently trapped below the pycnocline (top of the salt water layer) and do not reach surface waters readily. In the current modeling, impacts of this vertical stratification on hydrodynamics, sediment diagenesis, and subsequent release of phosphorus and nitrogen nutrients from bottom sediments during anoxic bottom-water conditions are simulated explicitly.

Flows

The approach used to determine daily flows of harbor water into the Basin was to extract the number of boat lockage cycles on each day of the years 1998 through 2002 from log books maintained by the Metropolitan District Commission (MDC) at the dam. Geometric data on the width, length, and upstream and downstream invert elevations of the 3 locks located along the southern end of the dam were then used to estimate daily volumes of harbor water passing upstream into the Basin. A major assumption of this analysis is that over the daily time scale of the flow calculations the harbor water surface elevation is equivalent to the long-term mean sea level (MSL). There are 2 smaller locks (25 feet wide by 200 feet long by 5.5 feet deep at MSL) used during most times for the passage of recreational boats. However, during extreme high demand periods, such as during the 4th of July week in summer, a much larger lock (40 feet wide by 300 feet long by 14.5 feet deep at MSL) is also used. The large lock is also used for very large boats and barges at any time of the year. Harbor water can only intrude upstream when boats pass in the upstream direction from harbor to river. Although the MDC records do include direction of travel, this information was not extracted because of time and budget constraints. Thus, it was also assumed that harbor water intrusion occurred once during each lockage cycle, regardless of direction of boat travel. Over a time scale of days, this assumption is likely valid, since most boats return to their point of origin within this time period. It was also assumed that during peak usage periods, when more than 120 lockage cycles occur during a given day, that the 2 smaller and one large locks are used for 2/3 and 1/3 of the daily lockage, respectively. Harbor water intrusion flow rates and salt flux rates determined by the above method were found to be very similar to those estimated previously by USGS (Breault et al. 2001) and the Massachusetts Institute of Technology (MIT).

Figure 4.55 shows the number of lock activations (cycles times 2) occurring during each day during the period between 1998 and 2002. The annual cycle of increased lockage during summer months, particularly during the 4th of July week and other weekends, is evident. Based on these data and the geometric considerations described above, daily harbor water intrusion rates were calculated. Results for each day are shown in Figure 4.56 along with the corresponding total discharge reaching the New Charles River Dam from upstream. During portions of each summer the harbor water intrusion flow rate is of similar magnitude to the total river discharge rate. This phenomenon is a key contributor to the extensive salt wedge found in downstream portions of the Basin during much of each year.

Water Quality Constituent Loads

Concentrations of water quality constituent state variables used in the model must also be specified for the harbor water intrusion flow discussed above. Surface water quality data collected near the New England Aquarium by MWRA where used to fulfill this need. The

MWRA data were collected on a bi-weekly basis during the years 1997 through 2002. MWRA data were also available at the U.S. Coast Guard station, located in Boston's North End. The Coast Guard station is closer to the New Charles River Dam than the New England Aquarium. However, data at the Coast Guard station is only available on an intermittent basis during the above years. Surface water quality data at these two stations were compared and found to be very similar, with somewhat more influence from the Charles River freshwater discharge seen at the Coast Guard station during wet-weather events. Surface water quality data were chosen to characterize the harbor intrusion flow since these waters best represent the water drawn into the locks from the harbor during boat lockage.

MWRA analyzed surface samples collected at the New England Aquarium for the following water quality parameters: chlorophyll *a*, phaeopigments, total nitrogen, dissolved organic nitrogen, particulate organic nitrogen, total dissolved nitrogen, dissolved inorganic nitrogen, ammonium nitrogen, nitrite plus nitrate nitrogen, dissolved organic phosphorus, orthophosphorus, total phosphorus, particulate phosphorus, total dissolved phosphorus, particulate organic carbon, total suspended solids, temperature, salinity and dissolved oxygen. This extensive list of parameters was used, in conjunction with lockage intrusion flow predictions, in order to define model state variable concentrations and loads at the New Charles River Dam locks. Figures 4.57 through 4.67 show the surface concentrations of the above measured water quality constituents near the New England Aquarium during the years 1998 through 2002.

4.3.5 Kendall Power Station Cooling Water Intake and Discharge

The Kendall Power Station withdraws cooling water from the Basin via a pipe located at its northern shoreline, a short distance upstream of the Longfellow Bridge. This water passes through the plant as non-contact cooling water and is subsequently heated and discharged back into the Basin via a canal located at its northern shoreline just downstream of the Longfellow Bridge.

Flows

Short-term (hourly) cooling water discharge flow rates and water temperature data were obtained from the Kendall Power Station owners (Mirant) for the summer months (June through September/October) in the years 1999, and 2000 through 2002. No data were available for 2001 and only total daily flow rates and temperatures were available for all of 1998 and the non-summer months of 1999 and 2000. No daily flow and temperature data were available for non-summer months of 2002. Accordingly, daily flow rates and temperatures for non-summer months in 1998 were also used as model input for non-summer months in 2002. This was necessary since the period from June through October of 2002 was selected for water quality model calibration.

Water Quality Constituent Loads

Cooling water withdrawn from the Basin by the Kendall Power Station is assumed to have the same water quality properties upon discharge, with the exception of temperature. Cooling water

discharge temperature was specified using the data described above for the Kendall Power Station.

4.3.6 Atmospheric Boundary Conditions

Hourly meteorological data collected by the NCDC at Logan Airport were used to specify wind, water volume, heat, and water quality parameter mass fluxes passing across the air water interface of the hydrodynamic and water quality models. Model input meteorological data included: solar radiation, precipitation, air temperature and relative humidity, wind speed and direction, and cloud cover. These data were specified at hourly intervals in an input file to the EFDC hydrodynamic and water quality models.

4.4 Model Implementation

Source code for the linked EFDC hydrodynamic and EFDC-WQM models were implemented on personal computers using INTEL Fortran 90 and Absoft Fortran 95 (Macintosh computers). Five-year simulations using the 57-cell grid, 8 vertical layer linked models required approximately 24 hours for completion on a 2.3 gigahertz Pentium 4-based IBM compatible computer.

4.4.1 Pre- and Post-Processing Software Development

Testing (calibration and verification) of the linked hydrodynamic and water quality models required that a large number of simulations be made within a short time frame in order to test the response of the linked models to alternative model parameter data sets and reasonable flow and water quality boundary condition assumptions. Therefore, several software utilities had to be developed specifically for this modeling project.

Model Input Builder

A utility program was developed to automate the generation and manipulation of model input flow and water quality load boundary condition time series at each of the 92 input boundary locations. Input files to be used by this utility include: daily input flow and water quality parameter concentrations measured at the Watertown Dam, calculated daily harbor water intrusion flow and total outflows at the New Charles River Dam, daily water quality parameter concentrations at the New England Aquarium (applied to intrusion flows), SYNOP rainfall event statistics for the Ward Street Rainfall Gage, dry- and wet-weather EMC regression coefficients for various stormwater inputs, and finally SWMM predicted daily flows for stormwater and CSO inputs at each of the 92 boundary locations. MAKWQBC was used to generate the following input files to the linked hydrodynamic and water quality models: qser.inp and wqpsl.inp. These files contain daily total flow rates and loads for the 92 boundary condition input points to the Basin model.

Post-processing Utility

Outputs from the hydrodynamic and water quality models are in the form of time series predictions of water temperature and salinity (hydrodynamic sub-model) and water quality state variable concentrations (water quality sub-model), at specified locations within the model spatial domain. These time series files are in a fixed (static) format, which can be readily post-processed to yield time series plots for comparison to field data.

The approach chosen was to develop and apply a post-processing software utility to combine hydrodynamic and water quality model-predicted time series with field data available at 18 specified locations within the model spatial domain. Output from this utility does not change in format from model run to model run. As a result, these post-processed files may be pasted into spreadsheets containing pre-developed plots, which are then automatically updated to reflect current model predictions.

4.5 Water Quality Model Calibration and Verification

Model testing is often carried out in two steps, calibration and verification or validation. First, calibration is done for one historical time period when adequate field data are available. During calibration, model process controlling parameters are adjusted within reasonable bounds until model predictions mimic field data within acceptable limits. The calibrated model is then used to simulate an independent historical time period for which field data under different environmental conditions are available for comparison. This is known as verification or validation. For the verification run most model process controlling parameters, except those for which field measurements are available, are held at values used during model calibration. Results of the verification run are then compared with field data for the same time period and a decision is made if predictions and observations are close enough to consider the model valid for predictive purposes. If verification results are not adequately close, then model process controlling parameters are adjusted accordingly and the calibration and verification process is repeated iteratively until results are adequate to consider the model valid for predictive purposes.

For the current study, calibration was carried out for the 5-month time period between June 1 and October 31, 2002. Verification was carried out for the approximately 4.5-year time period between January 1, 1998 and May 31, 2002. Model time series results at a total of 18 locations were saved at 12-hour intervals, over each 4.5-year long simulation for comparison with field monitoring data collected by MWRA (Museum of Science only) and EPA (18 locations). EPA monitoring station locations are shown in Figure 4.68.

4.5.1 MWRA Science Museum Monitoring Data

The MWRA Museum of Science station is located in the vicinity of EPA station TMDL28 and CRBL11. Monitoring data at the MWRA Science Museum station were collected near the water surface on a bi-weekly basis, year-round since 1997. Plots of these data are shown in Figures 4.69 through 4.80. Due to the large amount of data points available for this important location (approximately 255 for each constituent), the data are presented prior to comparison with model results in order to allow the reader an opportunity to observe the unique behavior of water quality

in this portion of the Basin from season to season and year to year. Water quality data collected by EPA at CRBL11 are also presented for comparison with the MWRA data. It is important to note that EPA chlorophyll data were not corrected for phaeopigments. However, EPA total chlorophyll values have been corrected to chlorophyll *a* in these plots, using ratios of total chlorophyll to chlorophyll *a* measured by MWRA during the closest previous day.

Figure 4.69 shows measured levels of dissolved oxygen in surface waters at the MWRA Science Museum monitoring station for the period between January 1, 1998 and October 27, 2002. EPA data collected at nearby station CRBL11 during summer months are also shown for comparison. Dissolved oxygen levels vary sinusoidally over each year with higher concentrations during winter months when water temperatures are low, and with lower levels during summer months when water temperatures are higher. Major processes controlling surface water dissolved oxygen levels at this site and throughout the Basin include atmospheric re-aeration, sediment oxygen demand and intermittent vertical mixing of the resulting low dissolved oxygen bottom waters, oxidation of reduced nitrogenous compounds such as ammonium and nitrite-nitrogen, and algal photosynthesis and respiration. Atmospheric re-aeration is also reduced during the summer months because of lower river flows and quiescent circulation conditions in the Basin.

Figure 4.70 shows measured levels of the algal photosynthetic pigment chlorophyll *a* in surface waters at the MWRA Science Museum monitoring station. EPA data collected at nearby station CRBL11 during summer months are also shown for comparison. Chlorophyll *a* levels vary in a general sinusoidal manner over each year, with higher concentrations during summer months when water temperatures are high and algal blooms occur, and with lower levels during winter months when water temperatures are lower and algal activity is restricted to cold water species such as diatoms. During most years two distinct chlorophyll *a* peaks occur during the warm months. Modeling results suggest that the early summer chlorophyll *a* peaks are primarily due to diatoms. Chlorophyll *a* peaks seen during latter periods of each summer and extending into fall are likely due to the increased activity of other algal assemblages, such as cyanophytes (blue-greens) and chrysophytes (greens and others).

Figures 4.71, 4.74, and 4.75 show measured levels of inorganic algal nutrients (PO4-P, NH4-N, and the sum of NO2-N and NO3-N, respectively) in surface waters at the MWRA Science Museum monitoring station. Algal nutrient levels vary in a general sinusoidal manner over each year with higher concentrations during winter months when water temperatures are low and algal activity is reduced. In contrast, the much lower levels of algal nutrients seen during summer months are likely due to the higher water temperatures and sunlight, which are optimal for supporting significant algal blooms and increased algal nutrient uptake.

Figures 4.72 and 4.76 show measured levels of organic phosphorus and nitrogen, respectively, in surface waters at the MWRA Science Museum monitoring station. In general, organic nitrogen and phosphorus tend to increase somewhat during summer months, as the result of increased algal uptake of inorganic nutrients and their subsequent excretion of dissolved organic forms.

Figures 4.73 and 4.77 show measured levels of total phosphorus and total nitrogen, respectively, in surface waters at the MWRA Science Museum monitoring station. These data capture the

complex effects of input nitrogen and phosphorus loads, algal activity, and other water column and bottom sediment processes, such as settling, vertical mixing, and stratification.

Figure 4.78 shows measured levels of total suspended sediment in surface waters at the MWRA Science Museum monitoring station. Sorption of inorganic phosphorus onto suspended sediments and subsequent deposition if these sediments onto the river bottom are important mechanisms for removal of inorganic phosphorus from surface waters. These suspended sediment data were used during the modeling to estimate a long-term suspended sediment concentration of 4 mg/l throughout the Basin. The model was then used to account for sorption of inorganic phosphorus to these solids and their subsequent deposition to the river bottom sediments for diagenesis.

Figures 4.79 and 4.80 shows measured salinity and water temperature, respectively, in surface waters at the MWRA Science Museum monitoring station. Surface salinity is seen to increase periodically during summer periods when salt water intrusion through the locks at the New Charles River Dam result in a high salinity bottom layer in the Basin. However, the fact that surface salinity during summer months is generally below 1.5 ppt, whereas bottom salinity may exceed 25 ppt during these periods, suggests that vertical mixing of the salt wedge is minimal during the summer. This lack of vertical mixing has an impact on existing water quality in the Basin. Water temperature exhibits periodic seasonal variations during every year, with lowest temperatures during January and highest temperatures during August and September. Surface water temperatures at the Science Museum monitoring location approached 30 °C (88 degrees Fahrenheit) during the summer of 2002.

4.5.2 EPA Monitoring Data

Water quality sampling by EPA consists of near-surface (1 meter depth) grabs at 15 locations (1998 through 2002) and vertical sampling at multiple depths for 3 stations (2002 only) in the downstream, lake-like, portion of the Basin (between the BU Bridge and the Science Museum). EPA sampling was conducted on a bi-weekly basis each year, during the period between June and October. The EPA data are presented along with the modeling results in subsequent report sections. All total chlorophyll data have been corrected to chlorophyll *a* using the procedure outline above for the MWRA Science Museum station.

Sampling results at several key locations from this set are presented in the following section, along with modeling results. A plot of daily precipitation measured at the MWRA Ward Street Headwork Facility during this period is given in Figure 4.81. Model predictions and observations are often seen to respond rapidly during days with rainfall, due to its impact on stormwater and CSO input flows and related water quality parameter loads to the Basin.

4.5.3 Water Quality Model Calibration

During early phases of the Lower Charles River Basin TMDL modeling project the EFDC and EFDC-WQM models and simulation options were modified numerous times, in an effort to reduce predicted effective vertical mixing rates to those observed in the Basin. The current model utilizes suspended sediment sorption of a fraction of the water column dissolved PO4-P as

a defensible method to reduce net vertical transport of phosphorus from bottom waters to surface waters. Observed bottom-water phosphorus and nitrogen buildup occurs during summer months, due to anoxic bottom-water conditions and subsequent sediment diagenesis process releases.

Near-surface (top 12 percent of the water column) modeling results and field data for the period between June 1 and October 30, 2002 are presented as a measure of model calibration. Model runs included the impacts of organic phosphorus, carbon and nitrogen deposition and subsequent sediment diagenesis, including SOD exertion on bottom waters, and the release of phosphorus and nitrogen nutrients during anoxic conditions.

Due to the large number of monitoring locations, predictions, and observations in the Basin, results and data for several key reaches were spatially averaged. These include: (1) between the Longfellow Bride and the Science Museum (Lower Basin), (2) between the Harvard (Massachusetts Avenue) Bridge and the Longfellow Bridge (Upper Basin), and (3) in the vicinity of the BU Bridge (BU Basin). However, predictions and observations at the following locations were plotted without spatial averaging: CRBL12, Science Museum, TMDL21, CRBL02, and CRBL03.

Near-Surface Results

Calibration plots for June 1 through October 30, 2002 are presented for CRBL12 (Figures 4.83 through 4.94), Science Museum (Figures 4.95 through 4.106), Lower Basin (Figures 4.107 through 4.118), TMDL21 (Figures 4.119 through 4.130), Upper Basin (Figures 4.131 through 4.142), BU Basin (Figures 4.143 through 4.154), CRBL03 (Figures 4.155 through 4.166) and CRBL02 (Figures 4.167 through 4.178). As seen in the plots, the water quality model predicts most of the water quality constituents reasonably well during the 2002 monitoring period. The calibration simulation was made for the full 5-year period between 1998 and 2002. The plots only depict model results for the summer period in 2002 when extensive field data are available for comparison.

In addition to the visual comparisons of model predictions and field observations, statistical measures of wellness-of-fit were also developed. The RMA statistic was calculated for each predicted water quality constituent for each day on which corresponding field observations were available at the 5 individual stations and over multiple stations located within the 3 spatially averaged reaches. RMA is equal to the sum of the absolute values of the differences in concentration between each observed and predicted pair divided by the sum of all the observed concentrations over the specified time period. Model results were also averaged over time periods of 1, 2, and 4 weeks centered on each monitoring date and corresponding RMA statistics were calculated. RMA values for predicted water quality parameters exhibiting large short-term variability (PO4-P and chlorophyll *a*) were reduced significantly following time averaging and best results were found for a 2-week averaging period. Separate sets of RMA calculations were made for the calibration period (June 1 through October 30, 2002) and the verification period (January 1, 1998 through May 31, 2002). Results for the calibration period in 2002 are given in Table 4-10 based on a 2-week time averaging period. Table 4-10 also gives the number of field data points used for each RMA calculation. The average RMA values given in Table 4-10 account for the fact that field data and model predictions for the lumped basins utilize data at

multiple locations. The Lower, Upper, and BU Basins consist of data at 5, 4, and 2 individual locations, respectively.

Table 4-10. Relative mean absolute error for the surface water calibration (6/1/2002 – 10/30/2002)

Relative Mean Absolute Error (Percent)

Parameter	Lower Basin	Upper Basin	BU Basin	Science Mus.	CRBL02	CRBL03	CRBL12	TMDL21	Average
DO	15	14	18	14	16	7	20	21	15
Chlor-a	114	117	99	76	137	80	130	76	108
PO4-P	55	39	118	56	92	164	48	63	68
TP	12	22	35	32	54	17	23	20	22
Tot Org-P	12	21	28	32	56	26	26	18	22
NH4-N	96	107	113	120	58	304	103	118	114
NO23-N	174	148	104	140	37	36	157	263	143
TN	47	44	32	59	7	17	46	51	40
Tot Org-N	6	10	26	32	19	29	9	14	14
Tot Org-C	30	5	53	0	85	25	12	0	28

Number of Field Data Points

Parameter	Lower Basin	Upper Basin	BU Basin	Science Mus.	CRBL02	CRBL03	CRBL12	TMDL21	Average
DO	13	13	13	21	13	6	6	6	91
Chlor-a	9	6	9	21	9	6	6	5	71
PO4-P	13	6	13	21	13	6	6	5	83
TP	13	6	13	21	13	6	6	6	84
Tot Org-P	13	6	13	21	13	6	6	5	83
NH4-N	12	6	12	21	12	6	6	6	81
NO23-N	13	6	13	21	13	6	6	5	83
TN	6	6	6	21	6	6	6	5	62
Tot Org-N	6	6	6	21	6	6	6	6	63
Tot Org-C	10	1	10	0	10	3	2	0	36

RMAs for total phosphorus ranged between 12 and 54 percent with an average value of 22 percent. RMAs for organic phosphorus ranged between 12 and 56 percent with an average value of 22 percent. RMAs for the algal nutrient PO4-P ranged between 39 and 164 percent with an average value of 68 percent. RMAs for total nitrogen ranged between 7 and 59 percent with an average value of 40 percent. RMAs for organic nitrogen ranged between 6 and 32 percent with an average value of 14 percent. RMAs for the algal nutrients NH4-N and NO3-N averaged 114 and 143 percent, respectively. RMAs for dissolved oxygen were between 7 and 21 percent with an average value of 15 percent. RMAs for chlorophyll *a* were found to be between 76 and 137 percent with an average value of 108 percent.

Near-Bottom Results

Verification plots comparing near-bottom modeling results and field data for the 3 monitoring locations for which vertical sampling was conducted for the calibration period in 2002 (TMDL22, TMDL25, and CRBL11), are shown in Figures 4.179 through 4.193. Statistical measures of the model's predictive capabilities are presented, in terms of percent RMA, in Table 4-11. RMAs are given for bottom water dissolved oxygen, chlorophyll *a*, PO4-P, total phosphorus, organic phosphorus, NH4-N, NOx-N, total nitrogen, organic nitrogen, and total organic carbon. Although many of the RMA values are relatively high, results suggest that the model is capable of simulating the general timing and magnitude of bottom-water dissolved oxygen anoxia, sediment diagenesis releases, and the observed build-up of phosphorus and nitrogen in the bottom-waters during the warm weather season in 2002. It is important to note

that RMA values can be quite high for water quality parameter concentrations that are either very small or are often non-detectable, such as was found for bottom-water dissolved oxygen.

Table 4-11. Relative mean absolute error for the bottom-water calibration (6/1/2002 – 10/30/2002)

	Relative Mean Absolute Error (%)			
Parameter	TMDL22	TMDL25	CRBL11	Average
DO	165	102	399	222
Chlor-a	195	224	280	233
PO4-P	70	70	32	57
TP	59	69	28	52
Tot Org-P	73	63	41	59
NH4-N	42	25	32	33
NO23-N	344	251	904	500
TN	45	19	36	33
Tot Org-N	60	23	33	39

	Number of Field Data Points			
Parameter	TMDL22	TMDL25	CRBL11	Average
DO	5	5	5	15
Chlor-a	6	6	5	17
PO4-P	6	6	6	18
TP	6	6	6	18
Tot Org-P	6	6	6	18
NH4-N	6	6	6	18
NO23-N	6	6	6	18
TN	6	6	6	18
Tot Org-N	6	6	6	18

4.5.4 Water Quality Model Verification

Model results were also plotted along with the field observations for the water quality model verification time period (January 1, 1998 through May 31, 2002). Taken together, the near-surface and near-bottom calibration results presented in Section 4.5.3 and analogous verification results presented here suggest that the model is capable of simulating the major processes controlling water quality and eutrophication in the Basin.

Near-Surface Results

Near-surface (top 12 percent of the water column) modeling results and field data for the period between January 1, 1998 and May 31, 2002 are presented as a measure of model verification.

Verification plots are presented for CRBL12 (Figures 4.194 through 4.205), Science Museum (Figures 4.206 through 4.217), Lower Basin (Figures 4.218 through 4.229), TMDL21 (Figures 4.230 through 4.241), Upper Basin (Figures 4.242 through 4.253), BU Basin (Figures 4.254 through 4.265), CRBL03 (Figures 4.266 through 4.277), and CRBL02 (Figures 4.278 through 4.289). The water quality model predicts most of the water quality constituents adequately during the verification time period.

In addition to the visual comparisons of model predictions and field observations, statistical measures of wellness-of-fit were also developed for the verification time period. Results for near-surface stations and basins are given in Table 4-12. Details on assumptions and methods used to develop RMA statistics for the verification time period were presented previously in the model calibration section (Section 4.5.3).

Table 4-12. Relative mean absolute error for the surface water verification (1/1/1998 – 5/31/2002)

Relative Mean Absolute Error (Percent)

Parameter	Lower Basin	Upper Basin	BU Basin	Science Mus.	CRBL02	CRBL03	CRBL12	TMDL21	Average
DO	13	0	12	11	15	11	14	0	12
Chlor-a	59	0	51	51	46	65	62	0	56
PO4-P	135	0	469	50	137	136	72	0	182
TP	33	0	23	29	42	42	36	0	32
Tot Org-P	35	0	38	26	43	38	39	0	36
NH4-N	86	0	145	70	48	247	107	0	108
NO23-N	0	0	0	36	0	0	0	0	36
TN	0	0	0	22	0	0	0	0	22
Tot Org-N	0	0	0	22	0	0	0	0	22
Tot Org-C	40	0	32	0	34	27	29	0	35

Number of Field Data Points

Parameter	Lower Basin	Upper Basin	BU Basin	Science Mus.	CRBL02	CRBL03	CRBL12	TMDL21	Average
DO	27	0	28	235	22	14	14	0	340
Chlor-a	19	0	19	235	19	11	11	0	314
PO4-P	22	0	22	235	22	10	10	0	321
TP	23	0	23	235	23	11	11	0	326
Tot Org-P	22	0	22	233	22	10	10	0	319
NH4-N	23	0	23	235	22	11	11	0	325
NO23-N	0	0	0	235	0	0	0	0	235
TN	0	0	0	235	0	0	0	0	235
Tot Org-N	0	0	0	234	0	0	0	0	234
Tot Org-C	23	0	23	0	23	11	11	0	91

Verification RMAs for total phosphorus ranged between 23 and 42 percent with an average value of 32 percent. RMAs for the algal nutrient PO4-P ranged between 72 and 469 percent with an average value of 182 percent. RMAs for organic phosphorus ranged between 26 and 43 percent with an average value of 36 percent. The RMA for total nitrogen at the Science Museum was 22 percent. Organic nitrogen data were only available for the Science Museum monitoring location during the verification time period. As a result verification RMAs for total and organic nitrogen could not be determined for the other monitoring locations. RMAs for the algal nutrients NH4-N and NO3-N averaged 108 and 36 percent, respectively. RMAs for dissolved oxygen were between 11 and 15 percent with an average value of 12 percent. RMAs for chlorophyll *a* were found to be between 46 and 65 percent with an average value of 56 percent. RMAs for total organic carbon were found to be between 27 and 40 percent with an average value of 35 percent.

Near-Bottom Results

Verification plots giving near-bottom modeling results and field data for the 3 monitoring locations for which limited vertical sampling was available during the verification time period between January 1, 1998 and May 31, 2002 (TMDL22, TMDL25, and CRBL11) are shown in Figures 4.290 through 4.304. No statistical measures of the model's predictive capabilities were developed for the verification time period because of a lack of sufficient monitoring data at these

locations prior to June of 2002. Results for dissolved oxygen, PO4-P, total phosphorus, organic phosphorus and, NH4-N are plotted to demonstrate that the water quality model is capable of simulating seasonal bottom water dissolved oxygen anoxia and oxygenation, sediment diagenesis and release and the observed build-up and flushing of bottom-water phosphorus and nitrogen during multiple annual cycles.

4.5.5 EFDC-WQM Calibration Parameter Set

During the model testing process (calibration and verification), EFDC-WQM parameters controlling water column and sediment diagenesis water quality processes were initially set at those given in the EFDC-WQM model documentation (Hamrick et al. 1995). These values were previously used successfully during testing of the Chesapeake Bay Model (Cerco and Cole 1994). However, during model testing some parameters were changed in order to produce results that more closely simulate field observations throughout the Basin. Tables 4-13 through 4-17 present the final calibrated and verified model parameters used for this study. Many of the parameter values are identical to those of the Chesapeake Bay application and those that were changes fall within ranges of values used in accepted previous applications of EFDC-WQM.

Table 4-13. Water quality parameters related to algae in the water column

Parameter	Value[a]	Equation[b]
PM_c (day^{-1})	1.2 (2.5)	3-1a
PM_d (day^{-1})	2.2 (2.25)	3-1a
PM_g (day^{-1})	1.4 (2.5)	3-1a
KHN_x (g N m^{-3})	**0.01 (all groups)**	3-1c
KHP_x (g P m^{-3})	**0.001 (all groups)**	3-1c
FD	temporally-varying input	3-1e
I_o (langleys day^{-1})	temporally-varying input	3-1f
Ke_b (m^{-1})	0.05 (spatially varied)	3-1h
Ke_{TSS} (m^{-1} per g m^{-3})	0.015 (NA)	3-1h
Ke_{Chl} (m^{-1} per mg Chl m^{-3})	**0.017**	3-1h
$CChl_x$ (g C per mg Chl)	**0.060 (g)**, 0.100 (d), 0.250 (b-g) (0.060)	3-1h
$(D_{opt})_x$ (m)	**1.0 (g), 1.0 (d)**, 0.1 (b-g) (1.0 all groups)	3-1i
$(I_s)_{min}$ (langleys day^{-1})	**40.0**	3-1i
CI_a, CI_b & CI_c	**0.7, 0.2 & 0.1**	3-1j
$TMlow_c$, $TMlow_d$ & $TMlow_g$ (°C)	28, 14, 20 (NA)	3-1k
$TMupp_c$, $TMupp_d$ & $TMupp_g$ (°C)	35, 16, 23 (NA)	3-1k
$KTG1_c$ & $KTG2_c$ ($°C^{-2}$)	0.008 & 0.008 (0.005 & 0.004)	3-1k
$KTG1_d$ & $KTG2_d$ ($°C^{-2}$)	0.008 & 0.008 (0.004 & 0.006)	3-1k
$KTG1_g$ & $KTG2_g$ ($°C^{-2}$)	**0.008** & 0.008 (0.008 & 0.01)	3-1k
STOX (ppt)	**1.0**	3-1l
BMR_c (day^{-1})	0.010 (0.04)	3-1m
BMR_d (day^{-1})	**0.010**	3-1m
BMR_g (day^{-1})	**0.010**	3-1m
TR_x (°C)	**20.0 (all groups)**	3-1m
KTB_x ($°C^{-1}$)	**0.069 (all groups)**	3-1m
PRR_c (day^{-1})	0.02 (0.01)	3-1n
PRR_d (day^{-1})	0.05 (0.215)	3-1n
PRR_g (day^{-1})	0.05 (0.215)	3-1n
WS_c (m day^{-1})	0.07 (0.03)	3-1
WS_d (m day^{-1})	0.25 (0.215)	3-1
WS_g (m day^{-1})	0.1 (0.13)	3-1

[a]The evaluation of these values are detailed in Chapter IX of Cerco and Cole (1994).
[b]The equation number where the corresponding parameter is first shown and defined.
[c]Not available in Cerco and Cole (1994) since their formulations do not include these parameters.
Note: Values in **Bold** font are identical to those used in Chesapeake Bay Model (CBM) (Cerco and Cole 1994); If values different than in CBM, CBM values given as (CBM Value)

Table 4-14. Parameters related to organic carbon in the water column

Parameter	Value[a]	Equation[b]
FCRP	**0.35**	3-2
FCLP	**0.55**	3-3
FCDP	**0.10**	3-4
FCD_x	**0.0 (all groups)**	3-4
WS_{RP} (m day^{-1})	0.17 (1.0)	3-2
WS_{LP} (m day^{-1})	0.17 (1.0)	3-3
KHR_x (g O_2 m^{-3})	**0.5 (all groups)**	3-4
$KHOR_{DO}$ (g O_2 m^{-3})	**0.5**	3-4g
K_{RC} (day^{-1})	**0.005**	3-4h
K_{LC} (day^{-1})	**0.075**	3-4i
K_{DC} (day^{-1})	**0.010**	3-4j
K_{RCalg} (day^{-1} per g C m^{-3})	**0.03**	3-4h
K_{LCalg} (day^{-1} per g C m^{-3})	**0.03**	3-4i
K_{DCalg} (day^{-1} per g C m^{-3})	**0.03**	3-4j
TR_{HDR} (°C)	**20.0**	3-4h
TR_{MNL} (°C)	**20.0**	3-4j
KT_{HDR} ($°C^{-1}$)	**0.069**	3-4h
KT_{MNL} ($°C^{-1}$)	**0.069**	3-4j
$KHDN_N$ (g N m^{-3})	**0.1**	3-4l
AANOX	**0.5**	3-4l

[a]The evaluation of these values are detailed in Chapter IX of Cerco and Cole (1994).
[b]The equation number where the corresponding parameter is first shown and defined.
Note: Values in **Bold** font are identical to those used in Chesapeake Bay Model (CBM) (Cerco and Cole 1994)
If values different than in CBM, CBM values given as (CBM Value)

Table 4-15. Parameters related to phosphorus in the water column

Parameter	Value[a]	Equation[b]
FPRP	**0.1**	3-5
FPLP	**0.2**	3-6
FPDP	**0.5**	3-7
FPIP	**0.2**[c]	3-8
FPR_x	**0.0 (all groups)**	3-5
FPL_x	**0.0 (all groups)**	3-6
FPD_x	**1.0 (all groups)**	3-7
FPI_x	**0.0**[c] **(all groups)**	3-8
WS_s (m day^{-1})	0.17 (1.0)	3-8
K_{PO4p} (per g m^{-3}) for TSS	2.0 (NA)	3-8b
CP_{prm1} (g C per g P)	**42.0**	3-8e
CP_{prm2} (g C per g P)	**85.0**	3-8e
CP_{prm3} (per g P m^{-3})	**200.0**	3-8e
K_{RP} (day^{-1})	**0.005**	3-8f
K_{LP} (day^{-1})	**0.075**	3-8g
K_{DP} (day^{-1})	**0.130**	3-8h
K_{RPalg} (day^{-1} per g C m^{-3})	0.03 (0.0)	3-8f
K_{LPalg} (day^{-1} per g C m^{-3})	0.03 (0.0)	3-8g
K_{DPalg} (day^{-1} per g C m^{-3})	0.23 (0.0)	3-8h

[a]The evaluation of these values are detailed in Chapter IX of Cerco and Cole (1994).
[b]The equation number where the corresponding parameter is first shown and defined.
[c]Not available in Cerco and Cole (1994) since their formulations do not include these parameters: FPI_x is estimated from $FPR_x+FPL_x+FPD_x+FPI_x = 1$.
Note: Values in **Bold** font are identical to those used in Chesapeake Bay Model (CBM) (Cerco and Cole 1994); If values different than in CBM, CBM values given as (CBM Value)

Table 4-16. Parameters related to nitrogen in the water column

Parameter	Value[a]	Equation[b]
FNRP	**0.35**	3-9
FNLP	**0.55**	3-10
FNDP	**0.10**	3-11
FNIP	**0.0**	3-12
FNR_x	**0.0 (all groups)**	3-9
FNL_x	**0.0 (all groups)**	3-10
FND_x	**1.0 (all groups)**	3-11
FNI_x	**0.0 (all groups)**	3-12
ANC_x (g N per g C)	**0.167 (all groups)**	3-9
ANDC (g N per g C)	**0.933**	3-13
K_{RN} (day^{-1})	**0.005**	3-13b
K_{LN} (day^{-1})	**0.075**	3-13c
K_{DN} (day^{-1})	0.13 (0.015)	3-13d
K_{RNalg} (day^{-1} per g C m^{-3})	0.03 (0.0)	3-13b
K_{LNalg} (day^{-1} per g C m^{-3})	0.03 (0.0)	3-13c
K_{DNalg} (day^{-1} per g C m^{-3})	0.23 (0.0)	3-13d
Nit_m (g N m^{-3} day^{-1})	0.10 (0.07)	3-13g
$KHNit_{DO}$ (g O_2 m^{-3})	**1.0**	3-13g
$KHNit_N$ (g N m^{-3})	**1.0**	3-13g
TNit (°C)	**27.0**	3-13g-1
KNit1 ($°C^{-2}$)	**0.0045**	3-13g-1
KNit2 ($°C^{-2}$)	**0.0045**	3-13g-1

[a]The evaluation of these values are detailed in Chapter IX of Cerco and Cole (1994).
[b]The equation number where the corresponding parameter is first shown and defined.
Note: Values in **Bold** font are identical to those used in Chesapeake Bay Model (CBM) (Cerco and Cole 1994); If values different than in CBM, CBM values given as (CBM Value)

Table 4-17. Parameters related to chemical oxygen demand and dissolved oxygen in the water column

Parameter	Value[a]	Equation[b]
KH_{COD} (g O_2 m^{-3})	**1.5**	3-16
K_{CD} (day^{-1})	1.0 (2.0)	3-16a
TR_{COD} (°C)	**20.0**	3-16a
KT_{COD} ($°C^{-1}$)	**0.041**	3-16a
AOCR (g O_2 per g C)	**2.67**	3-17
AONT (g O_2 per g N)	**4.33**	3-17
K_{ro} (in MKS unit)	1.5 (3.933)	3-17e
KT_r	**1.024[c] (1.005 - 1.030)**	3-17e

[a]The evaluation of these values are detailed in Chapter IX of Cerco and Cole (1994).
[b]The equation number where the corresponding parameter is first shown and defined.
[c]Not available in Cerco and Cole (1994) since their formulations do not include these parameters: K_{ro} is from O'Connor & Dobbins (1958) and KT_r is from Thomann & Mueller (1987).
Note: Values in **Bold** font are identical to those used in Chesapeake Bay Model (CBM) (Cerco and Cole 1994); If values different than in CBM, CBM values given as (CBM Value)

Table 4-18. Sediment sub-model calibration parameter set

```
C05  DIFFUSION COEFFICIENT
C    DifT = diffusion coefficient for sediment temperature (m2/sec)
C05  DifT
    1.8E-7

C06 Spatially constant parameters to split depositional fluxes to Gi classes $
C   FNBc1 = fraction of PON from Cyanobacteria routed to G1 class
C   FNBc2 = fraction of PON from Cyanobacteria routed to G2 class
C   FNBc3 = fraction of PON from Cyanobacteria routed to G3 class
C         Note:  FNBc1 + FNBc2 + FNBc3 = 1.0
C   FNBd1 = fraction of PON from diatom algae group routed to G1 class
C   FNBd2 = fraction of PON from diatom algae group routed to G2 class
C   FNBd3 = fraction of PON from diatom algae group routed to G3 class
C         Note:  FNBd1 + FNBd2 + FNBd3 = 1.0
C   FNBg1 = fraction of PON from green algae group routed to G1 class
C   FNBg2 = fraction of PON from green algae group routed to G2 class
C   FNBg3 = fraction of PON from green algae group routed to G3 class
C         Note:  FNBg1 + FNBg2 + FNBg3 = 1.0
C06 FNBc1   FNBc2   FNBc3   FNBd1   FNBd2   FNBd3   FNBg1   FNBg2   FNBg3
        0.65      0.30      0.05      0.65      0.30      0.05      0.65      0.30      0.05

C07
C   FPBc1 = fraction of POP from Cyanobacteria routed to G1 class
C   FPBc2 = fraction of POP from Cyanobacteria routed to G2 class
C   FPBc3 = fraction of POP from Cyanobacteria routed to G3 class
C         Note:  FPBc1 + FPBc2 + FPBc3 = 1.0
C   FPBd1 = fraction of POP from diatom algae group routed to G1 class
C   FPBd2 = fraction of POP from diatom algae group routed to G2 class
C   FPBd3 = fraction of POP from diatom algae group routed to G3 class
C         Note:  FPBd1 + FPBd2 + FPBd3 = 1.0
C   FPBg1 = fraction of POP from green algae group routed to G1 class
C   FPBg2 = fraction of POP from green algae group routed to G2 class
C   FPBg3 = fraction of POP from green algae group routed to G3 class
C         Note:  FPBd1 + FPBd2 + FPBd3 = 1.0
C07 FPBc1   FPBc2   FPBc3   FPBd1   FPBd2   FPBd3   FPBg1   FPBg2   FPBg3
        0.65      0.30      0.05      0.65      0.30      0.05      0.65      0.30      0.05

C08
C   FCBc1 = fraction of POC from Cyanobacteria routed to G1 class
C   FCBc2 = fraction of POC from Cyanobacteria routed to G2 class
C   FCBc3 = fraction of POC from Cyanobacteria routed to G3 class
C         Note:  FCBc1 + FCBc2 + FCBc3 = 1.0
C   FCBd1 = fraction of POC from diatom algae group routed to G1 class
C   FCBd2 = fraction of POC from diatom algae group routed to G2 class
C   FCBd3 = fraction of POC from diatom algae group routed to G3 class
C         Note:  FCBd1 + FCBd2 + FCBd3 = 1.0
C   FCBg1 = fraction of POC from green algae group routed to G1 class
C   FCBg2 = fraction of POC from green algae group routed to G2 class
C   FCBg3 = fraction of POC from green algae group routed to G3 class
C         Note:  FCBd1 + FCBd2 + FCBd3 = 1.0
C08 FCBc1   FCBc2   FCBc3   FCBd1   FCBd2   FCBd3   FCBg1   FCBg2   FCBg3
        0.65      0.30      0.05      0.65      0.30      0.05      0.65      0.30      0.05
```

Table 4-18 (continued). Sediment sub-model calibration parameter set

```
C09 Spatially constant parameters for diagenesis
C09
C   KPON1 = Decay rate of PON at 20 degC in Layer 2 for G1 class (1/day)
C   KPON2 = Decay rate of PON at 20 degC in Layer 2 for G2 class (1/day)
C   KPON3 = Decay rate of PON at 20 degC in Layer 2 for G3 class (1/day)
C   KPOP1 = Decay rate of POP at 20 degC in Layer 2 for G1 class (1/day)
C   KPOP2 = Decay rate of POP at 20 degC in Layer 2 for G2 class (1/day)
C   KPOP3 = Decay rate of POP at 20 degC in Layer 2 for G3 class (1/day)
C   KPOC1 = Decay rate of POC at 20 degC in Layer 2 for G1 class (1/day)
C   KPOC2 = Decay rate of POC at 20 degC in Layer 2 for G2 class (1/day)
C   KPOC3 = Decay rate of POC at 20 degC in Layer 2 for G3 class (1/day)
C
C09 KPON1   KPON2   KPON3   KPOP1   KPOP2   KPOP3   KPOC1   KPOC2   KPOC3
        0.025   0.0015      0.0   0.025   0.0015      0.0   0.025   0.0015      0.0

C10
C   ThKN1 = Constant for temperature adjustment for KPON1 (unitless)
C   ThKN2 = Constant for temperature adjustment for KPON2 (unitless)
C   ThKN3 = Constant for temperature adjustment for KPON3 (unitless)
C   ThKP1 = Constant for temperature adjustment for KPOP1 (unitless)
C   ThKP2 = Constant for temperature adjustment for KPOP2 (unitless)
C   ThKP3 = Constant for temperature adjustment for KPOP3 (unitless)
C   ThKC1 = Constant for temperature adjustment for KPOC1 (unitless)
C   ThKC2 = Constant for temperature adjustment for KPOC2 (unitless)
C   ThKC3 = Constant for temperature adjustment for KPOC3 (unitless)
C
C10 ThKN1   ThKN2   ThKN3   ThKP1   ThKP2   ThKP3   ThKC1   ThKC2   ThKC3
          1.1    1.15     1.0     1.1    1.15     1.0     1.1    1.15     1.0

C11 Spatially constant parameters common to sediment flux
C11
C    rM1 = Solid concentrations in Layer 1 (Kg/L)
C    rM2 = Solid concentrations in Layer 2 (Kg/L)
C   ThDd = Constant for temperature adjustment for Dd (unitless)
C   ThDp = Constant for temperature adjustment for Dp (unitless)
C  GPOCr = Reference concentration for GPOC(1) (gC/m3)
C   KMDp = Particle mixing half-saturation constant for oxygen (mg/L)
C    KST = First-order decay rate for accumulated benthic stress (1/day)
C  DpMIN = Minimum diffusion coefficient for particle mixing (m^2/d)
C  RBIBT = Ratio of bio-irrigation to bioturbation (unitless)
C11 rM1    rM2    ThDd   ThDp   GPOCr  KMDp   KST    DpMIN  RBIBT
      0.5    0.5    1.08   1.117    50.0    2.0   0.03    3.0E-6     1.0
C-------------------------------------------------------------------------------
C12
C  O2BSc = Critical overlying oxygen concentration below which benthic
C          hysteresis occurs (mg/L)
C  TDMBS = Time duration for which the maximum or minimum stress is
C          retained (days)
C  TCMBS = Critical hypoxia duration; if less than this value, no
C          hysteresis occurs (days)
C
C12 O2BSc  TDMBS  TCMBS
          1.0    60.0    14.0
```

Table 4-18 (continued). Sediment sub-model calibration parameter set

```
C13 Spatially constant parameters for NH4, NO3 & PO4 flux
C13
C   P1NH4 = Partition coefficient, ratio of particulate to dissolved NH4
C         in layer 1 (L/Kg)
C   P2NH4 = Partition coefficient, ratio of particulate to dissolved NH4
C         in layer 2 (L/Kg)
C   KMNH4 = Nitrification half-sat. constant for ammonium (gN/m^3)
C KMNH4O2 = Nitrification half-sat. constant for dissolved oxygen (gO2/m^3)
C   ThNH4 = Constant for temperature adjustment for KNH4 (unitless)
C   ThNO3 = Constant for temperature adjustment for KNO31 and KNO32 (unitless)
C   P2PO4 = Partition coefficient, ratio of particulate to dissolved PO4
C          in layer 2 (L/Kg)
C  DOcPO4 = Critical dissolved oxygen for PO4 sorption (mg/L)
C         Note: increase this value to increase PO4 flux to water column
C
C13 P1NH4   P2NH4   KMNH4   KMNH4O2 ThNH4   ThNO3   P2PO4   DOcPO4
          1.0       1.0       1.5          3.68    1.17      1.08      10.         2.5

C14 Spatially constant parameters for H2S/CH4 flux and SOD
C14
C   P1H2S = Partition coefficient for H2S in Layer 1 (L/Kg)
C   P2H2S = Partition coefficient for H2S in Layer 2 (L/Kg)
C  KH2Sd1 = Reaction velocity for dissolved sulfide oxidation in
C         Layer 1 at 20 degC (m/day)
C  KH2Sp1 = Reaction velocity for particulate sulfide oxidation in
C         Layer 1 at 20 degC (m/day)
C   ThH2S = Constant for temperature adjustment for KH2Sd1 and KH2Sp1 (unitless)
C   KMH2S = Constant to normalize the sulfide oxidation rate for oxygen (mgO2/L)
C    KCH4 = Reaction velocity for methane oxidation in layer 1 at 20 degC (m/day)
C   ThCH4 = Constant for temperature adjustment for KCH4 (unitless)
C  cSHSCH = Critical salinity; less than this value CH4 is produced,
C         above this value H2S is produced (g/L)
C
C14 P1H2S   P2H2S   KH2Sd1  KH2Sp1  ThH2S   KMH2S   KCH4    ThCH4   cSHSCH
        100.0     100.0       0.2       0.4     1.17        4.0       0.2       1.08        1.0

C15
C    aO2C = Stoichiometric coefficient for carbon diagenesis consumed
C         by H2S oxidation (gO2/gC)
C  aO2NO3 = Stoichiometric coefficient for carbon diagenesis consumed
C         by denitritrification (gO2/gN)
C  aO2NH4 = Stoichiometric coefficient for carbon diagenesis consumed
C         by nitrification (gO2/gN)
C
C15    aO2C     aO2NO3   aO2NH4
     2.66667      2.85714       4.33
```

Table 4-18 (continued). Sediment sub-model calibration parameter set

```
C19 Spatially varying parameters: physical and rate velocity
C    ISMz = zone for spatially variable parameters in SPM
C    Hsed = Total active sediment thickness (meters)
C      W2 = sediment burial rate (cm/year)
C      Dd = diffusion coefficient in pore water (m2/day)
C      Dp = apparent diffusion coefficient for particle mixing (m2/day)
C    KNH4 = optimal reaction velocity for nitrification at 20 degC (m/day)
C   KNO31 = reaction velocity for denitrification in layer 1 at 20 degC (m/day)
C   KNO32 = reaction velocity for denitrification in layer 2 at 20 degC (m/day)
C  DP1PO4 = factor to enhance sorption of PO4 in layer 1 when DO is
C           greater than DOcPO4 (unitless)
C           Note: decrease DP1PO4 and/or increase DOcPO4 to increase the
C                 benthic flux of PO4 to the water column
C SODmult = factor to enhance magnitude of sediment oxygen demand (unitless)
$  ISMZ    Hsed  W2       Dd       Dp      KNH4   KNO31   KNO32   DP1PO4 SODmult
          1    0.80  0.10  0.0100  1.2E-4       0.14       0.12       0.18      150.00       1.00

C20 Spatially varying parameters: distribution coefficients for RPOM
C20
C    ISMZ = zone index for spatially variable parameters
C   FNRP1 = fraction of water column refractory PON routed to G-class 1
C   FNRP2 = fraction of water column refractory PON routed to G-class 2
C   FNRP3 = fraction of water column refractory PON routed to G-class 3
C           Note:  FNRP1 + FNRP2 + FNRP3 = 1.0
C   FPRP1 = fraction of water column refractory POP routed to G-class 1
C   FPRP2 = fraction of water column refractory POP routed to G-class 2
C   FPRP3 = fraction of water column refractory POP routed to G-class 3
C           Note:  FPRP1 + FPRP2 + FPRP3 = 1.0
C   FCRP1 = fraction of water column refractory POC routed to G-class 1
C   FCRP2 = fraction of water column refractory POC routed to G-class 2
C   FCRP3 = fraction of water column refractory POC routed to G-class 3
C           Note:  FCRP1 + FCRP2 + FCRP3 = 1.0
C
C20 ONE TITLE CARD FOLLOWS:
$  ISMZ   FNRP1   FNRP2   FNRP3   FPRP1   FPRP2   FPRP3   FCRP1   FCRP2   FCRP3
          1      0.10       0.80       0.10       0.10       0.80       0.10       0.10       0.80       0.10
```

4.6 Additional Model Testing

Following calibration and verification of the model, several additional tests runs were conducted. The first test consisted of running the calibrated and verified model for a 10-year time period, repeating daily water quality parameter loading time series used to simulate 1998. The objective of this test was to determine if initial conditions specified for bottom sediment particulate organic carbon, phosphorus, and nitrogen during the calibration and verification runs were consistent with long-term fluxes of these parameters across the water column-bottom interface. A finding that the concentrations of these parameters in bottom sediments remains relatively constant over the long-term suggests that initial conditions used in the model testing were appropriate. Results of this test are presented in Figure 4.305 for the model cell corresponding to the Science Museum monitoring station. Particulate organic carbon, phosphorus, and nitrogen vary over the 10-year simulation due to seasonal changes in sediment loadings and variable sediment diagenesis processes. However, long-term average concentrations do not exhibit a significant drift downward or upward relative to initial conditions following the first year of the simulation.

The second test consisted of running the model for the 5-year period between January 1, 1998 and October 31, 2002, specifying a constant (over time) 50 percent reduction in daily boundary input loads of algal phosphorus and nitrogen nutrients, including PO4-P, organic phosphorus, NH4-N, NOx-N and organic nitrogen. This test provided insight into algal nutrient and chlorophyll *a* reductions likely to result from implementation of nutrient load reduction scenarios, such as those to be investigated during TMDL development. Results of this nutrient reduction test run are shown in Figures 4.306, 4.307, and 4.308, for chlorophyll *a*, total phosphorus, and total nitrogen before and after 50 percent load reduction, respectively. Following a 50 percent reduction in nutrients, chlorophyll *a* would likely be reduced significantly. Peak growing season algal bloom chlorophyll *a* levels predicted for 1998 would likely be reduced from 47 to 32 µg/l and growing season average chlorophyll *a* levels would likely be reduced from 20 to 12 µg/l under this scenario.

An additional time series plot of chlorophyll *a* levels of each of the three modeled algal groups has been developed based on the full 5-year model run under existing loading conditions. This plot (Figure 4.309) has been developed to demonstrate the predicted seasonal succession of these three algal groups and to show their relative contributions to total algal chlorophyll *a* levels predicted by the model at the Science Museum monitoring location. It is seen that during the winter, early summer and fall, diatoms dominate the total phytoplankton. As water temperatures increase during the summer months, algal groups other than diatoms start to dominate the assemblage, with blue-green algae peaking during the warmest periods of each summer. In terms of biomass, it is important to realize that in the model and prototype, blue-greens exhibit a biomass to chlorophyll *a* ratio that is over 4 times larger than that of the green algae (greens and other groups) and over 2 times larger than that of diatoms. Although they may account for a relatively small portion of the total measured or predicted chlorophyll *a* during summer, they have a very large impact on ambient carbon, phosphorus, and nitrogen levels and dissolved oxygen because of their correspondingly large biomass.

5 CONCLUSIONS AND RECOMMENDATIONS

A transient linked hydrodynamic and water quality model has been developed and tested as a tool for use in subsequent TMDL analyses. Calibration and verification results indicate that the model, in general, successfully predicts observed hydrodynamic and water quality conditions throughout the Lower Charles River Basin. Error statistics developed for the calibration and verification time periods generally fall within ranges established as adequate in previous applications of the EFDC model. Error statistics for several water quality parameters, including: chlorophyll-a, PO4-P, NH4-N and NOx-N were found to exceed literature ranges, at several monitoring locations.

It is important to note that, due to the size of model computational cells, model predictions should be viewed as being indicative of water quality conditions over hundreds of meters longitudinally and laterally within the river, in which water quality parameter loadings are assumed to be completely mixed horizontally. This spatial averaging may result in attenuation of water quality parameter concentrations due to nearby discharges. Conversely, spatial averaging may result in accentuating the influence of more distant discharges. Field monitoring data is indicative of water quality conditions at a point horizontally within the river. Due to local circulation patterns a monitoring point may fall within or outside individual plumes of shoreline discharges, either accentuating or attenuating their influence on water quality parameter concentrations. Model predictions at a given time should also be viewed as being indicative of average water quality conditions over periods on the order of 12 hours, whereas monitoring data indicates water quality conditions at an instant in time. Differences in both the spatial and temporal characteristics of model predictions and field observations may contribute significantly to the relatively high error statistics cited above.

In order to investigate impacts of the above differences in the temporal characteristics of model predictions and field observations, a sensitivity analysis of time averaging of model results and field data was conducted. Model predictions (every 12 hours) and field data at the Science Museum monitoring site were averaged over time periods of 0.5, 7, 17, 30, 51, 77 and 153 days, for the growing season (June 1 through October 31) in each year between 1998 and 2002. Results of the sensitivity analysis, in terms of relative mean absolute errors for the seven different time averaging periods, are given in Table 5-1 It is seen that RMAs decrease rapidly with the length of the time averaging period, and that a 1-month period results in error statistics that are acceptable for subsequent TMDL modeling. Seasonal average (153 days) error values for all water quality parameters are well within suggested error guidelines for TMDL modeling.

Following calibration and verification of the water quality model, the model will be used to evaluate point and nonpoint source loading allocations and reduction alternates, considering critical conditions and established TMDL endpoints. There are numerous combinations of loads that can meet the TMDL endpoint. Using the information provided through stakeholder interaction, alternatives that best meet the stakeholder's needs will be assessed and adjusted to produce acceptable loading alternatives. In addition, watershed and in stream BMPs will be considered for nonpoint source load reduction.

TMDL scenario simulations will be designed based on current load allocations and various alternative load allocations developed in conjunction with the stakeholders, regulatory agencies and the technical advisory group. The calibrated and verified hydrodynamic and water quality models will be reconfigured as appropriate and TMDL allocation simulation scenarios using both calibration kinetic parameters and implicit safety factor parameters derived from sensitivity and uncertainty analyses. The simulation scenario results and analysis, including a comparison of implicit and explicit factor of safety approaches, will be documented in a report.

Table 5-1. Impact of time averaging on error statistics, Science Museum (1998-2002)

Time Averaging Period (Days) June-October	Relative Mean Absolute Error (Percent)								
	DO	Chlor-a	PO4-P	Total P	Org-P	NH4-N	NO23-N	Total N	Org-N
1	16	61	106	49	33	123	81	38	23
7	14	59	77	39	31	114	84	35	22
17	11	53	59	34	27	107	78	33	19
30	10	44	47	31	24	98	73	31	15
51	9	44	47	30	23	82	64	29	14
77	7	28	39	23	18	48	40	19	10
153 (June-Oct)	5	30	26	20	15	37	26	12	8

6 REFERENCES

Ambrose, R. B., T. A. Wool, and J. L. Martin, 1993: The water quality analysis and simulation program, WASP5: Part A, model documentation version 5.1. U. S. EPA, Athens Environmental Research Laboratory, 210 pp.

Banks, R.B. & Herrera, F.F. 1977: Effect of wind and rain on surface reaeration. J. of the Environmental Engineering Division, ASCE, 103(EE3): 489-504.

Blumberg, A.F. and D.M. Goodrich. 1990. Modeling of wind-induced destratification in Chesapeake Bay. *Estuaries*, 13, 236-249.

Boni, L., Carpené, E., Wynne, D., & Reti, M. 1989: Alkaline phosphatase activity in *Protogonyaulax tamarensis*. J. of Plankton Research, 11(5): 879-885.

Breault, R.F., J.R. Sorenson, and P.K. Weiskel. 2002. Streamflow, water quality, and contaminant loads in the Lower Charles River Watershed, Massachusetts, 1999-2000. USGS, Northbrough, Massachusetts, WRIR 02-4137.

Carritt, D.E. & Goodgal, S. 1954. Sorption reactions and some ecological implications. Deep-Sea Research, 1: 224-243.

Cerco, C.F. and T.M. Cole. 1994. Three-Dimensional Eutrophication Model of Chesapeake Bay. Volume I: Main Report. Technical Report EL-94-4. U.S. Army Corps of Engineers, Waterways Experiment Station, Vicksburg, MS, May 1994.

Chróst, R.J. & Overbek, J. 1987. Kinetics of alkaline phosphatase activity and phosphorus availability for phytoplankton and bacterioplankton in Lake Plußsee (North German eutrophic lake). Microbial Ecology, 13: 229-248.

Devore, J.L. 1982. *Probability and Statistics for Engineering and the Sciences*. Brooks-Cole, Monterey, CA.

DiToro, D.M. 1980. Applicability of cellular equilibrium and Monod theory to phytoplankton growth kinetics. Ecological Modelling, 8: 201-218.

DiToro, D.M. & Fitzpatrick, J.J. 1993. Chesapeake bay sediment flux model. Contract Report EL-93-2, US Army Engineer Waterways Experiment Station, Vicksburg, MS, 316 pp.

Froelich, P.N. 1988. Kinetic control of dissolved phosphate in natural rivers and estuaries: a primer on the phosphate buffer mechanism. Limnology and Oceanography, 33(4, part 2): 649-668.

Galperin, B., L.H. Kantha, S. Hassid, and A. Rosati. 1988. A quasi-equilibrium turbulent energy model for geophysical flows. *J. Atmos. Sci.,* 45, 55-62.

Genet, L.A., Smith, D.J. & Sonnen, M.B. 1974. Computer program documentation for the dynamic estuary model. Prepared for US EPA, Systems Development Branch, Washington, D.C.

Hamrick, J.M. 1992. A Three-Dimensional Environmental Fluid Dynamics Computer Code: Theoretical and Computational Aspects. The College of William and Mary, Virginia Institute of Marine Science. Special Report 317.

Hamrick, J.M. and T.S. Wu. 1997. Computational design and optimization of the EFDC/HEM3D surface water hydrodynamic and eutrophication models. *Next Generation Environmental Models* and *Computational Methods,* G. Delich and M.F. Wheeler, Eds., Society of Industrial and Applied Mathematics, Philadelphia, 143-156.

Huber, W.C., and Dickinson, R.E., 1988. Stormwater Management Model User's Manual, Version 4.0, U.S. Environmental Protection Agency, EPA/600/3-88/001a, 569 p.

MADEP (Massachusetts Department of Environmental Protection). 2000. Massachusetts Water Quality Standards, 314 CMR 4.00: Massachusetts Surface Water Quality Standards. Division of Water Pollution Control. May 12, 2000.

MAEOEA (Massachusetts Executive Office of Environmental Affairs). 2003. Massachusetts year 2002 integrated list of waters, Part 1 - Context and rationale for assessing and reporting the quality of Massachusetts surface waters. CN: 125.1.

MAEOEA (Massachusetts Executive Office of Environmental Affairs). 2003. Massachusetts year 2002 integrated list of waters, Part 2 - Proposed listing of individual categories of water. CN: 125.2.

MAEOEA (Massachusetts Executive Office of Environmental Affairs). 2004. Massachusetts year 2004 integrated list of waters, Proposed listing of the condition of Massachusetts' waters pursuant to Sections 303(d) and 305(b) of the Clean Water Act. CN: 176.0.

Mellor, G.L. and T. Yamada. 1982. Development of a turbulence closure model for geophysical fluid problems. *Rev. Geophys. Space Phys.*, 20, 851-875.

Metcalf and Eddy, Inc. 1994. Sub-Task 2.5.5. Final Technical Memorandum, Estimation of Stormwater Flows and Loads, Master Planning and CSO Facility Planning. Submitted to MWRA, November 1994.

Metcalf and Eddy, Inc. 2000. MWRA Combined Sewer Overflow Model, Annual Overflow Simulation Results for 2000, Wakefield, MA.

Metcalf and Eddy, Inc. 2001. MWRA Combined Sewer Overflow Model, Annual Overflow Simulation Results for 2001. Wakefield, MA.

Metcalf and Eddy, Inc. 2002. MWRA Combined Sewer Overflow Model, Annual Overflow Simulation Results for 2002. Wakefield, MA.
Morel. 1983.

Morel, F. 1983. Principles of Aquatic Chemistry. John Wiley & Sons, New York, NY, 446 pp.

Numeric Environmental Services. 2002. Lower Charles River TMDL Modeling Project – Historical Data Review.

O'Connor, D.J. & Dobbins, W.E. 1958. Mechanism of reaeration in natural streams. Transactions of the Americal Society of Civil Engineers, 123(2934): 641-684.

Odum, E.P. 1971. Fundamentals of ecology (third edition). W.B. Saunders Co., Philadelphia, PA, 574pp.

Park, K., A. Y. Kuo, J. Shen, and J. M. Hamrick, 1995: A three-dimensional hydrodynamic-eutrophication model (HEM3D): description of water quality and sediment processes submodels. The College of William and Mary, Virginia Institute of Marine Science. Special Report 327, 113 pp.

Parsons, T.R., Takahashi, M. & Hargrave, B. 1984. Biological oceanographic processes (third edition). Pergamon Press, 330 pp.

Redfield, A.C., Ketchum, B.H. & Richards, F.A. 1963. The influence of organisms on the composition of sea-water (Chapter 2) pp 26-77. In: M.N. Hill (ed.), The Sea - Ideas and Observations on Progress in the Study of the Seas: Vol. 2, Composition of Sea Water, Comparative and Descriptive Oceanography, Interscience Publishers.

Ryskin, G. and L.G. Leal. 1983. Orthogonal mapping. *J. Comp. Phys.*, 50, 71-100.

Steele, J.H. 1962. Environmental control of photosynthesis in the sea. Limnology and Oceanography, 7(2): 137-150.

Stumm, W. & Morgan, J.J. 1981. Aquatic chemistry, an introduction emphasizing chemical equilibria in natural waters (second edition). John Wiley & Sons, Inc., 780 pp.

Tetra Tech, Inc., 2002: User's Manual for Environmental Fluid Dynamics Code, prepared for U. S. EPA, Region 1.

Tetra Tech, Inc. 2005. DRAFT – Total Maximum Daily Load for Eutrophication in the Lower Charles River Basin.

Thomann, R.V. 1982. Verification of water quality models. *J. Environ. Engrg. Div., ASCE*. 108, 923-940.

Thomann, R.V. & Mueller, J.A. 1987. Principles of surface water quality modeling and control. Harper & Row, Publishers, Inc., 644 pp.

USEPA (United States Environmental Protection Agency). 1990. Technical Guidance Manual for Performing Waste Load Allocations, Book III Estuaries, Part 2, Application of Estuarine Waste Load Allocation Models. EPA 823-R-92-003.

Voorhees, M. 2005. Personal communication. United States Environmental Protection Agency, Region I. Boston, Massachusetts.

Westrich, J.T. & Berner, R.A. 1984. The role of sedimentary organic matter in bacterial sulfate reduction: the G model tested. Limnology and Oceanography, 29(2): 236-249.

Willmont, C.J. 1982. Some comments on the evaluation of model performance. *Bull. Am. Meteor. Soc*., 63, 1309-1313.

Willmont, C.J., R.E. Davis, J.J. Feddema, K.M. Klink, D.R. Legates, C.M. Rowe, S.G. Ackelson, and J. O'Donnell. 1985. Statistics for the evaluation and comparison of models. *J. Geophys. Res*., 90, 8995-9005.

Woodward-Clyde. Synoptic analysis of selected rainfall gages throughout the United States: Oakland, CA.

Zarriello, P.J. and L.K. Barlow. 2002. Measured and simulated runoff to the Lower Charles River, Massachusetts, October 1999-September 2000. USGS, Northbrough, Massachusetts, WRIR 02-4129.

APPENDIX A: SUMMARY OF EFDC HYDRODYNAMIC MODEL FORMULATIONS

The equations used in the EFDC hydrodynamic model are the horizontal momentum equations:

$$\begin{aligned}&\partial_t(m_x m_y Hu)+\partial_x(m_y Huu)+\partial_y(m_x Hvu)+\partial_z(m_x m_y wu)-f_e m_x m_y Hv\\&=-m_y H\partial_x(p+p_{atm}+\phi)+m_y(\partial_x z_b^*+z\partial_x H)\partial_z p+\partial_z\left(m_x m_y\frac{A_v}{H}\partial_z u\right)+Q_x\end{aligned}\tag{A.1}$$

$$\begin{aligned}&\partial_t(m_x m_y Hv)+\partial_x(m_y Huv)+\partial_y(m_x Hvv)+\partial_z(m_x m_y wv)+f_e m_x m_y Hu\\&=-m_x H\partial_y(p+p_{atm}+\phi)+m_x(\partial_y z_b^*+z\partial_y H)\partial_z p+\partial_z\left(m_x m_y\frac{A_v}{H}\partial_z v\right)+Q_y\end{aligned}\tag{A.2}$$

$$m_x m_y f_e = m_x m_y f - u\partial_y m_x + v\partial_x m_y \tag{A.3}$$

$$(\tau_{xz},\tau_{yz})=A_v H^{-1}\partial_z(u,v) \tag{A.4}$$

where u and v are the horizontal velocity components in the curvilinear horizontal coordinates x and y, respectively. The scale factors of the horizontal coordinates are m_x and m_y. The vertical velocity in the stretched vertical coordinate z is w. The physical vertical coordinates of the free surface and bottom bed are z_s*, and z_b* respectively. The total water column depth is H, and ϕ is the free surface potential, which is equal to $g\,z_s$*. The effective Coriolis acceleration f_e incorporates the curvature acceleration terms according to (A.3). The Q terms in (A.1 and A.2) represent optional horizontal momentum diffusion terms. The vertical turbulent viscosity A_v relates the shear stresses to the vertical shear of the horizontal velocity components by (A.4). The kinematic atmospheric pressure, referenced to water density, is p_{atm}; the excess hydrostatic pressure in the water column is given by

$$\partial_z p = -gHb = -gH(\rho-\rho_o)\rho_o^{-1} \tag{A.5}$$

where ρ and ρ_o are the actual and reference water densities and b is the buoyancy. The three-dimensional continuity equation in the stretched vertical and curvilinear horizontal coordinate system is

$$\partial_t(m_x m_y H)+\partial_x(m_y Hu)+\partial_y(m_x Hv)+\partial_z(m_x m_y w)=Q_H \tag{A.6}$$

with Q_H representing volume sources and sinks including rainfall, evaporation, infiltration, and lateral inflows and outflows having negligible momentum fluxes. The generic three-dimensional transport and transformation equation for a dissolved or suspended material represented by the concentration variable C is

$$\partial_t\left(m_x m_y HC\right)+\partial_x\left(m_y HuC\right)+\partial_y\left(m_x HvC\right)+\partial_z\left(m_x m_y wC\right)$$
$$=\partial_x\left(\frac{m_y}{m_x}HA_H\partial_x C\right)+\partial_y\left(\frac{m_x}{m_y}HA_H\partial_y C\right)+\partial_z\left(\frac{m_x m_y}{H}A_b\partial_z C\right)+m_x m_y HR_C \qquad \text{(A.7)}$$

where A_H and A_b are horizontal and vertical turbulent mass diffusion coefficients and R_C represents physical and biogeochemical sources and sinks. The horizontal mass diffusion terms in (A.7) are generally omitted in the numerical solution when the model is configured for three-dimensional simulation.

Vertical boundary conditions for the solution of the momentum equations are based on the specification of the kinematic shear stresses

$$\left(\tau_{xz},\tau_{yz}\right)=\left(\tau_{bx},\tau_{by}\right)=c_b\sqrt{u_1^2+v_1^2}\left(u_1,v_1\right) \qquad \text{(A.8)}$$

and

$$\left(\tau_{xz},\tau_{yz}\right)=\left(\tau_{sx},\tau_{sy}\right)=c_s\sqrt{U_w^2+V_w^2}\left(U_w,V_w\right) \qquad \text{(A.9)}$$

at the bottom, $z=0$, and free surface, $z=1$, respectively, with U_w and V_w being the components of the wind velocity at 10 meters above the water surface. The subscript *1* refers to velocity and elevation at the mid-point of the bottom layer. The bottom drag coefficient is given by

$$c_b=\left(\frac{\kappa}{\ln(\Delta_1/2z_o)}\right)^2 \qquad \text{(A.10)}$$

where κ, is the von Karman constant, Δ_1 is the dimensionless thickness of the bottom layer, and $z_o=z_o^*/H$ is the dimensionless roughness height. The wind stress coefficient is given by

$$c_s=0.001\frac{\rho_a}{\rho_w}\left(0.8+0.065\sqrt{U_w^2+V_w^2}\right) \qquad \text{(A.11)}$$

for the wind velocity components in meters per second, with ρ_a and ρ_w denoting air and water densities. respectively. A no flux vertical boundary condition is used for the transport equation (A.7) when C represents salinity. Turbulent viscosity and diffusion coefficients in the momentum and transport equations, respectively, are determined using a turbulence closure model (Galperin et al. 1988; Mellor and Yamada 1982). The numerical solution procedures used in the EFDC model are documented by Hamrick (1992) and summarized in Hamrick and Wu (1997).

For thermal transport and temperature simulations, the water surface heat flux for the transport equation (A.7), when C represents heat ($C=\rho wcpwT$) is:

$$J_{TS} = \varepsilon\sigma T_s^4\left(0.39 - 0.05e_a^{1/2}\right)\left(1 - B_c C_c\right) + 4\varepsilon\sigma T_s^3\left(T_s - T_a\right)$$
$$+c_h\rho_a c_{pa}\sqrt{U_w^2 + V_w^2}\left(T_s - T_a\right) + c_e\rho_a L\sqrt{U_w^2 + V_w^2}\left(e_{ss} - R_h e_{sa}\right)\left(0.622\, p_a^{-1}\right) - I_S \qquad \text{(A.12)}$$

where *cpw* is the specific heat of water. The heat fluxes on the right of (17) are based on the NOAA Geophysical Fluid Dynamic Laboratory's atmospheric heat exchange formulation[31]. The first two terms represent net longwave back radiation where *Ts* and *Ta* are the water surface and atmospheric temperatures, ε is the emissivity, σ is the Stefan-Boltzman constant, *ea* is the atmospheric vapor pressure in millibars, *Cc* is the fractional cloud cover, and *Bc* is an empirical constant equal to 0.8. The third term is the convective or sensible heat flux where *ch* is a dimensionless transfer coefficient on the order of 10^{-3} in magnitude, □*a* is the atmospheric density, and *cpa* is the specific heat of air. The last term represents latent heat transfer where *ce* is a dimensionless transfer coefficient on the order of 10^{-3} in magnitude, *L* is the latent heat of evaporation, *ess* and *esa* are the saturation vapor pressures in millibars corresponding to the water surface and atmospheric temperatures respectively, *Rh* is the fractional relative humidity, and *pa* is the atmospheric pressure in millibars.

The incident shortwave solar radiation, *Is* at the water surface (watts/square meter) is given by

$$I_s = 0.5 I_o\left(1 - A_\alpha + \tau^{\sec\psi}\right)\left(1 - \alpha\right)\left(1 - 0.62 C_c + 0.0019\beta\right) \qquad \text{(A.13)}$$

where I_s is the shortwave solar radiation at the top of the atmosphere, A_a is water vapor plus ozone adsorption coefficient (0.09), τ is the atmospheric attenuation coefficient (0.7), ψ is the zenith angle, α is the surface albedo, and β is the solar noon angle in degrees.

The bottom heat flux is

$$J_{TB} = c_{hb}\rho_w c_{pw}\sqrt{u_1^2 + v_1^2}\left(T_B - T\right) - I_B \qquad \text{(A.14)}$$

where *Tb* is the bed temperature, *Hb* is the active thermal thickness of the bed, ρb is the density and *cpb* is the specific heat of the water-solid bed mixture, *chb* is a dimensionless convective heat exchange coefficient on the order of 1E-3. The remaining irradiance at the sediment bed-water interface being adsorbed into the sediment bed is

$$I_B = rI_S\exp\left(-\beta_f H\right) + \left(1 - r\right)I_S\exp\left(-\beta_s H\right) \qquad \text{(A.15)}$$

where β_f and β_s are fast and slow scale attenuation coefficients (1/meters), and *r* is a distribution fraction between zero and one. For shallow water environments, *r* is set to one and β_f generally falls within the range of 0.2 to 4 per meter. The thermal balance for the bed is given by

$$\partial_t\left(\rho_b c_{pb} H_b T_b\right) = I_b - c_{hb}\rho_w c_{pw}\sqrt{u_1^2 + v_1^2}\left(T_b - T_1\right) \qquad \text{(A.16)}$$

Equation (A.16) serves to couple the bed with the water column.

APPENDIX B: WATER QUALITY MODEL FORMULATION

This section summarizes the basic theory of the water quality-eutrophication component of the EFDC model. The kinetic processes included in the EFDC water quality model are mostly from the Chesapeake Bay three-dimensional water quality model, CE-QUAL-ICM (Cerco and Cole 1994). A more detailed description of the water quality model can be found in the report by Park et al. (1995). Table B-1 lists the model's complete set of state variables and their interactions are illustrated in Figure B-1. As opposed to earlier water quality model's such as WASP (Ambrose et al. 1992), which use biochemical oxygen demand to represent oxygen demanding organic material, the EFDC water quality model is carbon based. The four algae species are represented in carbon units. The three organic carbon variables play an equivalent role to BOD. Organic carbon, nitrogen and phosphorous can be represented by up to three reactive sub-classes, refractory particulate, labile particulate and labile dissolve. The use of the sub-classes allows a more realistic distribution of organic material by reactive classes when data is to estimate distribution factors. The following sub-sections discuss the role of each variable and summarize there kinetic interaction processes. The kinetic processes include the exchange of fluxes at the sediment-water interface, including sediment oxygen demand. The description of the EFDC water column water quality model in this section is from Park et al. (1995).

Table B-1. EFDC model water quality state variables

(1) cyanobacteria	(12) labile particulate organic nitrogen
(2) diatom algae	(13) dissolved organic nitrogen
(3) green algae	(14) ammonia nitrogen
(4) refractory particulate organic carbon	(15) nitrate nitrogen
(5) labile particulate organic carbon	(16) particulate biogenic silica
(6) dissolved organic carbon	(17) dissolved available silica
(7) refractory particulate organic phosphorus	(18) chemical oxygen demand
(8) labile particulate organic phosphorus	(19) dissolved oxygen
(9) dissolved organic phosphorus	(20) total active metal
(10) total phosphate	(21) fecal coliform bacteria
(11) refractory particulate organic nitrogen	

B.1 Model State Variables

B.1.1 Algae

Algae are grouped into four model classes: cyanobacteria, diatoms, greens, and macroalgae. The grouping is based upon the distinctive characteristics of each class and upon the significant role the characteristics play in the ecosystem. Cyanobacteria, commonly called blue-green algae, are characterized by their abundance (as picoplankton) in saline water and by their bloom-forming characteristics in fresh water. Cyanobacteria are unique in that some species fix atmospheric nitrogen, although nitrogen fixers are not believed to be predominant in many river systems. Diatoms are distinguished by their requirement of silica as a nutrient to form cell walls. Diatoms are large algae characterized by high settling velocities. Settling of spring diatom blooms to the

sediments may be a significant source of carbon for sediment oxygen demand. Algae that do not fall into the preceding two groups are lumped into the heading of green algae. Green algae settle at a rate intermediate between cyanobacteria and diatoms and are subject to greater grazing pressure than cyanobacteria.

B.1.2 Organic Carbon

Three organic carbon state variables are considered: dissolved, labile particulate, and refractory particulate. Labile and refractory distinctions are based upon the time scale of decomposition. Labile organic carbon decomposes on a time scale of days to weeks whereas refractory organic carbon requires more time. Labile organic carbon decomposes rapidly in the water column or the sediments. Refractory organic carbon decomposes slowly, primarily in the sediments, and may contribute to sediment oxygen demand years after deposition.

B.1.3 Nitrogen

Nitrogen is first divided into organic and mineral fractions. Organic nitrogen state variables are dissolved organic nitrogen, labile particulate organic nitrogen, and refractory particulate organic nitrogen. Two mineral nitrogen forms are considered: ammonium and nitrate. Both are utilized to satisfy algal nutrient requirements, although ammonium is preferred from thermodynamic considerations. The primary reason for distinguishing the two is that ammonium is oxidized by nitrifying bacteria into nitrate. This oxidation can be a significant sink of oxygen in the water column and sediments. An intermediate in the complete oxidation of ammonium, nitrite, also exists. Nitrite concentrations are usually much less than nitrate, and for modeling purposes, nitrite is combined with nitrate. Hence the nitrate state variable actually represents the sum of nitrate plus nitrite.

B.1.4 Phosphorus

As with carbon and nitrogen, organic phosphorus is considered in three states: dissolved, labile particulate, and refractory particulate. Only a single mineral form, total phosphate, is considered. Total phosphate exists as several states within the model ecosystem: dissolved phosphate, phosphate sorbed to inorganic solids, and phosphate incorporated in algal cells. Equilibrium partition coefficients are used to distribute the total among the three states.

B.1.5 Silica

Silica is divided into two state variables: available silica and particulate biogenic silica. Available silica is primarily dissolved and can be utilized by diatoms. Particulate biogenic silica cannot be utilized. In the model, particulate biogenic silica is produced through diatom mortality. Particulate biogenic silica undergoes dissolution to available silica or else settles to the bottom sediments.

B.1.6 Chemical Oxygen Demand

In the context of this study, chemical oxygen demand is the concentration of reduced substances that are oxidizable by inorganic means. The primary component of chemical oxygen demand is sulfide released from sediments. Oxidation of sulfide to sulfate may remove substantial quantities of dissolved oxygen from the water column.

B.1.7 Dissolved Oxygen

Dissolved oxygen is required for the existence of higher life forms. Oxygen availability determines the distribution of organisms and the flows of energy and nutrients in an ecosystem. Dissolved oxygen is a central component of the water quality model.

B.1.8 Total Active Metal

Both phosphate and dissolved silica sorb to inorganic solids, primarily iron and manganese. Sorption and subsequent settling is one pathway for removal of phosphate and silica from the water column. Consequently, the concentration and transport of iron and manganese are represented in the model. However, limited data do not allow a complete treatment of iron and manganese chemistry. Rather, a single-state variable, total active metal, is defined as the total concentration of metals that are active in phosphate and silica transport. Total active metal is partitioned between particulate and dissolved phases by an oxygen-dependent partition coefficient.

B.1.9 Salinity

Salinity is a conservative tracer that provides verification of the transport component of the model and facilitates examination of conservation of mass. Salinity also influences the dissolved oxygen saturation concentration and is used in the determination of kinetics constants that differ in saline and fresh water. Salinity is simulated in the hydrodynamic component of the model.

B.1.10 Temperature

Temperature is a primary determinant of the rate of biochemical reactions. Reaction rates increase as a function of temperature, although extreme temperatures result in the mortality of organisms. Temperature is simulated in the hydrodynamic component of the model.

B.2 Conservation of Mass Equation

The governing mass-balance equation for each of the water quality state variables may be expressed as:

$$\frac{\partial C}{\partial t} + \frac{\partial (u C)}{\partial x} + \frac{\partial (v C)}{\partial y} + \frac{\partial (w C)}{\partial z} = \frac{\partial}{\partial x}\left(K_x \frac{\partial C}{\partial x}\right) + \frac{\partial}{\partial y}\left(K_y \frac{\partial C}{\partial y}\right) + \frac{\partial}{\partial z}\left(K_z \frac{\partial C}{\partial z}\right) + S_C \qquad \text{(B.1)}$$

where

C = concentration of a water quality state variable
u, v, w = velocity components in the x-, y-, and z-directions, respectively
K_x, K_y, K_z = turbulent diffusivities in the x-, y-, and z-directions, respectively
SC = internal and external sources and sinks per unit volume.

The last three terms on the left-hand side (LHS) of equation B.1 account for the advective transport, and the first three terms on the right-hand side (RHS) of equation B.1 account for the diffusive transport. These six terms for physical transport are analogous to, and thus the numerical method of solution is the same as, those in the mass-balance equation for salinity in

the hydrodynamic model (Hamrick 1992). The last term in equation B.1 represents the kinetic processes and external loads for each of the state variables. The present model solves equation B.1 after decoupling the kinetic terms from the physical transport terms. The solution scheme for both the physical transport (Hamrick 1992) and the kinetic equations is second-order accurate.

The governing mass-balance equation for water quality state variables (equation B.1) consists of physical transport, advective and diffusive, and kinetic processes. When solving equation B.1, the kinetic terms are decoupled from the physical transport terms. The mass-balance equation for physical transport only, which takes the same form as the salt-balance equation, is:

$$\frac{\partial C}{\partial t}+\frac{\partial (uC)}{\partial x}+\frac{\partial (vC)}{\partial y}+\frac{\partial (wC)}{\partial z}=\frac{\partial}{\partial x}\left(K_x\frac{\partial C}{\partial x}\right)+\frac{\partial}{\partial y}\left(K_y\frac{\partial C}{\partial y}\right)+\frac{\partial}{\partial z}\left(K_z\frac{\partial C}{\partial z}\right) \qquad \text{(B.2)}$$

The equation for kinetic processes only, which will be referred to as the kinetic equation, is:

$$\frac{\partial C}{\partial t}=S_C \qquad \text{(B.3)}$$

which may be expressed as:

$$\frac{\partial C}{\partial t}=K\bullet C+R \qquad \text{(B.4)}$$

where K is kinetic rate (time^{-1}) and R is source/sink term (mass volume^{-1} time^{-1}). Equation B.4 is obtained by linearizing some terms in the kinetic equations, mostly Monod type expressions. Hence, K and R are known values in equation B.4. Equation B.2 is identical to, and thus its numerical method of solution is the same as, the mass-balance equation for salinity (Hamrick 1992).

The remainder of this chapter details the kinetics portion of the mass-conservation equation for each state variable. Parameters are defined where they first appear. All parameters are listed, in alphabetical order, in an appendix. For consistency with reported rate coefficients, kinetics are detailed using a temporal dimension of days. Within the CE-QUAL-ICM computer code, kinetics sources and sinks are converted to a dimension of seconds before employment in the mass-conservation equation.

B.2.1 Algae

Algae, which occupy a central role in the model (Figure B-1), are grouped into three model state variables: cyanobacteria (blue-green algae), diatoms, and green algae. The subscript, ***x***, is used to denote four algal groups: **c** for cyanobacteria, **d** for diatoms, **g** for green algae, and **m** for macroalgae. Sources and sinks included in the model are:

- Growth (production)
- Basal metabolism

- Predation
- Settling
- External loads

Equations describing these processes are largely the same for the four algal groups with differences in the values of parameters in the equations. The kinetic equation describing these processes is:

$$\frac{\partial B_x}{\partial t} = (P_x - BM_x - PR_x) B_x + \frac{\partial}{\partial z}(WS_x \bullet B_x) + \frac{WB_x}{V} \qquad \text{(B.5)}$$

B_x = algal biomass of algal group x (g C m^{-3})
t = time (day)
P_x = production rate of algal group x (day^{-1})
BM_x = basal metabolism rate of algal group x (day^{-1})
PR_x = predation rate of algal group x (day^{-1})
WS_x = settling velocity of algal group x (m day^{-1})
WB_x = external loads of algal group x (g C day^{-1})
V = cell volume (m^3).

Production (Algal Growth)

Algal growth depends on nutrient availability, ambient light, and temperature. The effects of these processes are considered to be multiplicative:

$$P_x = PM_x \bullet f_1(N) \bullet f_2(I) \bullet f_3(T) \qquad \text{(B.6)}$$

PM_x = maximum growth rate under optimal conditions for algal group x (day^{-1})
$f_1(N)$ = effect of suboptimal nutrient concentration ($0 \le f_1 \le 1$)
$f_2(I)$ = effect of suboptimal light intensity ($0 \le f_2 \le 1$)
$f_3(T)$ = effect of suboptimal temperature ($0 \le f_3 \le 1$).

The freshwater cyanobacteria may undergo rapid mortality in salt water, e.g., freshwater organisms in the Potomac River (Thomann et al. 1985). For the freshwater organisms, the increased mortality may be included in the model by retaining the salinity toxicity term in the growth equation for cyanobacteria:

$$P_c = PM_c \bullet f_1(N) \bullet f_2(I) \bullet f_3(T) \bullet f_4(S) \qquad \text{(B.7)}$$

$f_4(S)$ = effect of salinity on cyanobacteria growth ($0 \le f_4 \le 1$).

Activation of the salinity toxicity term, f_4 (S), is an option in the source code.

Effect of Nutrients on Algal Growth

Using Liebig's "law of the minimum" (Odum 1971) that growth is determined by the nutrient in least supply, the nutrient limitation for growth of cyanobacteria and green algae is expressed as:

$$f_1(N) = minimum\left(\frac{NH4 + NO3}{KHN_x + NH4 + NO3}, \frac{PO4d}{KHP_x + PO4d}\right) \quad \text{(B.8)}$$

NH4 = ammonium nitrogen concentration (g N m^{-3})
NO3 = nitrate nitrogen concentration (g N m^{-3})
KHN_x = half-saturation constant for nitrogen uptake for algal group *x* (g N m^{-3})
PO4d = dissolved phosphate phosphorus concentration (g P m^{-3})
KHP_x = half-saturation constant for phosphorus uptake for algal group *x* (g P m^{-3}).

Some cyanobacteria (e.g., *Anabaena*) can fix nitrogen from atmosphere and thus are not limited by nitrogen. Hence, equation B.8 is not applicable to the growth of nitrogen fixers.

Since diatoms require silica as well as nitrogen and phosphorus for growth, the nutrient limitation for diatoms is expressed as:

$$f_1(N) = minimum\left(\frac{NH4 + NO3}{KHN_d + NH4 + NO3}, \frac{PO4d}{KHP_d + PO4d}, \frac{SAd}{KHS + SAd}\right) \quad \text{(B.9)}$$

SAd = concentration of dissolved available silica (g Si m^{-3})
KHS = half-saturation constant for silica uptake for diatoms (g Si m^{-3}).

Effect of Light on Algal Growth

The daily and vertically integrated form of Steele's equation is:

$$f_2(I) = \frac{2.718 \bullet FD}{Kess \bullet \Delta z}\left(e^{-\alpha_B} - e^{-\alpha_T}\right) \quad \text{(B.10)}$$

$$\alpha_B = \frac{I_o}{FD \bullet (I_s)_x} \bullet \exp\left(-Kess\,[H_T + \Delta z]\right) \quad \text{(B.11)}$$

$$\alpha_T = \frac{I_o}{FD \bullet (I_s)_x} \bullet \exp\left(-Kess \bullet H_T\right) \quad \text{(B.12)}$$

FD = fractional daylength ($0 \le FD \le 1$)
Kess = total light extinction coefficient (m^{-1})
Δz = layer thickness (m)

I_o = daily total light intensity at water surface (langleys day^{-1})
$(I_s)_x$ = optimal light intensity for algal group x (langleys day^{-1})
H_T = depth from the free surface to the top of the layer (m).

Light extinction in the water column consists of three fractions in the model: a background value dependent on water color, extinction due to suspended particles, and extinction due to light absorption by ambient chlorophyll:

$$Kess = Ke_b + Ke_{TSS} \bullet TSS + Ke_{Chl} \bullet \sum_{x=c,d,g} \left(\frac{B_x}{CChl_x}\right) \qquad \text{(B.13)}$$

Ke_b = background light extinction (m^{-1})
Ke_{TSS} = light extinction coefficient for total suspended solid (m^{-1} per g m^{-3})
TSS = total suspended solid concentration (g m^{-3}) provided from the hydrodynamic model
Ke_{Chl} = light extinction coefficient for chlorophyll 'a' (m^{-1} per mg Chl m^{-3})
$CChl_x$ = carbon-to-chlorophyll ratio in algal group x (g C per mg Chl).

For a model application that does not simulate TSS, the Ke_{TSS} term may be set to zero and Ke_b may be estimated to include light extinction due to suspended solid.

Optimal light intensity (I_s) for photosynthesis depends on algal taxonomy, duration of exposure, temperature, nutritional status, and previous acclimation. Variations in I_s are largely due to adaptations by algae intended to maximize production in a variable environment. Steel (1962) noted the result of adaptations is that optimal intensity is a consistent fraction (approximately 50 percent) of daily intensity. Kremer and Nixon (1978) reported an analogous finding that maximum algal growth occurs at a constant depth (approximately 1 m) in the water column. Their approach is adopted so that optimal intensity is expressed as:

$$(I_s)_x = maximum\left\{(I_o)_{avg} \bullet e^{-Kess \bullet (D_{opt})_x}, (I_s)_{\min}\right\} \qquad \text{(B.14)}$$

$(D_{opt})_x$ = depth of maximum algal growth for algal group x (m)
$(I_o)_{avg}$ = adjusted surface light intensity (langleys day^{-1}).

A minimum, $(I_s)_{\min}$, in equation B.14 is specified so that algae do not thrive at extremely low light levels. The time required for algae to adapt to changes in light intensity is recognized by estimating $(I_s)_x$ based on a time-weighted average of daily light intensity:

$$(I_o)_{avg} = CI_a \bullet I_o + CI_b \bullet I_1 + CI_c \bullet I_2 \qquad \text{(B.15)}$$

I_1 = daily light intensity 1 day preceding model day (langleys day^{-1})
I_2 = daily light intensity 2 days preceding model day (langleys day^{-1})
CI_a, CI_b, CI_c = weighting factors for I_0, I_1 and I_2, respectively: $CI_a + CI_b + CI_c = 1$.

Effect of Temperature on Algal Growth

A Gaussian probability curve is used to represent temperature dependency of algal growth:

$$f_3(T) = \exp\left(-KTG1_x [T - TM_x]^2\right) \quad if \quad T \le TM_x$$
$$= \exp\left(-KTG2_x [TM_x - T]^2\right) \quad if \quad T > TM_x \qquad \text{(B.16)}$$

T = temperature (°C) provided from the hydrodynamic model
TM_x = optimal temperature for algal growth for algal group x (°C)
$KTG1_x$ = effect of temperature below TM_x on growth for algal group x ($°C^{-2}$)
$KTG2_x$ = effect of temperature above TM_x on growth for algal group x ($°C^{-2}$).

Effect of Salinity on Growth of Freshwater Cyanobacteria

The growth of freshwater cyanobacteria in salt water is limited by:

$$f_4(S) = \frac{STOX^2}{STOX^2 + S^2} \qquad \text{(B.17)}$$

$STOX$ = salinity at which Microcystis growth is halved (ppt)
S = salinity in water column (ppt) provided from the hydrodynamic model.

Algal Basal Metabolism

Algal biomass in the present model decreases through basal metabolism (respiration and excretion) and predation. Basal metabolism in the present model is the sum of all internal processes that decrease algal biomass and consists of two parts; respiration and excretion. In basal metabolism, algal matter (carbon, nitrogen, phosphorus, and silica) is returned to organic and inorganic pools in the environment, mainly to dissolved organic and inorganic matter. Respiration, which may be viewed as a reversal of production, consumes dissolved oxygen. Basal metabolism is considered to be an exponentially increasing function of temperature:

$$BM_x = BMR_x \bullet \exp\left(KTB_x [T - TR_x]\right) \qquad \text{(B.18)}$$

BMR_x = basal metabolism rate at TR_x for algal group x (day^{-1})
KTB_x = effect of temperature on metabolism for algal group x ($°C^{-1}$)
TR_x = reference temperature for basal metabolism for algal group x (°C).

Algal Predation

The present model does not include zooplankton. Instead, a constant rate is specified for algal predation, which implicitly assumes zooplankton biomass is a constant fraction of algal biomass. An equation similar to that for basal metabolism (equation B.18) is used for predation:

$$PR_x = PRR_x \bullet \exp\left(KTB_x\,[T - TR_x]\right) \qquad \text{(B.19)}$$

PRR_x = predation rate at TR_x for algal group x (day^{-1}).

The difference between predation and basal metabolism lies in the distribution of the end products of the two processes. In predation, algal matter (carbon, nitrogen, phosphorus, and silica) is returned to organic and inorganic pools in the environment, mainly to particulate organic matter.

Algal Settling

Settling velocities for four algal groups, WS_c, WS_d, WS_g, and WS_m, are specified as an input. Seasonal variations in settling velocity of diatoms can be accounted for by specifying time-varying WS_d.

B.2.2 Organic Carbon

The present model has three state variables for organic carbon: refractory particulate, labile particulate, and dissolved.

Particulate Organic Carbon

Labile and refractory distinctions are based on the time scale of decomposition. Labile particulate organic carbon with a decomposition time scale of days to weeks decomposes rapidly in the water column or in the sediments. Refractory particulate organic carbon with a longer-than-weeks decomposition time scale decomposes slowly, primarily in the sediments, and may contribute to sediment oxygen demand years after decomposition. For labile and refractory particulate organic carbon, sources and sinks included in the model are (Figure B-1):

- Algal predation
- Dissolution to dissolved organic carbon
- Settling
- External loads.

The governing equations for refractory and labile particulate organic carbons are:

$$\frac{\partial\, RPOC}{\partial t} = \sum_{x=c,d,g,m} FCRP \bullet PR_x \bullet B_x - K_{RPOC} \bullet RPOC + \frac{\partial}{\partial z}\left(WS_{RP} \bullet RPOC\right) + \frac{WRPOC}{V} \qquad \text{(B.20)}$$

$$\frac{\partial\, LPOC}{\partial t} = \sum_{x=c,d,g,m} FCLP \bullet PR_x \bullet B_x - K_{LPOC} \bullet LPOC + \frac{\partial}{\partial z}\left(WS_{LP} \bullet LPOC\right) + \frac{WLPOC}{V} \qquad \text{(B.21)}$$

$RPOC$ = concentration of refractory particulate organic carbon (g C m^{-3})
$LPOC$ = concentration of labile particulate organic carbon (g C m^{-3})

$FCRP$ = fraction of predated carbon produced as refractory particulate organic carbon
$FCLP$ = fraction of predated carbon produced as labile particulate organic carbon
K_{RPOC} = dissolution rate of refractory particulate organic carbon (day^{-1})
K_{LPOC} = dissolution rate of labile particulate organic carbon (day^{-1})
WS_{RP} = settling velocity of refractory particulate organic matter (m day^{-1})
WS_{LP} = settling velocity of labile particulate organic matter (m day^{-1})
$WRPOC$ = external loads of refractory particulate organic carbon (g C day^{-1})
$WLPOC$ = external loads of labile particulate organic carbon (g C day^{-1}).

Dissolved Organic Carbon

Sources and sinks for dissolved organic carbon included in the model are (Figure B-1):

- Algal excretion (exudation) and predation
- Dissolution from refractory and labile particulate organic carbon
- Heterotrophic respiration of dissolved organic carbon (decomposition)
- Denitrification
- External loads

The kinetic equation describing these processes is:

$$\frac{\partial DOC}{\partial t} = \sum_{x=c,d,g,m} \left(\left[FCD_x + (1 - FCD_x) \frac{KHR_x}{KHR_x + DO} \right] \bullet BM_x + FCDP \bullet PR_x \right) \bullet B_x$$

$$+ K_{RPOC} \bullet RPOC + K_{LPOC} \bullet LPOC - K_{HR} \bullet DOC - Denit \bullet DOC + \frac{WDOC}{V} \qquad \text{(B.22)}$$

DOC = concentration of dissolved organic carbon (g C m^{-3})
FCD_x = fraction of basal metabolism exuded as dissolved organic carbon at infinite dissolved oxygen concentration for algal group x
KHR_x = half-saturation constant of dissolved oxygen for algal dissolved organic carbon excretion for group x (g O_2 m^{-3})
DO = dissolved oxygen concentration (g O_2 m^{-3})
$FCDP$ = fraction of predated carbon produced as dissolved organic carbon
K_{HR} = heterotrophic respiration rate of dissolved organic carbon (day^{-1})
$Denit$ = denitrification rate (day^{-1}) given in equation B.34
$WDOC$ = external loads of dissolved organic carbon (g C day^{-1}).

The remainder of this section explains each term in equations B.20 to B.22.

Effect of Algae on Organic Carbon

The terms within summation ($\sum$) in equations B.20 to B.22 account for the effects of algae on organic carbon through basal metabolism and predation.

Basal Metabolism.

Basal metabolism, consisting of respiration and excretion, returns algal matter (carbon, nitrogen, phosphorus, and silica) back to the environment. Loss of algal biomass through basal metabolism is (Eq. C.18):

$$\frac{\partial B_x}{\partial t} = -BM_x \bullet B_x \qquad \text{(B.23)}$$

which indicates that the total loss of algal biomass due to basal metabolism is independent of ambient dissolved oxygen concentration. In this model, it is assumed that the distribution of total loss between respiration and excretion is constant as long as there is sufficient dissolved oxygen for algae to respire. Under that condition, the losses by respiration and excretion may be written as:

$$(1 - FCD_x) \bullet BM_x \bullet B_x \text{ due to respiration} \qquad \text{(B.24)}$$

$$FCD_x \bullet BM_x \bullet B_x \text{ due to excretion} \qquad \text{(B.25)}$$

where FCD_x is a constant of value between 0 and 1. Algae cannot respire in the absence of oxygen, however. Although the total loss of algal biomass due to basal metabolism is oxygen-independent (equation B.23), the distribution of total loss between respiration and excretion is oxygen-dependent. When oxygen level is high, respiration is a large fraction of the total. As dissolved oxygen becomes scarce, excretion becomes dominant. Thus, equation B.24 represents the loss by respiration only at high oxygen levels. In general, equation B.24 can be decomposed into two fractions as a function of dissolved oxygen availability:

$$(1 - FCD_x) \frac{DO}{KHR_x + DO} BM_x \bullet B_x \text{ due to respiration} \qquad \text{(B.26)}$$

$$(1 - FCD_x) \frac{KHR_x}{KHR_x + DO} BM_x \bullet B_x \text{ due to excretion} \qquad \text{(B.27)}$$

Equation B.26 represents the loss of algal biomass by respiration, and equation B.27 represents additional excretion due to insufficient dissolved oxygen concentration. The parameter KHR_x, which is defined as the half-saturation constant of dissolved oxygen for algal dissolved organic carbon excretion in equation B.22, can also be defined as the half-saturation constant of dissolved oxygen for algal respiration in equation B.26.

Combining equations B.25 and B.27, the total loss due to excretion is:

$$\left(FCD_x + (1 - FCD_x) \frac{KHR_x}{KHR_x + DO} \right) BM_x \bullet B_x \qquad \text{(B.28)}$$

Equations B.26 and B.28 combine to give the total loss of algal biomass due to basal metabolism, $BM_x \cdot B_x$ (equation B.23). The definition of FCD_x in equation B.22 becomes apparent in equation B.28 (i.e., fraction of basal metabolism exuded as dissolved organic carbon at infinite dissolved oxygen concentration). At zero oxygen level, 100 percent of total loss due to basal metabolism is by excretion regardless of FCD_x. The end carbon product of respiration is primarily carbon dioxide, an inorganic form not considered in the present model, while the end carbon product of excretion is primarily dissolved organic carbon. Therefore, equation B.28, that appears in equation B.22, represents the contribution of excretion to dissolved organic carbon, and there is no source term for particulate organic carbon from algal basal metabolism in equations B.20 and B.21.

Predation.

Algae produce organic carbon through the effects of predation. Zooplankton take up and redistribute algal carbon through grazing, assimilation, respiration, and excretion. Since zooplankton are not included in the model, routing of algal carbon through zooplankton predation is simulated by empirical distribution coefficients in equations B.20 to B.22; *FCRP*, *FCLP*, and *FCDP*. The sum of these three predation fractions should be unity.

Heterotrophic Respiration and Dissolution

The second term on the RHS of Equations B.20 and B.21 represents dissolution of particulate to dissolved organic carbon and the third term in the second line of equation B.22 represents heterotrophic respiration of dissolved organic carbon. The oxic heterotrophic respiration is a function of dissolved oxygen: the lower the dissolved oxygen, the smaller the respiration term becomes. Heterotrophic respiration rate, therefore, is expressed using a Monod function of dissolved oxygen:

$$K_{HR} = \frac{DO}{KHOR_{DO} + DO} K_{DOC} \qquad \text{(B.29)}$$

$KHOR_{DO}$ = oxic respiration half-saturation constant for dissolved oxygen (g O_2 m^{-3})
K_{DOC} = heterotrophic respiration rate of dissolved organic carbon at infinite dissolved oxygen concentration (day^{-1}).

Dissolution and heterotrophic respiration rates depend on the availability of carbonaceous substrate and on heterotrophic activity. Algae produce labile carbon that fuels heterotrophic activity: dissolution and heterotrophic respiration do not require the presence of algae though, and may be fueled entirely by external carbon inputs. In the model, algal biomass, as a surrogate for heterotrophic activity, is incorporated into formulations of dissolution and heterotrophic

respiration rates. Formulations of these rates require specification of algal-dependent and algal-independent rates:

$$K_{RPOC} = \left(K_{RC} + K_{RCalg} \sum_{x=c,d,g} B_x \right) \exp\left(KT_{HDR} \left(T - TR_{HDR} \right) \right) \quad \text{(B.30)}$$

$$K_{LPOC} = \left(K_{LC} + K_{LCalg} \sum_{x=c,d,g} B_x \right) \exp\left(KT_{HDR} \left(T - TR_{HDR} \right) \right) \quad \text{(B.31)}$$

$$K_{DOC} = \left(K_{DC} + K_{DCalg} \sum_{x=c,d,g} B_x \right) \exp\left(KT_{HDR} \left(T - TR_{HDR} \right) \right) \quad \text{(B.32)}$$

K_{RC} = minimum dissolution rate of refractory particulate organic carbon (day^{-1})
K_{LC} = minimum dissolution rate of labile particulate organic carbon (day^{-1})
K_{DC} = minimum respiration rate of dissolved organic carbon (day^{-1})
K_{RCalg}, K_{LCalg} = constants that relate dissolution of refractory and labile particulate organic carbon, respectively, to algal biomass (day^{-1} per g C m^{-3})
K_{DCalg} = constant that relates respiration to algal biomass (day^{-1} per g C m^{-3})
KT_{HDR} = effect of temperature on hydrolysis of particulate organic matter ($°C^{-1}$)
TR_{HDR} = reference temperature for hydrolysis of particulate organic matter (°C)
KT_{MNL} = effect of temperature on mineralization of dissolved organic matter ($°C^{-1}$)
TR_{MNL} = reference temperature for mineralization of dissolved organic matter (°C).

Equations B.30 to B.32 have exponential functions that relate rates to temperature.

In the present model, the term "hydrolysis" is defined as the process by which particulate organic matter is converted to dissolved organic form, and thus includes both dissolution of particulate carbon and hydrolysis of particulate phosphorus and nitrogen. Therefore, the parameters, KT_{HDR} and TR_{HDR}, are also used for the temperature effects on hydrolysis of particulate phosphorus (equations B.28 and B.29) and nitrogen (equations B.53 and B.54). The term "mineralization" is defined as the process by which dissolved organic matter is converted to dissolved inorganic form, and thus includes both heterotrophic respiration of dissolved organic carbon and mineralization of dissolved organic phosphorus and nitrogen. Therefore, the parameters, KT_{MNL} and TR_{MNL}, are also used for the temperature effects on mineralization of dissolved phosphorus (equation B.45) and nitrogen (equation B.55).

Effect of Denitrification on Dissolved Organic Carbon

As oxygen is depleted from natural systems, organic matter is oxidized by the reduction of alternate electron acceptors. Thermodynamically, the first alternate acceptor reduced in the absence of oxygen is nitrate. The reduction of nitrate by a large number of heterotrophic

anaerobes is referred to as denitrification, and the stoichiometry of this reaction is (Stumm and Morgan 1981):

$$4\,NO_3^- + 4\,H^+ + 5\,CH_2O \rightarrow 2\,N_2 + 7\,H_2O + 5\,CO_2 \qquad \text{(B.33)}$$

The last term in equation B.22 accounts for the effect of denitrification on dissolved organic carbon. The kinetics of denitrification in the model are first-order:

$$Denit = \frac{KHOR_{DO}}{KHOR_{DO} + DO} \frac{NO3}{KHDN_N + NO3} AANOX \bullet K_{DOC} \qquad \text{(B.34)}$$

$KHDN_N$ = denitrification half-saturation constant for nitrate (g N m^{-3})
$AANOX$ = ratio of denitrification rate to oxic dissolved organic carbon respiration rate.

In equation B.34, the dissolved organic carbon respiration rate, K_{DOC}, is modified so that significant decomposition via denitrification occurs only when nitrate is freely available and dissolved oxygen is depleted. The ratio, $AANOX$, makes the anoxic respiration slower than oxic respiration. Note that K_{DOC}, defined in equation B.32, includes the temperature effect on denitrification.

B.2.3 Phosphorus

The present model has four state variables for phosphorus: three organic forms (refractory particulate, labile particulate, and dissolved) and one inorganic form (total phosphate).

Particulate Organic Phosphorus

For refractory and labile particulate organic phosphorus, sources and sinks included in the model are (Figure B-1):

- Algal basal metabolism and predation
- Dissolution to dissolved organic phosphorus
- Settling
- External loads.

The kinetic equations for refractory and labile particulate organic phosphorus are:

$$\frac{\partial RPOP}{\partial t} = \sum_{x=c,d,g,m} (FPR_x \bullet BM_x + FPRP \bullet PR_x)\, APC \bullet B_x - K_{RPOP} \bullet RPOP + \frac{\partial}{\partial z}(WS_{RP} \bullet RPOP) + \frac{WRPOP}{V} \qquad \text{(B.35)}$$

$$\frac{\partial LPOP}{\partial t} = \sum_{x=c,d,g,m} (FPL_x \bullet BM_x + FPLP \bullet PR_x) APC \bullet B_x - K_{LPOP} \bullet LPOP + \frac{\partial}{\partial z}(WS_{LP} \bullet LPOP) + \frac{WLPOP}{V} \quad \text{(B.36)}$$

$RPOP$ = concentration of refractory particulate organic phosphorus (g P m^{-3})
$LPOP$ = concentration of labile particulate organic phosphorus (g P m^{-3})
FPR_x = fraction of metabolized phosphorus by algal group x produced as refractory particulate organic phosphorus
FPL_x = fraction of metabolized phosphorus by algal group x produced as labile particulate organic phosphorus
$FPRP$ = fraction of predated phosphorus produced as refractory particulate organic phosphorus
$FPLP$ = fraction of predated phosphorus produced as labile particulate organic phosphorus
APC = mean algal phosphorus-to-carbon ratio for all algal groups (g P per g C)
K_{RPOP} = hydrolysis rate of refractory particulate organic phosphorus (day^{-1})
K_{LPOP} = hydrolysis rate of labile particulate organic phosphorus (day^{-1})
$WRPOP$ = external loads of refractory particulate organic phosphorus (g P day^{-1})
$WLPOP$ = external loads of labile particulate organic phosphorus (g P day^{-1}).

Dissolved Organic Phosphorus

Sources and sinks for dissolved organic phosphorus included in the model are (Figure B-1):

- Algal basal metabolism and predation
- Dissolution from refractory and labile particulate organic phosphorus
- Mineralization to phosphate phosphorus
- External loads.

The kinetic equation describing these processes is:

$$\frac{\partial DOP}{\partial t} = \sum_{x=c,d,g,m} (FPD_x \bullet BM_x + FPDP \bullet PR_x) APC \bullet B_x + K_{RPOP} \bullet RPOP + K_{LPOP} \bullet LPOP - K_{DOP} \bullet DOP + \frac{WDOP}{V} \quad \text{(B.37)}$$

DOP = concentration of dissolved organic phosphorus (g P m^{-3})
FPD_x = fraction of metabolized phosphorus by algal group x produced as dissolved organic phosphorus
$FPDP$ = fraction of predated phosphorus produced as dissolved organic phosphorus
K_{DOP} = mineralization rate of dissolved organic phosphorus (day^{-1})
$WDOP$ = external loads of dissolved organic phosphorus (g P day^{-1}).

Total Phosphate

For total phosphate that includes both dissolved and sorbed phosphate, sources and sinks included in the model are (Figure B-1):

- Algal basal metabolism, predation, and uptake
- Mineralization from dissolved organic phosphorus
- Settling of sorbed phosphate
- Sediment-water exchange of dissolved phosphate for the bottom layer only
- External loads

The kinetic equation describing these processes is:

$$\frac{\partial PO4t}{\partial t} = \sum_{x=c,d,g,m} (FPI_x \bullet BM_x + FPIP \bullet PR_x - P_x)\, APC \bullet B_x + K_{DOP} \bullet DOP + \frac{\partial}{\partial z}(WS_{TSS} \bullet PO4p) + \frac{BFPO4d}{\Delta z} + \frac{WPO4t}{V} \quad \text{(B.38)}$$

$PO4t$ = total phosphate (g P m^{-3}) = PO4d + PO4p
$PO4d$ = dissolved phosphate (g P m^{-3})
$PO4p$ = particulate (sorbed) phosphate (g P m^{-3})
FPI_x = fraction of metabolized phosphorus by algal group x produced as inorganic phosphorus
$FPIP$ = fraction of predated phosphorus produced as inorganic phosphorus
WS_{TSS} = settling velocity of suspended solid (m day^{-1}), provided by the hydrodynamic model
$BFPO4d$ = sediment-water exchange flux of phosphate (g P m^{-2} day^{-1}), applied to the bottom layer only
$WPO4t$ = external loads of total phosphate (g P day^{-1}).

In equation B.38, if total active metal is chosen as a measure of sorption site, the settling velocity of total suspended solid, WS_{TSS}, is replaced by that of particulate metal, WS_s. The remainder of this section explains each term in equations B.35 to B.38, except $BFPO4d$ (benthic flux of dissolved orthophosphate).

Total Phosphate System

Suspended and bottom sediment particles (clay, silt, and metal hydroxides) adsorb and desorb phosphate in river and estuarine waters. This adsorption-desorption process has been suggested to buffer phosphate concentration in water column and to enhance the transport of phosphate away from its external sources (Carritt and Goodgal 1954, Froelich 1988). To ease the computational complication due to the adsorption-desorption of phosphate, dissolved and sorbed phosphate are treated and transported as a single state variable. Therefore, the model phosphate state variable, total phosphate, is defined as the sum of dissolved and sorbed phosphate (equation B.39), and the concentrations for each fraction are determined by equilibrium partitioning of their sum.

In CE-QUAL-ICM, sorption of phosphate to particulate species of metals including iron and manganese was considered based on a phenomenon observed in the monitoring data from the mainstem of the Chesapeake Bay: phosphate was rapidly depleted from anoxic bottom waters during the autumn reaeration event (Cerco and Cole 1994). Their hypothesis was that reaeration of bottom waters caused dissolved iron and manganese to precipitate, and phosphate sorbed to newly formed metal particles and rapidly settled to the bottom. One state variable, total active metal, in CE-QUAL-ICM was defined as the sum of all metals that act as sorption sites, and the total active metal was partitioned into particulate and dissolved fractions via an equilibrium partitioning coefficient. Then phosphate was assumed to sorb to only the particulate fraction of the total active metal.

In the treatment of phosphate sorption in CE-QUAL-ICM, the particulate fraction of metal hydroxides was emphasized as a sorption site in bottom waters under anoxic conditions. Phosphorus is a highly particle-reactive element, and phosphate in solution reacts quickly with a wide variety of surfaces, being taken up by and released from particles (Froelich 1988). The present model has two options, total suspended solid and total active metal, as a measure of a sorption site for phosphate, and dissolved and sorbed fractions are determined by equilibrium partitioning of their sum as a function of total suspended solid or total active metal concentration:

$$PO4p = \frac{K_{PO}4p \bullet TSS}{1 + K_{PO}4p \bullet TSS} PO4t \quad \text{or} \quad PO4p = \frac{K_{PO}4p \bullet TAMp}{1 + K_{PO}4p \bullet TAMp} PO4t$$

$$PO4d = \frac{1}{1 + K_{PO}4p \bullet TSS} PO4t \quad \text{or} \quad PO4d = \frac{1}{1 + K_{PO}4p \bullet TAMp} PO4t \qquad \text{(B.39)}$$

$$= PO4t - PO4p \qquad \text{(B.40)}$$

$K_{PO}4p$ = empirical coefficient relating phosphate sorption to total suspended solid (per g m^{-3}) or particulate total active metal (per mol m^{-3}) concentration
$TAMp$ = particulate total active metal (mol m^{-3}).

Dividing equation B.39 by equation B.40 gives:

$$K_{PO}4p = \frac{PO4p}{PO4d} \frac{1}{TSS} \quad \text{or} \quad K_{PO}4p = \frac{PO4p}{PO4d} \frac{1}{TAMp} \qquad \text{(B.41)}$$

where the meaning of $K_{PO}4p$ becomes apparent, i.e., the ratio of sorbed to dissolved phosphate per unit concentration of total suspended solid or particulate total active metal (i.e., per unit sorption site available).

Algal Phosphorus-to-Carbon Ratio (APC)

Algal biomass is quantified in units of carbon per volume of water. In order to express the effects of algal biomass on phosphorus and nitrogen, the ratios of phosphorus-to-carbon and nitrogen-to-carbon in algal biomass must be specified. Although global mean values of these ratios are well known (Redfield et al. 1963), algal composition varies especially as a function of nutrient availability. As phosphorus and nitrogen become scarce, algae adjust their composition so that smaller quantities of these vital nutrients are required to produce carbonaceous biomass (DiToro 1980, Parsons et al. 1984). Examining the field data from the surface of upper Chesapeake Bay, Cerco and Cole (1993) showed that the variation of nitrogen-to-carbon stoichiometry was small and thus used a constant algal nitrogen-to-carbon ratio, ANC_x. Large variations, however, were observed for algal phosphorus-to-carbon ratio indicating the adaptation of algae to ambient phosphorus concentration (Cerco and Cole 1993): algal phosphorus content is high when ambient phosphorus is abundant and is low when ambient phosphorus is scarce. Thus, a variable algal phosphorus-to-carbon ratio, *APC*, is used in model formulation. A mean ratio for all algal groups, *APC*, is described by an empirical approximation to the trend observed in field data (Cerco and Cole 1994):

$$APC = \left(CP_{prm}1 + CP_{prm}2 \bullet \exp\left[-CP_{prm}3 \bullet PO4d \right] \right)^{-1} \qquad \text{(B.42)}$$

$CP_{prm}1$ = minimum carbon-to-phosphorus ratio (g C per g P)
$CP_{prm}2$ = difference between minimum and maximum carbon-to-phosphorus ratio (g C per g P)
$CP_{prm}3$ = effect of dissolved phosphate concentration on carbon-to-phosphorus ratio (per g P m^{-3}).

Effect of Algae on Phosphorus

The terms within summation in equations B.35 to B.38 account for the effects of algae on phosphorus. Both basal metabolism (respiration and excretion) and predation are considered, and thus formulated, to contribute to organic and phosphate phosphorus. That is, the total loss by basal metabolism ($BM_x \cdot B_x$ in equation B.5) is distributed using distribution coefficients (FPR_x, FPL_x, FPD_x, and FPI_x). The total loss by predation ($PR_x \cdot B_x$ in equation B.5), is also distributed using distribution coefficients (*FPRP, FPLP, FPDP*, and *FPIP*). The sum of four distribution coefficients for basal metabolism should be unity, and so is that for predation. Algae take up dissolved phosphate for growth, and algae uptake of phosphate is represented by ($- \sum P_x \cdot APC \cdot B_x$) in equation B.38.

Mineralization and Hydrolysis

The third term on the RHS of equations B.35 and B.36 represents hydrolysis of particulate organic phosphorus and the last term in equation B.7 represents mineralization of dissolved organic phosphorus. Mineralization of organic phosphorus is mediated by the release of nucleotidase and phosphatase enzymes by bacteria (Chróst and Overbek 1987) and algae (Boni et al. 1989). Since the algae themselves release the enzymes and bacterial abundance is related to

algal biomass, the rate of organic phosphorus mineralization is related to algal biomass in model formulation. Another mechanism included in model

formulation is that algae stimulate production of an enzyme that mineralizes organic phosphorus to phosphate when phosphate is scarce (Chróst and Overbek 1987, Boni et al. 1989). The formulations for hydrolysis and mineralization rates including these processes are:

$$K_{RPOP} = \left(K_{RP} + \frac{KHP}{KHP + PO4d} K_{RPalg} \sum_{x=c,d,g} B_x \right) \exp\left(KT_{HDR} \left(T - TR_{HDR} \right) \right) \qquad \text{(B.43)}$$

$$K_{LPOP} = \left(K_{LP} + \frac{KHP}{KHP + PO4d} K_{LPalg} \sum_{x=c,d,g} B_x \right) \exp\left(KT_{HDR} \left(T - TR_{HDR} \right) \right) \qquad \text{(B.44)}$$

$$K_{DOP} = \left(K_{DP} + \frac{KHP}{KHP + PO4d} K_{DPalg} \sum_{x=c,d,g} B_x \right) \exp\left(KT_{HDR} \left(T - TR_{HDR} \right) \right) \qquad \text{(B.45)}$$

K_{RP} = minimum hydrolysis rate of refractory particulate organic phosphorus (day^{-1})
K_{LP} = minimum hydrolysis rate of labile particulate organic phosphorus (day^{-1})
K_{DP} = minimum mineralization rate of dissolved organic phosphorus (day^{-1})
K_{RPalg}, K_{LPalg} = constants that relate hydrolysis of refractory and labile particulate organic phosphorus, respectively, to algal biomass (day^{-1} per g C m^{-3})
K_{DPalg} = constant that relates mineralization to algal biomass (day^{-1} per g C m^{-3})
KHP = mean half-saturation constant for algal phosphorus uptake (g P m^{-3})

$$= \frac{1}{3} \sum_{x=c,d,g} KHP_x \qquad \text{(B.46)}$$

When phosphate is abundant relative to *KHP*, the rates become close to the minimum values with little influence from algal biomass. When phosphate becomes scarce relative to *KHP*, the rates increase with the magnitude of increase depending on algal biomass. Equations B.43 to B.45 have exponential functions that relate rates to temperature.

B.2.4 Nitrogen

The present model has five state variables for nitrogen: three organic forms (refractory particulate, labile particulate, and dissolved) and two inorganic forms (ammonium and nitrate). The nitrate state variable in the model represents the sum of nitrate and nitrite.

Particulate Organic Nitrogen

For refractory and labile particulate organic nitrogen, sources and sinks included in the model are (Figure B-1):

- Algal basal metabolism and predation
- Dissolution to dissolved organic nitrogen
- Settling
- External loads

The kinetic equations for refractory and labile particulate organic nitrogen are:

$$\frac{\partial RPON}{\partial t} = \sum_{x=c,d,g,m} (FNR_x \bullet BM_x + FNRP \bullet PR_x) ANC_x \bullet B_x - K_{RPON} \bullet RPON + \frac{\partial}{\partial z}(WS_{RP} \bullet RPON) + \frac{WRPON}{V} \quad \text{(B.47)}$$

$$\frac{\partial LPON}{\partial t} = \sum_{x=c,d,g,m} (FNL_x \bullet BM_x + FNLP \bullet PR_x) ANC_x \bullet B_x - K_{LPON} \bullet LPON + \frac{\partial}{\partial z}(WS_{LP} \bullet LPON) + \frac{WLPON}{V} \quad \text{(B.48)}$$

$RPON$ = concentration of refractory particulate organic nitrogen (g N m^{-3})
$LPON$ = concentration of labile particulate organic nitrogen (g N m^{-3})
FNR_x = fraction metabolized nitrogen by algal group x as refractory particulate organic nitrogen
FNL_x = fraction of metabolized nitrogen by algal group x produced as labile particulate organic nitrogen
$FNRP$ = fraction of predated nitrogen produced as refractory particulate organic nitrogen
$FNLP$ = fraction of predated nitrogen produced as labile particulate organic nitrogen
ANC_x = nitrogen-to-carbon ratio in algal group x (g N per g C)
K_{RPON} = hydrolysis rate of refractory particulate organic nitrogen (day^{-1})
K_{LPON} = hydrolysis rate of labile particulate organic nitrogen (day^{-1})
$WRPON$ = external loads of refractory particulate organic nitrogen (g N day^{-1})
$WLPON$ = external loads of labile particulate organic nitrogen (g N day^{-1})

Dissolved Organic Nitrogen

Sources and sinks for dissolved organic nitrogen included in the model are (Figure B-1):

- Algal basal metabolism and predation
- Dissolution from refractory and labile particulate organic nitrogen
- Mineralization to ammonium
- External loads.

The kinetic equation describing these processes is:

$$\frac{\partial DON}{\partial t} = \sum_{x=c,d,g,m} (FND_x \bullet BM_x + FNDP \bullet PR_x) ANC_x \bullet B_x + K_{RPON} \bullet RPON + K_{LPON} \bullet LPON - K_{DON} \bullet DON + \frac{WDON}{V} \quad \text{(B.49)}$$

DON = concentration of dissolved organic nitrogen (g N m^{-3})
FND_x = fraction of metabolized nitrogen by algal group *x* produced as dissolved organic nitrogen
FNDP = fraction of predated nitrogen produced as dissolved organic nitrogen
K_{DON} = mineralization rate of dissolved organic nitrogen (day^{-1})
WDON = external loads of dissolved organic nitrogen (g N day^{-1}).

Ammonium Nitrogen

Sources and sinks for ammonia nitrogen included in the model are (Figure B-1):

- Algal basal metabolism, predation, and uptake
- Mineralization from dissolved organic nitrogen
- Nitrification to nitrate
- Sediment-water exchange for the bottom layer only
- External loads

The kinetic equation describing these processes is:

$$\frac{\partial NH4}{\partial t} = \sum_{x=c,d,g,m} (FNI_x \bullet BM_x + FNIP \bullet PR_x - PN_x \bullet P_x) ANC_x \bullet B_x + K_{DON} \bullet DON - Nit \bullet NH4 + \frac{BFNH4}{\Delta z} + \frac{WNH4}{V} \quad \text{(B.50)}$$

FNI_x = fraction of metabolized nitrogen by algal group *x* produced as inorganic nitrogen
FNIP = fraction of predated nitrogen produced as inorganic nitrogen
PN_x = preference for ammonium uptake by algal group *x* ($0 \le PN_x \le 1$)
Nit = nitrification rate (day^{-1}) given in equation B.58
BFNH4 = sediment-water exchange flux of ammonium (g N m^{-2} day^{-1}), applied to the bottom layer only
WNH4 = external loads of ammonium (g N day^{-1})

Nitrate Nitrogen

Sources and sinks for nitrate nitrogen included in the model are (Figure B-1):

- Algal uptake
- Nitrification from ammonium
- Denitrification to nitrogen gas
- Sediment-water exchange for the bottom layer only
- External loads

The kinetic equation describing these processes is:

$$\frac{\partial NO3}{\partial t} = \sum_{x=c,d,g,m} (1 - PN_x)\, P_x \bullet ANC_x \bullet B_x + Nit \bullet NH4 - ANDC \bullet Denit \bullet DOC + \frac{BFNO3}{\Delta z} + \frac{WNO3}{V} \qquad \text{(B.51)}$$

ANDC = mass of nitrate nitrogen reduced per mass of dissolved organic carbon oxidized (0.933 g N per g C from equation B.33)
BFNO3 = sediment-water exchange flux of nitrate (g N m^{-2} day^{-1}), applied to the bottom layer only
WNO3 = external loads of nitrate (g N day^{-1})

The remainder of this section explains each term in equations B.47 to B.51, except *BFNH4* and *BFNO3* which are described in Chapter 5.

Effect of Algae on Nitrogen

The terms within summation in equations B.47 to B.51 account for the effects of algae on nitrogen. As in phosphorus, both basal metabolism (respiration and excretion) and predation are considered, and thus formulated, to contribute to organic and ammonium nitrogen. That is, algal nitrogen released by both basal metabolism and predation are represented by distribution coefficients (FNR_x, FNL_x, FND_x, FNI_x, *FNRP, FNLP, FNDP,* and *FNIP*). The sum of four distribution coefficients for basal metabolism should be unity; the sum of the predation distribution coefficients should also be unity.

Algae take up ammonium and nitrate for growth, and ammonium is preferred from thermodynamic considerations. The preference of algae for ammonium is expressed as:

$$PN_x = NH4 \frac{NO3}{(KHN_x + NH4)(KHN_x + NO3)} + NH4 \frac{KHN_x}{(NH4 + NO3)(KHN_x + NO3)} \qquad \text{(B.52)}$$

This equation forces the preference for ammonium to be unity when nitrate is absent, and to be zero when ammonium is absent.

Mineralization and Hydrolysis

The third term on the RHS of equations B.47 and B.48 represents hydrolysis of particulate organic nitrogen and the last term in equation B.49 represents mineralization of dissolved organic nitrogen. Including a mechanism for accelerated hydrolysis and mineralization during nutrient-limited conditions, the formulations for these processes are:

$$K_{RPON} = \left(K_{RN} + \frac{KHN}{KHN + NH4 + NO3} K_{RNalg} \sum_{x=c,d,g} B_x \right) \exp\left(KT_{HDR} \left(T - TR_{HDR} \right) \right) \qquad \text{(B.53)}$$

$$K_{LPON} = \left(K_{LN} + \frac{KHN}{KHN + NH4 + NO3} K_{LNalg} \sum_{x=c,d,g} B_x \right) \exp\left(KT_{HDR} \left(T - TR_{HDR} \right) \right) \qquad \text{(B.54)}$$

$$K_{DON} = \left(K_{DN} + \frac{KHN}{KHN + NH4 + NO3} K_{DNalg} \sum_{x=c,d,g} B_x \right) \exp\left(KT_{HDR} \left(T - TR_{HDR} \right) \right) \qquad \text{(B.55)}$$

K_{RN} = minimum hydrolysis rate of refractory particulate organic nitrogen (day^{-1})
K_{LN} = minimum hydrolysis rate of labile particulate organic nitrogen (day^{-1})
K_{DN} = minimum mineralization rate of dissolved organic nitrogen (day^{-1})
K_{RNalg}, K_{LNalg} = constants that relate hydrolysis of refractory and labile particulate organic nitrogen, respectively, to algal biomass (day^{-1} per g C m^{-3})
K_{DNalg} = constant that relates mineralization to algal biomass (day^{-1} per g C m^{-3})
KHN = mean half-saturation constant for algal nitrogen uptake (g N m^{-3})

$$= \frac{1}{3} \sum_{x=c,d,g} KHN_x \qquad \text{(B.56)}$$

Equations B.53 to B.55 have exponential functions that relate rates to temperature.

Nitrification

Nitrification is a process mediated by autotrophic nitrifying bacteria that obtain energy through the oxidation of ammonium to nitrite and of nitrite to nitrate. The stoichiometry of complete reaction is (Bowie et al. 1985):

$$NH_4^+ + 2\,O_2 \rightarrow NO_3^- + H_2O + 2\,H^+ \qquad \text{(B.57)}$$

The first term in the second line of equation B.50 and its corresponding term in equation B.51 represent the effect of nitrification on ammonium and nitrate, respectively. The kinetics of

complete nitrification process are formulated as a function of available ammonium, dissolved oxygen and temperature:

$$Nit = \frac{DO}{KHNit_{DO} + DO} \frac{NH4}{KHNit_N + NH4} Nit_m \bullet f_{Nit}(T) \qquad \text{(B.58)}$$

$$\begin{aligned} f_{Nit}(T) &= \exp\left(-KNit1\,[T - TNit]^2\right) \quad if \quad T \le TNit \\ &= \exp\left(-KNit2\,[TNit - T]^2\right) \quad if \quad T > TNit \end{aligned} \qquad \text{(B.59)}$$

$KHNit_{DO}$ = nitrification half-saturation constant for dissolved oxygen (g O_2 m^{-3})
$KHNit_N$ = nitrification half-saturation constant for ammonium (g N m^{-3})
Nit_m = maximum nitrification rate at *TNit* (g N m^{-3} day^{-1})
TNit = optimum temperature for nitrification (°C)
KNit1 = effect of temperature below *TNit* on nitrification rate ($°C^{-2}$)
KNit2 = effect of temperature above *TNit* on nitrification rate ($°C^{-2}$)

The Monod function of dissolved oxygen in equation B.58 indicates the inhibition of nitrification at low oxygen level. The Monod function of ammonium indicates that when ammonium is abundant, the nitrification rate is limited by the availability of nitrifying bacteria. The effect of suboptimal temperature is represented using Gaussian form.

Denitrification

The effect of denitrification on dissolved organic carbon was described in Section 5.4.5. Denitrification removes nitrate from the system in stoichiometric proportion to carbon removal as determined by equation B.33. The last term in the first line of equation B.51 represents this removal of nitrate.

B.2.5 Silica

The present model has two state variables for silica: particulate biogenic silica and available silica.

Particulate Biogenic Silica

Sources and sinks for particulate biogenic silica included in the model are (Figure B-1):

- Diatom basal metabolism and predation
- Dissolution to available silica
- Settling
- External loads

The kinetic equation describing these processes is:

$$\frac{\partial SU}{\partial t} = (FSP_d \bullet BM_d + FSPP \bullet PR_d)\, ASC_d \bullet B_d - K_{SUA} \bullet SU + \frac{\partial}{\partial z}(WS_d \bullet SU) + \frac{WSU}{V} \qquad \text{(B.60)}$$

SU = concentration of particulate biogenic silica (g Si m^{-3})
FSP_d = fraction of metabolized silica by diatoms produced as particulate biogenic silica
$FSPP$ = fraction of predated diatom silica produced as particulate biogenic silica
ASC_d = silica-to-carbon ratio of diatoms (g Si per g C)
K_{SUA} = dissolution rate of particulate biogenic silica (day^{-1})
WSU = external loads of particulate biogenic silica (g Si day^{-1})

Available Silica

Sources and sinks for available silica included in the model are (Figure B-1):

- Diatom basal metabolism, predation, and uptake
- Settling of sorbed (particulate) available silica
- Dissolution from particulate biogenic silica
- Sediment-water exchange of dissolved silica for the bottom layer only
- External loads.

The kinetic equation describing these processes is:

$$\frac{\partial SA}{\partial t} = (FSI_d \bullet BM_d + FSIP \bullet PR_d - P_d)\, ASC_d \bullet B_d + K_{SUA} \bullet SU + \frac{\partial}{\partial z}(WS_{TSS} \bullet SAp) + \frac{BFSAd}{\Delta z} + \frac{WSA}{V} \qquad \text{(B.61)}$$

SA = concentration of available silica (g Si m^{-3}) = SAd + SAp
SAd = dissolved available silica (g Si m^{-3})
SAp = particulate (sorbed) available silica (g Si m^{-3})
FSI_d = fraction of metabolized silica by diatoms produced as available silica
$FSIP$ = fraction of predated diatom silica produced as available silica
$BFSAd$ = sediment-water exchange flux of available silica (g Si m^{-2} day^{-1}), applied to bottom layer only
WSA = external loads of available silica (g Si day^{-1})

In equation B.61, if total active metal is chosen as a measure of sorption site, the settling velocity of total suspended solid, WS_{TSS}, is replaced by that of particulate metal, WS_s (Sections 5.7.3 and 5.10).

Available Silica System

Analysis of Chesapeake Bay monitoring data indicates that silica shows similar behavior as phosphate in the adsorption-desorption process (Cerco and Cole 1993). As in phosphate, therefore, available silica is defined to include both dissolved and sorbed fractions (equation

B.62). Treatment of available silica is the same as total phosphate, and the same method to partition dissolved and sorbed phosphate is used to partition dissolved and sorbed available silica:

$$SAp = \frac{K_{SAp} \bullet TSS}{1 + K_{SAp} \bullet TSS} SA \quad \text{or} \quad SAp = \frac{K_{SAp} \bullet TAMp}{1 + K_{SAp} \bullet TAMp} SA$$

$$SAd = \frac{1}{1 + K_{SAp} \bullet TSS} SA \quad \text{or} \quad SAd = \frac{1}{1 + K_{SAp} \bullet TAMp} SA \qquad \text{(B.62)}$$

$$= SA - SAp \qquad \text{(B.63)}$$

K_{SAp} = empirical coefficient relating available silica sorption to total suspended solid (per g m^{-3}) or particulate total active metal (per mol m^{-3}) concentration.

As in $K_{PO}4p$ in Section 5.5.4, K_{SAp} is the ratio of sorbed to dissolved available silica per unit sorption site available.

Effect of Diatoms on Silica

In equations B.60 and B.61, those terms expressed as a function of diatom biomass (B_d) account for the effects of diatoms on silica. As in phosphorus and nitrogen, both basal metabolism (respiration and excretion) and predation are considered, and thus formulated, to contribute to particulate biogenic and available silica. That is, diatom silica released by both basal metabolism and predation are represented by distribution coefficients (FSP_d, FSI_d, $FSPP$, and $FSIP$). The sum of two distribution coefficients for basal metabolism should be unity and so is that for predation. Diatoms require silica as well as phosphorus and nitrogen, and diatom uptake of available silica is represented by ($- P_d \cdot ASC_d \cdot B_d$) in equation B.61.

Dissolution

The term ($- K_{SUA} \cdot SU$) in equation B.60 and its corresponding term in equation B.61 represent dissolution of particulate biogenic silica to available silica. The dissolution rate is expressed as an exponential function of temperature:

$$K_{SUA} = K_{SU} \bullet \exp\left(KT_{SUA}[T - TR_{SUA}]\right) \qquad \text{(B.64)}$$

K_{SU} = dissolution rate of particulate biogenic silica at TR_{SUA} (day^{-1})
KT_{SUA} = effect of temperature on dissolution of particulate biogenic silica ($°C^{-1}$)
TR_{SUA} = reference temperature for dissolution of particulate biogenic silica (°C)

B.2.6 Chemical Oxygen Demand

In the present model, chemical oxygen demand is the concentration of reduced substances that are oxidizable through inorganic means. The source of chemical oxygen demand in saline water is sulfide released from sediments. A cycle occurs in which sulfate is reduced to sulfide in the sediments and reoxidized to sulfate in the water column. In fresh water, methane is released to the water column by the sediment process model. Both sulfide and methane are quantified in units of oxygen demand and are treated with the same kinetic formulation. The kinetic equation, including external loads, if any, is:

$$\frac{\partial COD}{\partial t} = -\frac{DO}{KH_{COD} + DO} KCOD \bullet COD + \frac{BFCOD}{\Delta z} + \frac{WCOD}{V} \qquad \text{(B.65)}$$

COD = concentration of chemical oxygen demand (g O_2-equivalents m^{-3})
KH_{COD} = half-saturation constant of dissolved oxygen required for oxidation of chemical oxygen demand (g O_2 m^{-3})
$KCOD$ = oxidation rate of chemical oxygen demand (day^{-1})
$BFCOD$ = sediment flux of chemical oxygen demand (g O_2-equivalents m^{-2} day^{-1}), applied to bottom layer only
$WCOD$ = external loads of chemical oxygen demand (g O_2-equivalents day^{-1})

An exponential function is used to describe the temperature effect on the oxidation rate of chemical oxygen demand:

$$KCOD = K_{CD} \bullet \exp\left(KT_{COD} [T - TR_{COD}] \right) \qquad \text{(B.66)}$$

K_{CD} = oxidation rate of chemical oxygen demand at TR_{COD} (day^{-1})
KT_{COD} = effect of temperature on oxidation of chemical oxygen demand ($°C^{-1}$)
TR_{COD} = reference temperature for oxidation of chemical oxygen demand (°C)

B.2.7 Dissolved Oxygen

Sources and sinks of dissolved oxygen in the water column included in the model are (Figure B-1):

- Algal photosynthesis and respiration
- Nitrification
- Heterotrophic respiration of dissolved organic carbon
- Oxidation of chemical oxygen demand
- Surface reaeration for the surface layer only
- Sediment oxygen demand for the bottom layer only
- External loads

The kinetic equation describing these processes is:

$$\frac{\partial DO}{\partial t} = \sum_{x=c,d,g,m} \left((1.3 - 0.3 \bullet PN_x) P_x - (1 - FCD_x) \frac{DO}{KHR_x + DO} BM_x \right) AOCR \bullet B$$

$$- AONT \bullet Nit \bullet NH4 - AOCR \bullet K_{HR} \bullet DOC - \frac{DO}{KH_{COD} + DO} KCOD \bullet COD \qquad \text{(B.67)}$$

$$+ K_r (DO_s - DO) + \frac{SOD}{\Delta z} + \frac{WDO}{V}$$

$AONT$ = mass of dissolved oxygen consumed per unit mass of ammonium nitrogen nitrified (4.33 g O_2 per g N; see Section 5.9.2)
$AOCR$ = dissolved oxygen-to-carbon ratio in respiration (2.67 g O_2 per g C; see Section 5.9.1)
K_r = reaeration coefficient (day^{-1}): the reaeration term is applied to the surface layer only
DO_s = saturated concentration of dissolved oxygen (g O_2 m^{-3})
SOD = sediment oxygen demand (g O_2 m^{-2} day^{-1}), applied to the bottom layer only; positive is to the water column
WDO = external loads of dissolved oxygen (g O_2 day^{-1})

The two sink terms in equation B.67, heterotrophic respiration and chemical oxygen demand, are explained in Section 5.4.4 (equation C.29) and Section 5.8 (equation C.65), respectively. The remainder of this section explains the effects of algae, nitrification, and surface reaeration.

Effect of Algae on Dissolved Oxygen

The first line on the RHS of equation B.67 accounts for the effects of algae on dissolved oxygen. Algae produce oxygen through photosynthesis and consume oxygen through respiration. The quantity produced depends on the form of nitrogen utilized for growth. Equations describing production of dissolved oxygen are (Morel 1983):

$$106\ CO_2 + 16\ NH_4^+ + H_2PO_4^- + 106\ H_2O \rightarrow protoplasm + 106\ O_2 + 15\ H^+ \qquad \text{(B.68)}$$

$$106\ CO_2 + 16\ NO_3^- + H_2PO_4^- + 122\ H_2O + 17\ H^+ \rightarrow protoplasm + 138\ O_2 \qquad \text{(B.69)}$$

When ammonium is the nitrogen source, one mole of oxygen is produced per mole of carbon dioxide fixed. When nitrate is the nitrogen source, 1.3 moles of oxygen are produced per mole of carbon dioxide fixed. The quantity, (1.3 - 0.3·PN_x), in the first term of equation B.67 is the photosynthesis ratio and represents the molar quantity of oxygen produced per mole of carbon dioxide fixed. It approaches unity as the algal preference for ammonium approaches unity.

The last term in the first line of equation B.67 accounts for the oxygen consumption due to algal respiration (equation B.26). A simple representation of respiration process is:

$$CH_2O + O_2 = CO_2 + H_2O \qquad \text{(B.70)}$$

from which, $AOCR$ = 2.67 g O_2 per g C.

Effect of Nitrification on Dissolved Oxygen

The stoichiometry of nitrification reaction (equation B.57) indicates that two moles of oxygen are required to nitrify one mole of ammonium into nitrate. However, cell synthesis by nitrifying bacteria is accomplished by the fixation of carbon dioxide so that less than two moles of oxygen are consumed per mole ammonium utilized (Wezernak and Gannon 1968), i.e., $AONT$ = 4.33 g O_2 per g N.

Effect of Surface Reaeration on Dissolved Oxygen

The reaeration rate of dissolved oxygen at the air-water interface is proportional to the oxygen gradient across the interface, (DO_s - DO), when assuming the air is saturated with oxygen. The saturated concentration of dissolved oxygen, which decreases as temperature and salinity increase, is specified using an empirical formula (Genet et al. 1974):

$$\begin{aligned} DO_s &= 14.5532 - 0.38217 \bullet T + 5.4258 \times 10^{-3} \bullet T^2 \\ &- CL \bullet (1.665 \times 10^{-4} - 5.866 \times 10^{-6} \bullet T + 9.796 \times 10^{-8} \bullet T^2) \end{aligned} \qquad \text{(B.71)}$$

CL = chloride concentration (mg/L) = S/1.80655.

The reaeration coefficient includes the effect of turbulence generated by bottom friction (O'Connor and Dobbins 1958) and that by surface wind stress (Banks and Herrera 1977):

$$K_r = \left(K_{ro} \sqrt{\frac{u_{eq}}{h_{eq}}} + W_{rea} \right) \frac{1}{\Delta z} \bullet KT_r^{T-20} \qquad \text{(B.72)}$$

K_{ro} = proportionality constant = 3.933 in MKS unit
u_{eq} = weighted velocity over cross-section (m sec^{-1}) = $\sum(u_k V_k)/\sum(V_k)$
h_{eq} = weighted depth over cross-section (m) = $\sum(V_k)/B_\eta$
B_η = width at the free surface (m)
W_{rea} = wind-induced reaeration (m day^{-1})

$$= 0.728\, U_w^{0.5} - 0.317\, U_w + 0.0372\, U_w^2 \qquad \text{(B.73)}$$

U_w = wind speed (m sec^{-1}) at the height of 10 m above surface
KT_r = constant for temperature adjustment of dissolved oxygen reaeration rate.

B.2.8 Total Active Metal

The present model requires simulation of total active metal for adsorption of phosphate and silica if that option is chosen (Figure B-1). The total active metal state variable is the sum of iron and manganese concentrations, both particulate and dissolved. In the model, the origin of total active metal is benthic sediments. Since sediment release of metal is not explicit in the sediment model (see Chapter 5), release is specified in the kinetic portion of the water column model. The only other term included is settling of the particulate fraction. Then the kinetic equation for total active metal, including external loads, if any, may be written as:

$$\frac{\partial TAM}{\partial t} = \frac{KHbmf}{KHbmf + DO} \frac{BFTAM}{\Delta z} e^{Ktam(T-Ttam)} + \frac{\partial}{\partial z}(WS_s \bullet TAMp) + \frac{WTAM}{V} \qquad \text{(B.74)}$$

TAM = total active metal concentration (mol m^{-3}) = *TAMd* + *TAMp*
TAMd = dissolved total active metal (mol m^{-3})
TAMp = particulate total active metal (mol m^{-3})
KHbmf = dissolved oxygen concentration at which total active metal release is half the anoxic release rate (g O_2 m^{-3})
BFTAM = anoxic release rate of total active metal (mol m^{-2} day^{-1}), applied to the bottom layer only
Ktam = effect of temperature on sediment release of total active metal ($°C^{-1}$)
Ttam = reference temperature for sediment release of total active metal (°C)
WS_s = settling velocity of particulate metal (m day^{-1})
WTAM = external loads of total active metal (mol day^{-1})

In estuaries, iron and manganese exist in particular and dissolved forms depending on dissolved oxygen concentration. In the oxygenated water, most of the iron and manganese exist as particulate while under anoxic conditions, large fractions are dissolved, although solid-phase sulfides and carbonates exist and may predominate. The partitioning between particulate and dissolved phases is expressed using a concept that total active metal concentration must achieve a minimum level, which is a function of dissolved oxygen, before precipitation occurs:

$$TAMd = minimum\{TAMdmx \bullet \exp(-Kdotam \bullet DO), TAM\} \qquad \text{(B.75)}$$

$$TAMp = TAM - TAMd \qquad \text{(B.76)}$$

TAMdmx = solubility of total active metal under anoxic conditions (mol m^{-3})
Kdotam = constant that relates total active metal solubility to dissolved oxygen (per g O_2 m^{-3})

B.2.9 Fecal Coliform Bacteria

Fecal coliform bacteria are indicative of organisms from the intestinal tract of humans and other animals and can be used as an indicator bacteria as a measure of public health (Thomann and Mueller 1987). In the present model, fecal coliform bacteria have no interaction with other state variables, and have only one sink term, die-off. The kinetic equation, including external loads, may be written as:

$$\frac{\partial FCB}{\partial t} = -KFCB \bullet TFCB^{T-20} \bullet FCB + \frac{WFCB}{V} \qquad \text{(B.77)}$$

FCB = bacteria concentration (MPN per 100 ml)
KFCB = first order die-off rate at 20°C (day^{-1})
TFCB = effect of temperature on decay of bacteria ($°C^{-1}$)
WFCB = external loads of fecal coliform bacteria (MPN per 100 ml m^3 day^{-1})

B.2.10 Method of Solution

The kinetic equations for the 21 state variables in the EFDC water column water quality model can be expressed in a 21 × 21 matrix after linearizing some terms, mostly Monod type expressions:

$$\frac{\partial}{\partial t}[C] = [K] \bullet [C] + [R] \qquad \text{(B.78)}$$

where *[C]* is in mass $volume^{-1}$, *[K]* is in $time^{-1}$, and *[R]* is in mass $volume^{-1}$ $time^{-1}$. Since the settling of particulate matter from the overlying cell acts as an input for a given cell, when equation B.78 is applied to a cell of finite volume, it may be expressed as:

$$\frac{\partial}{\partial t}[C]_k = [K1]_k \bullet [C]_k + \lambda \bullet [K2]_k \bullet [C]_{k+1} + [R]_k \qquad \text{(B.79)}$$

where the four matrices *[C], [K1], [K2],* and *[R]* are defined in Appendix A of Park et al. (1995). The subscript *k* designates a cell at the k^{th} vertical layer. The layer index *k* increases upward with *KC* vertical layers; *k* = 1 is the bottom layer and *k* = *KC* is the surface layer. Then λ = 0 for k = *KC*; otherwise, λ = 1. The matrix [K2] is a diagonal matrix, and the non-zero elements account for the settling of particulate matter from the overlying cell.

Equation B.79 is solved using a second-order accurate trapezoidal scheme over a time step of θ, which may be expressed as:

$$[C]_k^N = \left([I] - \frac{\theta}{2}[K1]_k^O \right)^{-1} \bullet \left([C]_k^O + \frac{\theta}{2}\left\{ [K1]_k^O \bullet [C]_k^O + \lambda\, [K2]_k^O \bullet [C]_{k+1}^A \right\} + \theta\, [R]_k^O \right) \qquad \text{(B.80)}$$

where $\theta = 2 \cdot m \cdot \Delta t$ is the time step for the kinetic equations; *[I]* is a unit matrix; $[C]^A = [C]^N + [C]^O$; the superscripts *O* and *N* designate the variables before and after being adjusted for the relevant kinetic processes. Since equation B.80 is solved from the surface layer downward, the term with $[C]_{k+1}^A$ is known for the k^{th} layer and thus placed on the RHS. In equation B.80, inversion of a matrix can be avoided if the 21 state variables are solved in a proper order. The kinetic equations are solved in the order of the variables in the matrix *[C]* defined in Appendix A of Park et al. (1995).

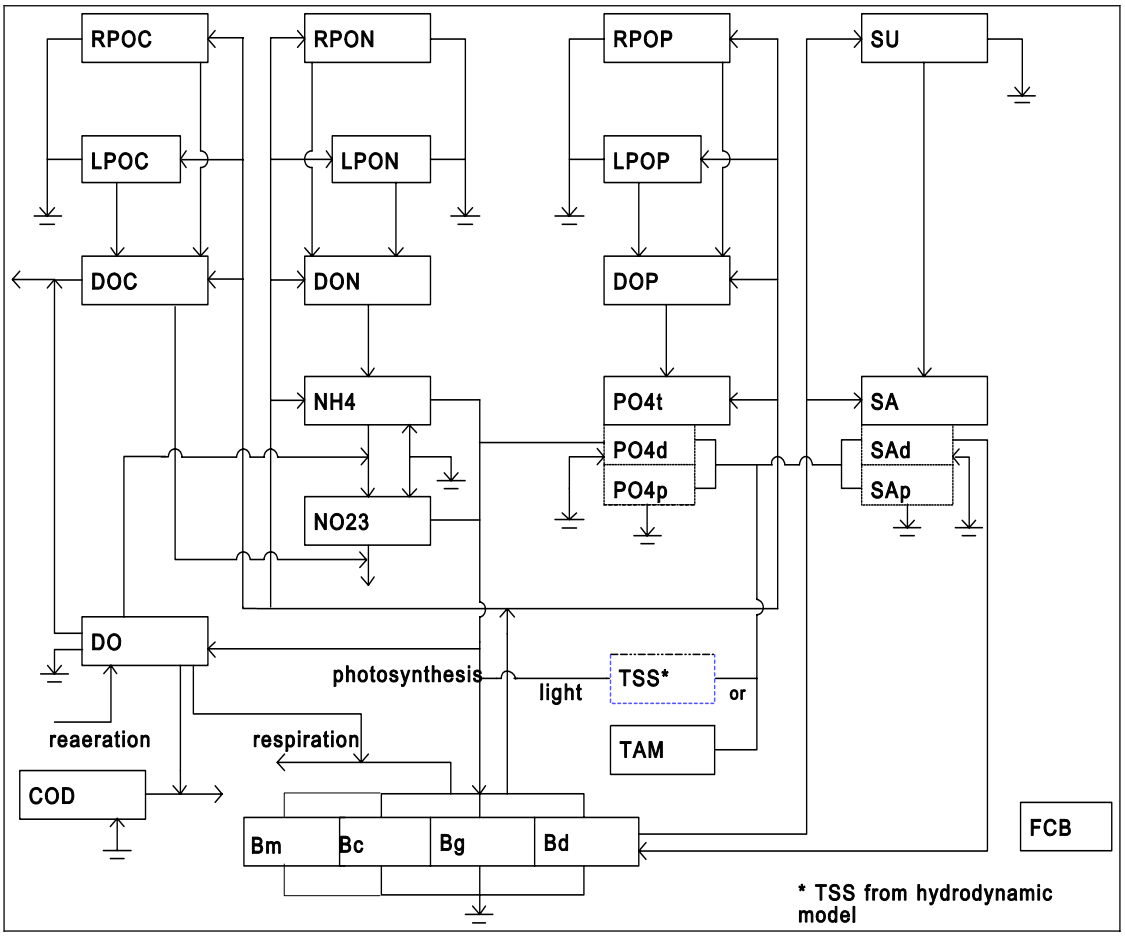

Figure B-1. Schematic diagram of EFDC water quality model structure.

APPENDIX C: CALIBRATION AND VERIFICATION MEASURES

To quantify the EFDC model's prediction of water surface elevation, salinity, and velocity, a number of statistical tests and time series analyses are used. This section summarizes general test and analysis procedures. Further discussion justifying the selection of particular tests and analyses for specific data types are presented in Section 5.

The statistical test that can be used for evaluating model predictions includes the mean error, mean absolute error, root mean square error, maximum absolute error, relative mean error and relative absolute mean error (Thomann 1982). Letting O and P denote observed and predicted values of a quantity at N observation times, the mean error is defined by

$$ME = \frac{1}{N}\sum_{n=1}^{N}\left(O^{(n)} - P^{(n)}\right) \qquad \text{(C.1)}$$

Positive values of the mean error indicate that the model tends to underpredict the observations whereas negative values indicate that the model tends to overpredict observations. The mean absolute error is defined by

$$MAE = \frac{1}{N}\sum_{n=1}^{N}\left|O^{(n)} - P^{(n)}\right| \qquad \text{(C.2)}$$

Although the mean absolute error provides no indication of overprediction or underprediction, it eliminates the canceling effects of positive and negative errors and can be viewed as a more extreme measure of observation-prediction agreement. The root mean square error is defined by

$$RMS = \sqrt{\frac{1}{N}\sum_{n=1}^{N}\left(O^{(n)} - P^{(n)}\right)^2} \qquad \text{(C.3)}$$

The root mean square error can be interpreted as a weighted equivalent to the mean absolute error with larger observation-prediction differences given larger weightings. The square root operation recovers the units of the data quantities. The RMA error is generally viewed as the most rigorous absolute error test. The maximum absolute error is defined by

$$MAX = \max\left|O^{(n)} - P^{(n)}\right| \quad : \quad n = 1, N \qquad \text{(C.4)}$$

and provides information on the largest discrepancy between corresponding values of observed and predicted quantities over an interval of N measurements.

Relative error measures can be used to eliminate data units and to provide a measure of error relative to the magnitude of the observational data. The relative mean error and the relative mean absolute error are defined by

$$RME = \frac{\sum_{n=1}^{N}\left(O^{(n)} - P^{(n)}\right)}{\sum_{n=1}^{N} O^{(n)}} \tag{C.5}$$

$$RMA = \frac{\sum_{n=1}^{N}\left|O^{(n)} - P^{(n)}\right|}{\sum_{n=1}^{N} O^{(n)}} \tag{C.6}$$

Caution should be employed in the use of these two relative error measures, particularly when observed and predicted quantities can have small values or values that have both positive and negative signs. An alternative relative error, hereafter referred to as the relative mean square error, is

$$RSE = \frac{\sum_{n=1}^{N}\left(O^{(n)} - P^{(n)}\right)^2}{\sum_{n=1}^{N}\left(\left(O^{(n)} - \overline{O}\right)^2 + \left(P^{(n)} - \overline{O}\right)^2\right)} \tag{C.7}$$

This error measure was proposed by Willmott (1982) and Willmont et al. (1982) and used by Blumberg and Goodrich (1990) to analyze the prediction skill of an estuarine model. The value of *RSE* always falls between zero and unity, with an increasing value corresponding to decreasing skill of the model.

Thomann (1982) suggested the use of linear regression for comparing model predictions with observations in the context of model calibration. Following Thomann, the linear equation relating observed and predicted values of the quantity *s* is written as

$$s_o = \alpha + \beta s_p \tag{C.8}$$

where alpha and beta are determined by

$$\alpha = \frac{1}{N}\left(\sum_{n=1}^{N} s_o^{(n)} - \beta\sum_{n=1}^{N} s_p^{(n)}\right) \tag{C.9}$$

$$\beta = \frac{\sum_{n=1}^{N}\left(s_o^{(n)} - s_o^{(avg)}\right)\left(s_p^{(n)} - s_p^{(avg)}\right)}{\sum_{n=1}^{N}\left(s_p^{(n)} - s_p^{(avg)}\right)^2} \tag{C.10}$$

(Devore, 1982). The null hypothesis for the linear regression is alpha, the intercept, equal to zero, and beta, the slope, equal to one. Also useful in the regression analysis is the correlation coefficient

$$r = \frac{N\sum_{n=1}^{N} s_p^{(n)} s_o^{(n)} - \left(\sum_{n=1}^{N} s_p^{(n)}\right)\left(\sum_{n=1}^{N} s_o^{(n)}\right)}{\sqrt{N\sum_{n=1}^{N} s_p^{(n)} s_p^{(n)} - \left(\sum_{n=1}^{N} s_p^{(n)}\right)^2}\sqrt{N\sum_{n=1}^{N} s_o^{(n)} s_o^{(n)} - \left(\sum_{n=1}^{N} s_o^{(n)}\right)^2}} \qquad \text{(C.11)}$$

For a good a fit or correlation between observations and predictions, the correlation coefficient should be near one. The square of the correlation coefficient equals the fractional proportion of variation of observations explained by the regression relationship between the observations and predictions (Devore 1982).

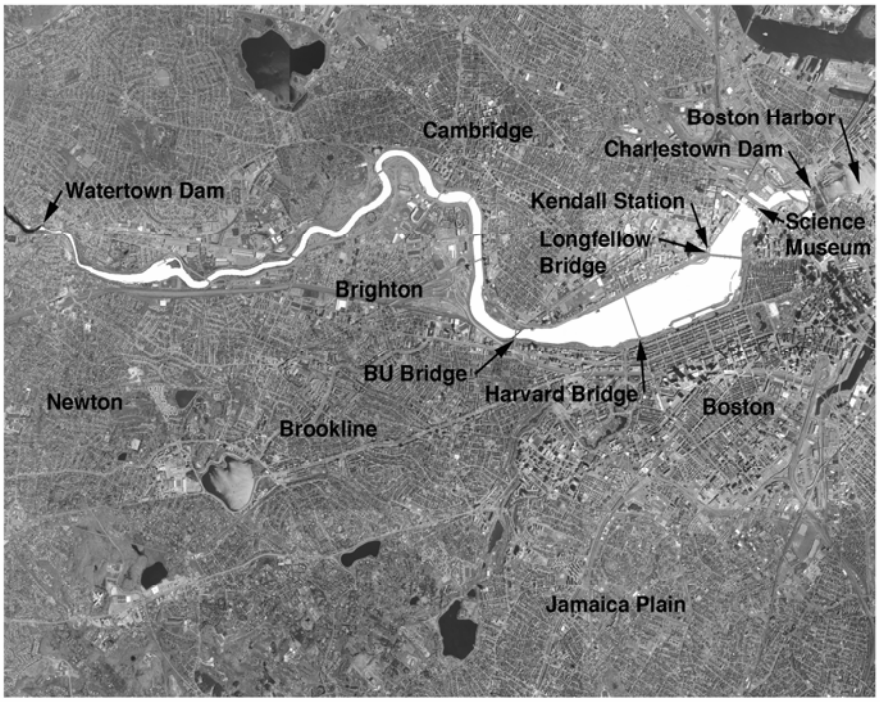

Figure 1.1 Lower Charles River Basin

Figure 2-1. Location and major tributary watersheds of the Charles River Basin.